INFORMATION TO USERS

This manuscript has been reproduced from the microfilm master. UMI films the text directly from the original or copy submitted. Thus, some thesis and dissertation copies are in typewriter face, while others may be from any type of computer printer.

The quality of this reproduction is dependent upon the quality of the copy submitted. Broken or indistinct print, colored or poor quality illustrations and photographs, print bleedthrough, substandard margins, and improper alignment can adversely affect reproduction.

In the unlikely event that the author did not send UMI a complete manuscript and there are missing pages, these will be noted. Also, if unauthorized copyright material had to be removed, a note will indicate the deletion.

Oversize materials (e.g., maps, drawings, charts) are reproduced by sectioning the original, beginning at the upper left-hand corner and continuing from left to right in equal sections with small overlaps.

Photographs included in the original manuscript have been reproduced xerographically in this copy. Higher quality 6" x 9" black and white photographic prints are available for any photographs or illustrations appearing in this copy for an additional charge. Contact UMI directly to order.

Bell & Howell Information and Learning
300 North Zeeb Road, Ann Arbor, MI 48106-1346 USA
800-521-0600

Investigation of the interaction of GdnHCl with poly-L-lysine, horseradish peroxidase and cytochrome c monitored via FTIR, CD and fluorescence spectroscopies

Christina Esposito

A Thesis

in

The Department

of

Chemistry & Biochemistry

Presented in Partial Fulfillment of the Requirements
for the Degree of Master of Science at
Concordia University
Montreal, Quebec, Canada

March 2000

ABSTRACT

Investigation of the interaction of GdnHCl with poly-L-lysine, horseradish peroxidase and cytochrome c monitored via FTIR, CD and fluorescence spectroscopies

Christina Esposito

Spectroscopic probes were utilized to study the interaction of GdnHCl with three model systems: poly-L-lysine (PLL), horseradish peroxidase (HRP) and cytochrome c. Probing the chemically denatured states of proteins by FTIR is a novel technique, which has only recently been reported. To aid in the interpretation of the FTIR results, fluorescence and CD were employed. The use of deuterated solvents, *i.e.* Gdn-d_5-DCl and D_2O, simplified data processing and is recommended for FTIR studies of protein chemical denaturation. PLL, a random coil, was used to model the interaction between Gdn-d_5-DCl and random structures. Spectroscopic evidence strongly suggested that Gdn-d_5-DCl associates with PLL, particularly with its lysyl side chains. The analysis of HRP indicated that it was not a suitable model due to complex time-dependent spectral changes. The study of cytochrome c in Gdn-d_5-DCl revealed that the denaturant preferentially interacted with random structures. The denatured states of horse and tuna c were characterized and subtle differences between the two species were reported. Curve-fitting of the FTIR amide I' mode (1600-1700 cm^{-1}) revealed that tuna c contained more residual structure in Gdn-d_5-DCl than horse c. It was successfully demonstrated that FTIR is a powerful tool for probing the chemically denatured states of model protein systems, with potential applications for other biomolecules.

ACKNOWLEDGEMENTS

I would like to thank the following people who were instrumental in the completion of this work: my research supervisor, Dr. Ann English for guiding me throughout my research, inspiring new ideas and critically editing this thesis; Dr. Joanne Turnbull and Dr. Peter Bird for being part of my research committee and reading this document; the lab group members especially Angelo Filosa, Andrea Romeo and Tyrone Shephard for all of their valuable help and making my time in the lab enjoyable; my parents and my brothers Rob and Dan, for their encouragement and support throughout these years; and my dearest Todd for motivating me, inspiring me, and most importantly for his love.

TABLE OF CONTENTS

TABLE OF CONTENTS
Continued

LIST OF FIGURES

LIST OF FIGURES
Continued

LIST OF FIGURES
Continued

LIST OF TABLES

LIST OF SPECIAL SYMBOLS

In order as they appear in the text

ΔG^b	Free energy of binding (kcal/mol)
ΔG^L	Free energy of protein-ligand interaction (kcal/mol)
ΔG^N	Free energy of protein-H_2O interaction (kcal/mol)
K_{ex}	Exchange constant
K	Resolution enhancement factor
γ	HWHH (cm^{-1})
γ'	Deconvolved HWHH (cm^{-1})
A_{peak}	Peak height (A.U.)
A'_{peak}	Deconvolved peak height (A.U.)
ΔA	Difference in absorbance (A.U.)
A_L	Absorption of left-handed circularly polarized light (A.U.)
A_R	Absorption of right-handed circularly polarized light (A.U.)
θ	Ellipticity (mdeg)
$[\theta]$	Molar ellipticity ($deg \cdot cm^2 \cdot dmol^{-1}$)
$\Delta\varepsilon$	Differential molar CD extinction coefficient
E	Efficiency of energy-transfer
R	Distance between fluorescent donor and acceptor (Å)
R_o	Distance between fluorescent donor and acceptor when the efficiency of energy-transfer is 50 % (Å)
M_r	Molecular weight (g/mole)
l	Cell pathlength (cm)
c	Molar concentration (M)
$\%F_{350}$	Percent relative fluorescence at 350 nm
F_{350}	Fluorescence at 350 nm

CHAPTER 1: INVESTIGATION OF PROTEIN CHEMICAL DENATURATION USING SPECTROSCOPIC PROBES

1.1 INTERACTION OF GUANIDINE HYDROCHLORIDE (GdnHCl) WITH PROTEINS

1.1.1 General Properties of Chemical Denaturants and Denaturation

The stability of proteins is of great concern since this is the factor which usually limits their usefulness (*1*). The conformational stability of the folded state of a protein can be investigated by denaturation studies. There exists a wide array of reagents that decrease protein stability when added to aqueous solvents. In 1911, Chick and Martin were the first to discover the process known as denaturation and distinguish it from aggregation (*2*). In 1929, Wu proposed that denaturation was an unfolding process (*3*).

Proteins are made up of regular repeated patterns of polypeptide chain folded in a three-dimensional network that is unique for every protein. This is referred to as the native state. The internal organization, known as secondary structure consists of helices, sheets and turns that are determined by the amino acid sequence. The secondary structure is formed as a result of hydrophobic interactions, chain-conformational entropies and electrostatic forces (*4*). In the native state, hydrophobic residues are buried in a nonpolar core and in the unfolded state, these residues become solvent exposed. Differences in hydrogen bonding within the secondary-structural elements determine the overall conformation of the protein. Understanding how these native structures form provides important insight in protein stability and folding.

The stability of the native state, which is defined as the difference in free energy between the native and denatured states (*4*) is very important. Denaturation involves the

disorganization of a folded protein structure to a more flexible open chain with a larger solvent-exposed surface area. Depending on the experimental conditions, the degree of polypeptide denaturation may vary from a compact species with residual structure to an expanded conformation.

Proteins do not always unfold to a simple reference state, *i.e.* to a random coil upon the addition of stresses such as chemical, heat, pressure or pH change. A random coil or unordered structure is characterized as an energetically well defined state that is highly solvated and in which no side chain interactions occur (*5*). Upon denaturation to a random coil, the polypeptide chain expands, becomes more flexible and is less structured since solvent-side-chain interactions are more favorable (*5*). Assuming that the denatured state is a featureless, random coil simplifies the interpretation of experimental data. However, many recent studies suggest that this assumption is *wrong*. Hammack *et al.* (*6*) stated that a single domain protein can be thought of as an ensemble of substructures or individual cooperative units. If this is the case, then these substructures provide the potential for the presence of residual structure in the denatured state. Shortle proposed a similar hypothesis, that the denatured state is not a single entity, but an ensemble of partially folded states (*5*).

There is mounting evidence that the denatured states of many proteins have residual structure and do not collapse into a random coil (*4, 7-9*). Residual structure was detected in ribonuclease A (Rnase A), staphylococcal nuclease (Snase) and cytochrome c from small-angle x-ray scattering studies (*5*), which characterized the global size and shape of the denatured state. The results indicated that the radii of gyration were lower than expected for a random-coil. According to Shortle (*5*), a detailed examination of the

denatured state revealed the presence of residual structure, which increased as the denaturation conditions were made less severe. Denaturation studies were also performed on Rnase A in GdnHCl, and substantial residual α-helical content was reported (*4*). Martensson (*10*) studied human carbonic anhydrase II in 1-2 M GdnHCl, and detected an ordered native-like β-sheet structure and a large hydrophobic cluster that are stable even at high concentrations of GdnHCl (>5 M).

For many single-domain proteins, reversible denaturation can be approximated by a 2-state $N \rightleftharpoons D$ process, where N and D denote the native and denatured states, respectively. The native state is located in a limited region of configurational space of the protein chain and is easily probed spectroscopically. The denatured state, on the other hand, can adopt a wide array of configurations and experimental characterization is considerably more challenging (*11*). A 2-state process is based on the assumption that conformational transitions within each state are fast, and transitions between states are relatively slow, therefore two molecular populations can be distinguished (*12*). When considering 2-state models, it is important to differentiate between variable and fixed states. Variable 2-state behavior refers to an ensemble of denatured states whose state-distinguishable properties vary with denaturant concentration (*13*). A state-distinguishable property is one that identifies an individual state (*4*); for example, the distinction between two NMR peaks in a spectrum, where one represents the native state and the other the denatured state (*4*). State-distinguishable properties that do not change with varying amounts of denaturant define fixed 2-state behavior (*13*). The reversible denaturation process can also be described by a 3-state mechanism, $N \rightleftharpoons I \rightleftharpoons D$ reaction, where I represents an intermediate population.

Denaturants like GdnHCl and urea act primarily on the non-native rather than the native state (*5*). It was initially thought that the denaturant acted by breaking protein hydrogen bonds. Recent studies have shown that hydrogen bonding is not the dominant force in protein folding (*14*). Hibbard *et al.* (*15*) proposed that the denaturing power of GdnHCl and urea is due to their ability to make water a better solvent for nonpolar side chains, *i.e.* they weaken hydrophobic interactions. They have hydrogen bonding capabilities comparable to water, but adopt different geometries (*16*). Segel (*17*) also pointed out that GdnHCl weakened hydrophobic interactions, therefore as the concentration of GdnHCl was increased, the number of hydrophobic interactions decreased, and the protein was driven towards a random-coil like structure. Breaking of these hydrophobic contacts in the denatured state is assumed to be a gradual process, and hence leads to the formation of a multiplicity of denatured states (*17*). Tanford (*18*) hypothesized that protein unfolding in chemical denaturants was due to the increased affinity of internal residues for solvent. As the denaturant was added, the unfolded state became more stable. Therefore, hydrogen bonding, hydrophobic effects, van der Waals interactions, conformational entropy and Gibbs free energy all drive protein folding (*19*).

1.1.2 Urea and GdnHCl

The most commonly used denaturants today are urea and GdnHCl shown in Figure 1.1. Both urea and GdnHCl are commercially available in highly purified forms. However, some lots of urea have been found to contain metal impurities and cyanates, while some batches of GdnHCl may contain fluorescent impurities (*1*). Stock aqueous

solutions of GdnHCl are stable for months, whereas urea stock solutions slowly decompose to form cyanate and ammonium ions (*1*).

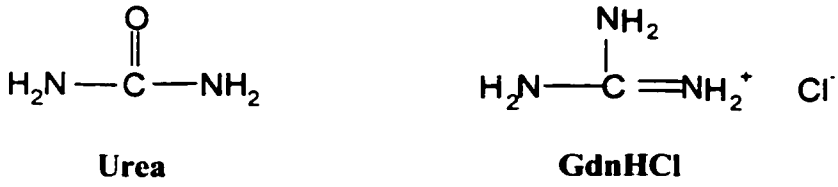

Urea **GdnHCl**

Figure 1.1 Structures of urea and GdnHCl denaturants.

Urea and GdnHCl are generally assumed to be comparable, and studies have shown that proteins unfolded by both solvents have very similar structures (*15*). However, the effects of GdnHCl on the conformational states of a protein are different from those of urea (*20*), which is not surprising given that GdnHCl is an ionic denaturant, and urea is non-ionic (*21*). Urea preferentially interacts with nonpolar groups and GdnHCl interacts more favorably with peptide groups (*22*). Overall, both exhibit polar and nonpolar interactions which makes them effective denaturants.

GdnHCl is a stronger denaturant compared to urea, such that higher concentrations of urea are needed to denature a protein. The solubilities of urea and GdnHCl in aqueous solutions at 25°C are 10.49 and 8.54 M, respectively (*1*). Another drawback of urea is that it has a titratable group with a pK_a of 0.1 (at 21°C) (*20*) and accurate experiments at low pH can not be performed. Therefore, GdnHCl is generally preferred as a protein denaturant (*20*).

GdnHCl was initially chosen over urea as a chemical denaturant for studies with horseradish peroxidase (HRP), which was the first protein examined in this work.

Denaturation of HRP by GdnHCl is preferred over urea because the protein does not undergo complete unfolding in 8 M urea. Pappa and Cass (*23*) observed a 50% loss of backbone CD signal when HRP was incubated in 8 M urea overnight, whereas no secondary structure was detected in 6 M GdnHCl.

1.1.3 Interaction of GdnHCl with Proteins and Peptides

As discussed earlier, GdnHCl is an ionic denaturant. Ions arising from GdnHCl modulate the electrostatics, and interact with the charged groups on the surface of a protein (*20*). The interaction of guanidinium ions (Gdn^+) with the protein will depend on the accessible surface area and the number and sign of the exposed charges (*19*). GdnHCl is expected to be more effective than most salts at eliminating unfavorable charge-charge interactions due to a 'screening effect' which may be enhanced by the binding of Gdn^+ and Cl^- ions to the protein surface (*19*). At neutral pH and low concentration of GdnHCl, chlorine anions interact with the positive charges on the protein surface and may stabilize the native state. For example, in 0.3 M GdnHCl, the native state of ribonuclease T_1 (at pH 5) was found to be slightly stabilized relative to its form in buffer (*20*). This is probably due to preferential interaction of the Gdn^+ with the protein.

Denaturants increase protein solubility. Studies have shown that they interact preferentially with the protein surface, and may even be bound to the polypeptide backbone (*16*). A schematic of favorable interactions of denaturant with a protein interface is shown in Figure 1.2. Under strong denaturation conditions, the concentration of Gdn^+ in the solvation shell of the protein is greater than in the bulk solvent.

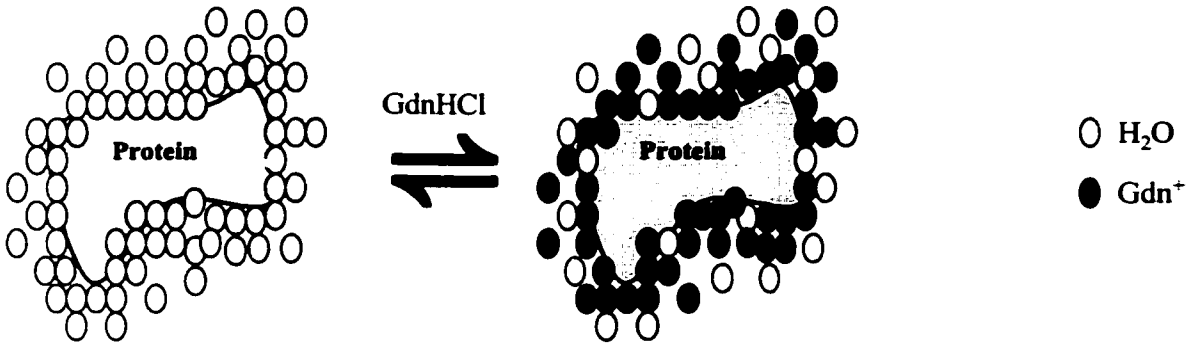

Figure 1.2 Schematic of preferential binding of guanidinium ions to a protein interface. Drawing on the left represents a native protein in water, and the one on the right represents a protein in a high concentration of GdnHCl. Adapted from Creighton (*16*).

The native states of proteins should be stabilized by substances that are worse at solvating nonpolar groups compared to water, for example sugars like glycerol (*24*). The effects of these stabilizers on protein stability are similar to interactions that are responsible for protein solubility. Preferential hydration occurs since the stabilizers are excluded from the protein surface (*16*). The concentration of these additives is greater in the bulk solvent than the vicinity of the protein.

The mechanism of action of GdnHCl, as well as urea, can be described as weak binding or adsorption to nonpolar surfaces (*5*). Since there are more nonpolar surfaces available for binding in the denatured state, GdnHCl promotes unfolding by association with the non-native state. The interaction of denaturants such as GdnHCl with proteins are classified as weak, because intrinsic binding constants for GdnHCl and H_2O are similar in magnitude (*25*). Therefore, if the binding constants are approximately the same, then there is an equal probability that H_2O or GdnHCl will bind to the protein. However, if the concentration of GdnHCl is high, then the probability of Gdn^+ binding to

the protein surface should be greater. Calorimetric measurements (*26*) were performed for the binding of GdnHCl and urea to unfolded proteins. Association of Gdn^+ with the protein contributed approximately 1.0 kcal/mol of free energy per Gdn^+ bound. Binding of urea to the protein generated only 0.2 kcal/mol of free energy per urea molecule bound.

Competitive solvation between GdnHCl an H_2O can be described by a preferential binding model developed by Timasheff *et al.* (*25*). All surface sites on the native protein are assumed to be occupied and in contact with H_2O molecules. The binding of a ligand molecule (GdnHCl) to a protein surface site must displace a H_2O molecule. Therefore, the free energy of binding at a particular site (ΔG^b) is defined as the difference in free energy of protein-ligand interaction (ΔG^L) and protein-H_2O interaction (ΔG^N) (*25*) given by equation 1.1.

$$\Delta G^b = \Delta G^L - \Delta G^N \qquad \textbf{1.1}$$

Protein interactions with denaturants can also be defined in terms of equilibrium competition according to equations 1.2 and 1.3 (*25*) where P and L represent the protein and ligand, respectively and K_{ex} is the exchange constant. Differences in affinity of GdnHCl *vs* H_2O for a given site on a protein influences the observed binding.

$$P\bullet(H_2O)_n + L \rightleftharpoons PL + nH_2O \qquad \textbf{1.2}$$

$$K_{ex} = \frac{[PL][H_2O]^n}{[P\bullet(H_2O)_n][L]} \qquad \textbf{1.3}$$

Two proteins (lysozyme and Rnase A) in GdnHCl and urea were used as models to study binding and occupancy of the protein's surface sites (*25*). In 6 M GdnHCl, Gdn^+ occupied 78% and 77% of the available surface sites of lysozyme and Rnase A, respectively. In 8 M urea, preferential binding of the denaturant was less prominent, *i.e.* 31% for lysozyme and 23% for Rnase A. The interactions with denaturants were favored as judged by an increase in free energy of ~15 kcal/mol in urea and ~30 kcal/mol in GdnHCl (*25*). Hence, these data provide evidence that competition for solvation sites favors Gdn^+ at high GdnHCl concentrations, and H_2O is displaced upon association of Gdn^+ with the polypeptide backbone.

Understanding protein-solvent interactions provides an important insight into protein structure, stability and unfolding. Denisov *et al.* (*27*) investigated the hydration of several GdnHCl-denatured proteins known to contain residual structure in their denatured states. Denisov's group utilized water ^{17}O NMR relaxation dispersion to monitor internal and external hydration of proteins in native and denatured forms. The proteins studied (lysozyme, α-lactalbumin and Rnase A) were not fully solvent exposed in their GdnHCl-denatured forms, as they contained strongly perturbed occluded H_2O. Long-lived (>10 ns) internal H_2O molecules were detected in the GdnHCl-denatured forms of all of three proteins, which is indicative of the presence of residual structure (*27*). These finding support the view that denatured proteins are not simply random coils (*27*).

Denisov *et al.* also performed MRD (magnetic relaxation dispersion) measurements using ^{17}O NMR longitudinal relaxation rates to characterize protein unfolding (*27*). Results revealed a large dynamic retardation for the denatured state,

which implies that H_2O penetrating the GdnHCl-denatured protein differs from that found in the hydration shell of a fully exposed polypeptide chain (*27*). This H_2O was four times more dynamically perturbed than H_2O in contact with a fully exposed random-coil like structure. Major hydration changes upon GdnHCl denaturation are correlated with disruption of secondary structure. According to Denisov, specific internal H_2O sites and secondary structure are lost simultaneously, accompanied by an influx of external solvent. Destabilization of sheets and helices is promoted by H_2O insertion and competition as a H-bonding partner (*28*). Therefore, even under strong solvent denaturing conditions, these proteins (lysozyme, α-lactalbumin and Rnase A) exhibit relatively compact non-native states, unlike that expected for a random coil.

Further analysis of the GdnHCl denaturation data generated by Denisov's group showed that the number of long-lived H_2O molecules decreased upon protein unfolding due to a gradual replacement of H_2O by Gdn^+ at the surface of the denatured protein (*27*). MRD studies with lysozyme revealed that competitive solvation occurred, and surface H_2O was replaced by Gdn^+ at high concentrations of denaturant. This effect was also modeled by weak binding of Gdn^+ at independent sites of α-lactalbumin, and yielded a Gdn^+ binding constant for the denatured state of K_b= 0.16 +/- 0.07 M (*29*). Therefore, GdnHCl does not only unfold the protein, but competes with H_2O for solvation sites.

Staniforth *et al.* (*30*) studied changes in the solvation free energy of internal amino acid residues upon the addition of varying amounts of denaturant. They proposed that the unfolding action of GdnHCl was due to the increased solvation energy generated as the amino acid side chains became exposed.

1.2 Review of Spectroscopic Probes Utilized to Study Chemical Denaturation

1.2.1 Fourier-Transform Infrared (FTIR) Spectroscopy

FTIR spectroscopy is a powerful tool for the structural characterization of biomolecules. For comprehensive reviews, refer to references by Jackson and Mantsch (*31*) as well as by Haris and Chapman (*32, 33*). Additional information on FTIR theory and instrumentation can be found in papers by Markovich and Haris (*33, 34*).

The amide I mode is normally utilized for secondary structural determination since it is a relatively pure mode (*31*). Its frequency (1600–1700 cm^{-1}) is mainly due to C–O stretching vibrations of the polypeptide backbone (80%) with minor contributions from C–N stretching vibrations and in-plane N–H bending (20%) (*16*). The amide I mode is sensitive to different H-bonding patterns between amide C=O and N–H groups, which gives rise to the characteristic frequencies of the secondary structures (*33*). The differences in H-bonding are attributed to varied lengths and directions of the H-bonds which alters the H-bond strength. The stronger the H-bond involving the amide C=O, the lower the electron density surrounding the carbonyl group, hence the lower the amide I mode absorption (*31*). H-bonding, as well as coupling between transition dipoles are the major factors responsible for the sensitivity of the amide I band to subtle changes in protein structure. Transition-dipole coupling leads to splitting of the amide I mode that is dependent on the direction and distance of interacting dipoles (*35*).

Characteristic secondary structure frequencies based on empirical rules are listed in Table 1.1 (*31, 36*). The exact position of these amide bands are dependent on the solvent and the nature of the side chains (*36*). The assignment of turns and sheets are the

most straightforward. Both α-helices and random structures, on the other hand, absorb at similar frequencies and may overlap, which can be problematic.

Table 1.1: Correlation between protein secondary structures and amide I frequencies

Secondary Structure	Amide I frequency (cm^{-1})
Aggregated strands	1610 – 1628
β-sheets	1625 – 1640
Unordered structures	1640 – 1648
α-helices	1648 – 1660
3_{10}-helices	1660 – 1670
β-turns	1660 – 1690
Antiparallel β-sheets	1675 – 1695

Protein secondary structures are assigned according to the frequencies listed in Table 1.1, however certain assumptions must be made (*37*):

i. Integrated absorption coefficients are equal for all secondary structures

ii. Contributions from amino acid side chains to the amide I band are negligible

iii. None of the secondary structural components overlap

The FTIR amino acid side-chain absorptions are listed in Table 1.2 (*38, 39*). The majority of the amino acids, with the exception of Lys, Arg, Asp and Glu, do not interfere with the amide I region (1700-1600 cm^{-1}), hence satisfy the second assumption listed above.

Table 1.2: FTIR absorptions due to amino acid side chains

Amino acid name	Symbol	Frequency (cm^{-1})
Glycine	G	N/A
Alanine	A	1465 (CH_2 bending)
Valine	V	1450 (CH_3 asymmetric bending)
Leucine	L	1375 (CH_3 symmetric bending)
Isoleucine	I	N/A
Serine	S	1350-1250 (OH deformation)
Cysteine	C	~2500 (S-H)
Threonine	T	N/A
Methionine	M	N/A
Phenylalanine	F	1494 (aromatic ring)
Tyrosine	Y	1518 (phenol ring)
Tryptophan	W	N/A
Proline	P	N/A
Histidine	H	1596 (ring)
Lysine	K	1629 (NH_3^+ asymmetric) & 1526 (NH_3^+ symmetric)
Arginine	R	1633 ($CN_3H_5^+$ symmetric) & 1673 ($CN_3H_5^+$ asymmetric)
Aspartic acid	D	1574 (COO^-) & 1718 (C=O)
Glutamic acid	E	1560 (COO^- asymmetric) & 1712 (COOH)
Asparagine	N	1678 (C=O) & 1622 (NH_2 bending)
Glutamine	Q	1670 (C=O) & 1615 (NH_2 bending)

The study of proteins in aqueous solutions is limited by strong OH-bending absorption of water at 1644 cm^{-1}, which overlaps with the amide I band (*31*). In addition, strong absorption of GdnHCl at ~ 1675 cm^{-1} interferes with the amide I mode. Careful digital subtraction procedures were developed by Dong *et al.* (*40, 41*) which remove

spectral contributions from the background. The subtraction steps are outlined in the Section 2.2.2.

The structure-sensitive amide I is made up of overlapping components which need to be resolved with mathematical techniques. Fourier-self deconvolution (FSD) and second-derivative procedures increase the separation of components under the broad amide I envelope, allowing the absorption due to different secondary structures to be identified according to frequencies listed in Table 1.1 (*32*). These methods do not achieve actual spectral resolution enhancement, which is only determined by the spectral settings (*37*). FSD resolves overlapping IR bands by narrowing bandwidths and increases peak heights without changing peak positions (*34*). Second-derivative treatment of data also deconvolutes the amide I band to resolve its components, without the input of parameters (*40*). This method is based on the fact that the height of the second derivative peak is proportional to the square of the original peak height (with the opposite sign) and the half bandwidth is inversely proportional to the square of the original half bandwidth (*42*).

The FTIR results shown in this present study were subjected to FSD rather than second-derivative treatment. However, second derivatives were used to verify the number and position of the bands under the amide I envelope. FSD introduces less distortions to the spectra compared to derivitization, and does not affect the integrated intensities (*35*). Unfortunately, the choice of correct deconvolution parameters is subjective and has to be manipulated by the operator. If bandwidths are overestimated, this will result in the appearance of side lobes at the edges of absorption bands. On the other hand, if spectra are under-deconvolved, absorption bands will appear unaltered and

no additional information will be gained. Derivatization modifies bandshapes and the relative integrated intensities (*31*). Good quality spectra with high signal-to-noise ratios and low water vapor contributions are needed since these mathematical procedures enhance spectral noise (*31*). Ideally, the use of derivatives in conjunction with FSD is the best way to interpret FTIR spectra.

Deconvolution of two functions is defined as the division of their transforms according to the convolution theorem (*34*). The resolution enhancement factor (K) and half width at half height (HWHH, γ) are related by the following expression (*34*):

$$K = \gamma / (\gamma - \gamma') = A'_{peak}/A_{peak} \qquad \textbf{1.4}$$

where γ and γ' are the measured and deconvolved HWHH values, and A_{peak} and A'_{peak} the measured and deconvolved peak heights, respectively. K values commonly used are in the range of 1.5 to 2.5 (*34*). As the HWHH parameter is decreased, deconvolution of the spectrum is increased. On the other hand, as the K-factor is decreased, deconvolution of the spectrum is decreased (*37*).

FTIR spectra of proteins can be studied in D_2O instead of H_2O, which has several advantages. Since the O-^{2}H band (~1200 cm^{-1}) is shifted to longer frequency compared to the O-^{1}H band (1644 cm^{-1}), a spectral window free of water absorption in the amide I' region exists in D_2O. Discrimination between α-helices and unordered structures that overlap in H_2O (Table 1.1) is facilitated. Absorption of unordered structures in D_2O red-shift by 10 cm^{-1}, whereas α-helices only red-shift by 5 cm^{-1} (*31*). This is because amide protons in ordered structures like helices are not expected to exchange as readily as the more solvent-exposed protons in random structures (*37*).

The amide II mode (1500–1600 cm^{-1}) is due to N–H bending (60%) and C–N stretching vibration (40%) of the amide groups (*31*). The frequency of these bands depends on the strength of the H-bonds involving backbone C=O and N–H groups. Hydrogen/deuterium exchange can be monitored by following changes in the amide II band at 1550 cm^{-1}, which is dominated by N–H bending vibrations. N–H to N–D isotopic substitution results in a shift of the amide II band by ~100 cm^{-1}. A less dramatic shift (~10-14 cm^{-1}) is observed for the amide I mode, since it is mostly made up of C=O stretching (*32*). The extent of H/D exchange can be used to examine solvent accessibility of amide protons. As amide protons exchange, the integrated area of the amide II band decreases. Any residual amide II intensity corresponds to amide N–H groups that are involved in strong H-bonds and/or are buried within the hydrophobic core of the protein (*31*).

A major problem with studying protein chemical denaturation by FTIR spectroscopy is the reliability of the background subtraction procedure. A strong GdnHCl absorption band (~1675 cm^{-1}) interferes with the high frequency region of the amide I mode, and careful digital subtraction is required to remove this spectral contribution. Alternatively, isotopically labeled GdnHCl can be used to shift the denaturant's absorption out of the amide I window, which circumvents any subtraction problems. The isotopically labeled denaturants used in this study were Gdn-^{13}C-HCl and Gdn-d_5-DCl (in D_2O).

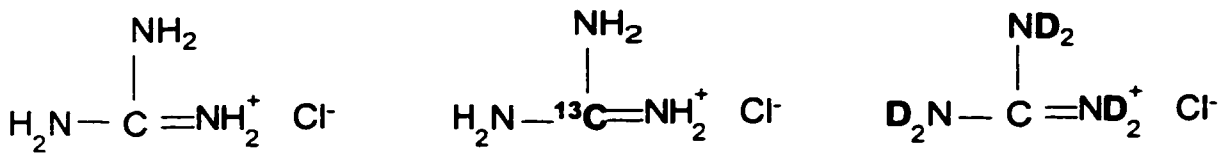

GdnHCl **Gdn-^{13}C-HCl** **Gdn-d_5-DCl**

Figure 1.3 Structures of isotopically labeled forms of GdnHCl.

The FTIR amide I spectra of the isotopic forms of GdnHCl are presented in Figure 1.4. The Gdn-^{13}C-HCl absorption (1652 cm^{-1}) is centered at the same frequency as the expected amide I α-helical absorption (Table 1.1). Therefore, it is the least desirable choice for FTIR-monitored denaturation studies. A ^{15}N-labeled denaturant is available, however labeling the denaturant with ^{13}C likely results in a much greater shift compared to ^{15}N, since the C–O contributions make up ~80% of the amide I, and C–N accounts for only ~20%. In D_2O, Gdn-d_5-DCl exhibits an absorption band at 1600 cm^{-1}, which is at the red-end of the amide I window and only slightly overlaps with the amide I′ mode. Thus, the Gdn-d_5-DCl isotopic form is the best choice for FTIR-monitored protein denaturation in GdnHCl.

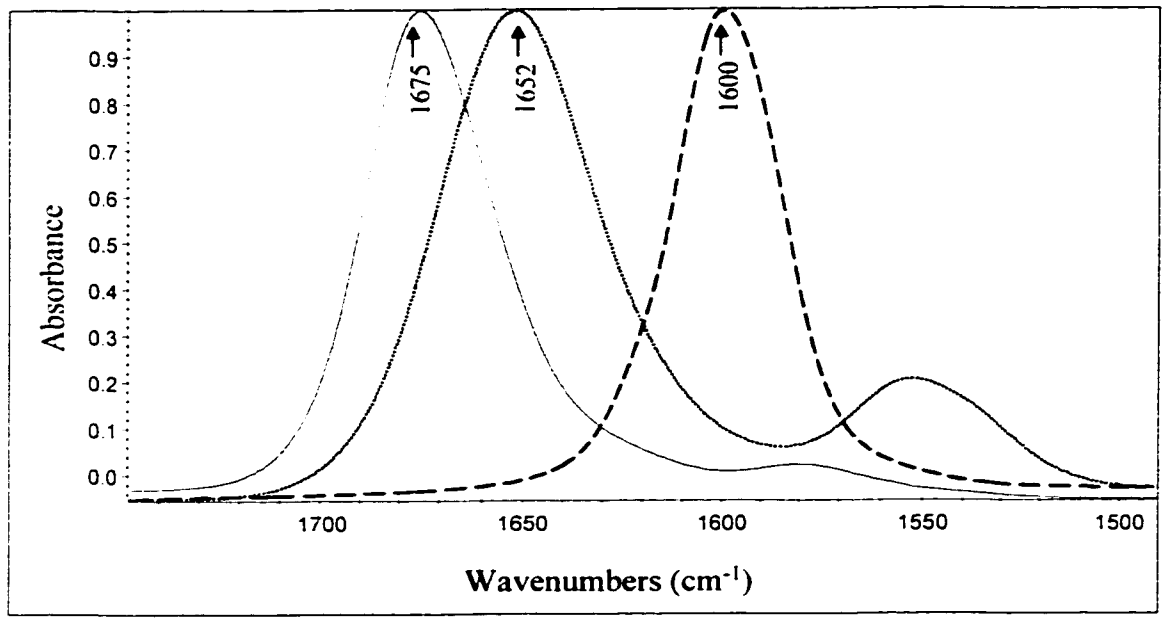

Figure 1.4 FTIR spectra of 3 M GdnHCl (solid line), Gdn-^{13}C-HCl (dotted line) and Gdn-d_5-DCl (dashed line) in 100 mM NaPi buffer (pH or pD 7.0). The spectra shown represent an average of 256 scans at a resolution of 2 cm^{-1}, acquired using CaF_2 windows with a 6 μM-pathlength.

FTIR offers many advantages for the characterization of protein structures. Subtle differences in structural forms in dynamic equilibrium can be detected due to the fast time scale of a vibration (10^{-12} – 10^{-13} s), which minimizes conformational averaging effects (*32*). FTIR absorption is sensitive to small changes in the protein's conformation, especially in the denatured state (*9*). The amide I band reports on all peptide C=O groups in the protein: therefore, in principle the unfolding of all parts of the protein can be monitored simultaneously (*7*). An entire spectrum can be recorded in about the same time required to observe one part of the spectrum by conventional spectroscopy (*43*). High quality data can be generated easily and rapidly with small amounts of protein in a variety of environments. Almost any physical state of a protein sample can be studied including aqueous or organic solutions, hydrated films, inhomogeneous dispersions and

solids (*31*). In addition, the FTIR spectrometer is inexpensive compared to X-ray diffraction, NMR and CD instruments (*32*).

Unfortunately, FTIR also has several pitfalls. Bulk secondary structure can be quantified, but not the precise location of a particular secondary structure within the primary sequence, due to low structural resolution (*9*, *7*). As discussed earlier, a major problem with aqueous protein solutions is the overlap of the amide I mode with strong absorptions from H_2O and GdnHCl. At high absorbance values, the response of the FTIR detector may be non-linear, which can result in distortion of band shapes and relative intensities of absorption (*31*). In addition, analysis of protein secondary structure in denaturants can be problematic. Assignment of secondary structural elements is based on empirical rules established from model proteins in aqueous solutions, but not in denaturants. Interaction of GdnHCl with the protein may shift characteristic amide I bands somewhat, and make assignments more difficult (*7*).

FTIR is complementary to many spectroscopic techniques such as NMR, CD and X-ray crystallography. NMR and FTIR spectroscopies are excellent techniques to use together. FTIR data is acquired on a fast time scale with low structural resolution, whereas NMR has a much slower time scale with a higher structural resolution (*31*). In NMR, the time scale is very long relative to FTIR and there are problems with structural averaging, *i.e.* one can not differentiate between rapidly interconverting structural forms (*36*). The FTIR spectrum is essentially a snapshot of the NMR time scale (*36*). The intensity of the Nuclear Overhauser effect (NOE) depends on the amount of time the chromophores are in contact. Therefore, short lifetimes result in weak NOEs, which may not be detected by NMR (*31*). Another disadvantage of using NMR is that spectra of

large proteins are very complex, therefore, applications are limited to small proteins (<20 kDa) (*33*). Protein size is not a problem in FTIR.

CD and FTIR spectroscopies are highly complementary techniques since the potential sources of error are not the same. These differences are due to the fact that CD spectroscopy monitors the protein backbone conformation, while FTIR spectroscopy is sensitive to the degree of H-bonding of the amide carbonyl groups (*31*). CD provides a better estimation of the α-helical content of a protein, whereas FTIR is preferred for the determination of sheets and turns (*35*). Therefore, both techniques used in conjunction provide useful information on secondary structure.

X-ray crystallography can be used to aid in the interpretation of FTIR results, since FTIR is limited by its low structural resolution (*31*). However, X-ray crystallography requires high quality single crystals, which may not be available for some proteins. Another major concern is that the static structure in a crystal may not be representative of a protein's conformation in solution or in living cells (*35*).

1.2.2 Circular Dichroism (CD) Spectroscopy

Circular dichroism is detected as the difference in absorbance (ΔA) or in ellipticity (θ) given by the following relationships (*1, 44*).

$$\Delta A = A_L - A_R \qquad \textbf{1.5}$$

$$\theta = 33\ \Delta A \qquad \textbf{1.6}$$

Where A_L is the absorption of left-handed circularly polarized light, A_R that of right-handed circularly polarized light and θ the observed ellipticity in degrees. Molar

ellipticity, [θ] can be converted to a differential molar CD extinction coefficient, Δε, and the numerical relationship between the two sets of units is (*1, 44*):

$$[\theta] = 3300\ \Delta\varepsilon \qquad \textbf{1.7}$$

where [θ] has units of deg•cm^2•dmol^{-1} and Δε has units of M^{-1}•cm^{-1}.

The CD spectrometer measures optical activity of an asymmetric molecule in solution (*1*). When a chromophore is part of an asymmetric system, left-handed and right-handed circularly polarized light are absorbed in varying amounts, and a CD signal is generated. The difference in absorbance of polarized light for proteins is typically in the range of 10^{-4} to 10^{-6} for a sample with a total absorbance of 1.0 (*1*). This difference in absorbance is very small, and hence it is possible to detect minor chromophoric modifications (*45*).

Proteins absorb light in the near- and far-UV CD regions. The near-UV region (250-300 nm) is made up of contributions from aromatic amino acids and disulfide bonds. Aromatic amino acids (Phe, Tyr and Trp) absorb between 250-290 nm, His absorbs at ~245 nm and disulfide bonds formed by Cys residues absorb from 240-290 nm (*44*). The overall fold of a protein, *i.e.* tertiary structure, causes the aromatic amino acid side chains to be in an optically active environment and generate a CD signal in the near-UV portion of the spectrum. Unfolded proteins, on the other hand, have an aromatic CD signal that is approximately zero (*1*). Individual peaks in the near-UV CD region can not be easily assigned to specific aromatic side chains since the signs, intensities and wavelengths depend on the local electronic environment of the asymmetric chromophores (*1*). However, the near-UV CD region can be utilized as a fingerprint tool to detect the presence of aromatic residues and disulfide bonds.

The far-UV CD or amide region (170-250 nm) is dominated by the absorption of peptide bonds, and is used to estimate the secondary structure of the protein. Differences in the peptide bonds associated with each secondary structure generate a distinct CD absorbance profile (*44*). Characteristic secondary-structure frequencies based on these CD patterns are summarized in Table 1.3. However, there are factors other than secondary structure, which contribute to the CD signal of a protein in the far-UV region, such as aromatic and sulfur-containing amino acid side chains.

Table 1.3: Correlation between protein secondary structure and far-UV CD absorbance

Secondary structure	Wavelength range (nm)	$\Delta\varepsilon$ (M^{-1} cm^{-1})
α-helices	193 208 222	+22 -10.5 -11.5
Antiparallel β-sheets	191-197 207-213	+2.5 to +5.0 -1.5 to +4.0
β-turns	198-202 208-212	+3.5 to +11.5 +3.5 to +6.5
3_{10} helices	190-198 210-220	-11.0 to -11.5 +3.0
Unordered structures	192-201 208-212	-11.0 to -14.5 -1.5 to +3.3

α-Helices display strong characteristic negative bands at 208 and 222 nm, which are easily recognized. Other secondary-structure absorptions, such as those due to sheets, turns and unordered structures are less intense and not as straightforward to assign. The following equations can be used to make a reliable estimate of the α-helical content of a protein (*44*), where $[\theta]_{208}$ and $[\theta]_{222}$ are the molar ellipticity values for α-helical bands at 208 and 222 nm, respectively.

$$\% \alpha\text{-helix} = \frac{[\theta]_{208} + 4000}{-29000} \times 100 \qquad \textbf{1.8}$$

$$\% \alpha\text{-helix} = \frac{[\theta]_{222} - 3000}{-39000} \times 100 \qquad \textbf{1.9}$$

The CD spectra of GdnHCl and Gdn-d_5-DCl are shown in Figure 1.5. The spectrum of GdnHCl (solid line) exhibits a major negative band at 198 nm accompanied by a shoulder at 199 nm and a band at 201 nm. The spectrum of Gdn-d_5-DCl (dashed line) reveals a major absorption at 197 nm with other bands at 202, 207 and 212 nm.

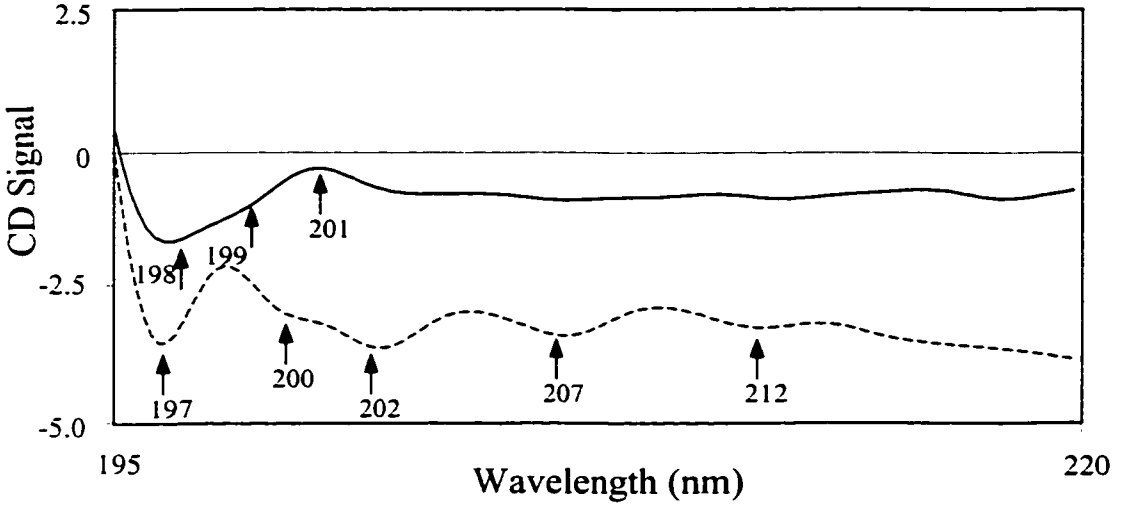

Figure 1.5 CD spectra of 3 M GdnHCl (solid line) and Gdn-d_5-DCl (dashed line) in 100 mM NaPi buffer (pH or pD 7.0). The spectra represent an average of 5 scans recorded using an FTIR cell (6-μM pathlength).

FTIR and CD spectroscopies are often used in conjunction as discussed in Section 1.2.1. CD is also complementary to NMR and X-ray crystallography, and it is less demanding than these techniques in terms of time and amount of sample required. CD can be used to examine the extent and rate of structural change in a protein's

conformation. Information on structure or the environment surrounding a particular chromophore (*44*) can be obtained. Additional information on CD theory and instrumentation is provided in references by Meyers (*44*) and Creighton (*1*).

1.2.3 Fluorescence Spectroscopy

Fluorescence emission of proteins originates from the aromatic residues, *i.e.* Trp, Tyr and Phe. Generally, fluorescence from Tyr and Phe aromatic amino acids is quenched by energy transfer to Trp, therefore steady-state fluorescence is dominated by Trp emission (*46*). In addition, excitation wavelengths for Trp are longer and quantum yields are much greater compared to any other aromatic amino acid, hence Trp is a good fluorescent probe (*1*). Intrinsic fluorescence from Trp residues is sensitive to the surrounding microenvironment and reports on localized structural changes.

The lifetime of the Trp fluorescence decay in heme proteins lies in the picosecond range, mainly due to the high efficiency energy transfer from the fluorescent donor to the heme acceptor (*47*). A single tryptophan residue in both HRP (Trp117) and cytochrome c (Trp59) can be used as a built-in fluorescent probe that is sensitive to the overall conformation and unfolding of the protein. In HRP, the Trp117 residue is located at a distance of ~1.2 nm from the heme center at neutral pH (*23*). In cytochrome c, the indole ring of Trp59 lies within 0.9 nm from the heme iron (*48*). Trp-heme energy transfer was used to study protein unfolding by fluorescence spectroscopy in this thesis.

In folded heme proteins, tryptophan fluorescence is almost completely quenched by energy transfer to the heme. Unfolding of the protein by adding denaturant results in increased fluorescence intensity due to an increase in the Trp-heme distance, and a

decrease in the efficiency of the energy transfer (*49*). The microenvironment surrounding the Trp is probed via shifts in the emission maximum. A red-shift from 320 to 350 nm is indicative of a change in Trp from a nonpolar (interior of the protein) to a polar (solvent-exposed) environment (*1*). Therefore, when a protein is denatured in GdnHCl, the Trp-heme distance should increase as well as the fluorescence intensity due to relief of heme quenching.

Fluorescence energy transfer to the heme group is the major mechanism that decreases fluorescence lifetimes in heme proteins. Förster's theory of resonance energy transfer (*47*) can be used to estimate the distance dependence of energy transfer:

$$E = \frac{R_o^6}{R^6 + R_o^6} \qquad \textbf{1.10}$$

where E is the efficiency of energy-transfer, R is the distance between the fluorescent donor and acceptor and R_o is the distance between these two groups when the energy-transfer efficiency is 50%. The energy-transfer efficiency is calculated using the distance between the centers of the fluorophore and acceptor. In heme proteins, the high efficiency of energy transfer results in picosecond decay lifetimes, which suppress all other deactivation pathways (*47*).

Fluorescence denaturation curves for a simple 2-state process between native (*N*) and denatured (D) forms: $N \rightleftharpoons D$ should have a sigmoidal shape. Since Trp can exist in only one of two states (hydrophobic or hydrophilic environment) depending on the denaturant concentration, 2-state behavior is typically observed (*23*). Additional information on fluorescence theory and instrumentation is given in the references by Skoog (*43*) and Creighton (*1*).

CHAPTER 2: INTERACTION OF GdnHCl WITH A RANDOM-COIL MODEL PEPTIDE: POLY-L-LYSINE

2.1 INTRODUCTION

In this chapter, the interaction of GdnHCl with poly-L-lysine (PLL) is probed by FTIR and CD spectroscopies. PLL is a basic polyelectrolyte of variable chain length determined by the number of Lys units (n) present (*50*).

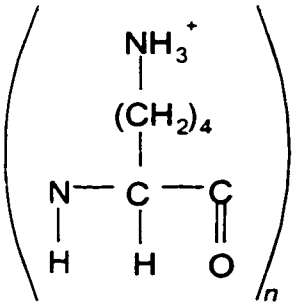

Figure 2.1 Structure of poly-L-lysine, where $n > 1$.

PLL can form three distinctly different secondary-structure conformations depending on the properties of the solution (*51*). Interconversion between structural forms occurs with changes in pH and heat. At neutral pH, PLL has protonated side chains and is in a random-coil conformation. In this state, repulsive forces between the charged side chains dominate over attractive ones (*51*). The α-helix form of PLL is induced by deprotonation in alkaline solution. The terminal ε-amino group has a pK_a of 10.0 to 10.3 (25°C, 0.1M KCl) (*52*), so that the lysyl side chain changes from positive to neutral when the bulk pH > 10, and deprotonation converts PLL to an α-helical conformation (*52*). For α-helices, a long-chain polypeptide is more stable than a short

one. The longer the chain, the lower the transition rates from α-helix to other secondary structures (*52*). Heating the α-helical conformation at alkaline pH generates the β-sheet form of PLL. As the pH is increased, the temperature required to induce an interconversion from α-helix to β-sheet is decreased. For example, at pH 10.6, the temperature must be raised to 43.5°C to yield a β-sheet, whereas at pH 11.9, interconversion occurs at 36.7°C as determined by differential scanning calorimetry (*53*).

The random-coil conformation of PLL is the most highly hydrated form (*54*). The surface of the α-helix is hydrated by 4-6 H_2O molecules per Lys residue (*54*). The β-sheet is the least hydrated structure, with less than 2 H_2O molecules per Lys residue (*54*).

PLL is a good peptide model system because of the ease of interconversion between its structural forms; however, only the random-coil conformation is studied in this chapter. Since it is speculated that GdnHCl preferentially interacts with random structures upon denaturation, it is advantageous to use a simple model system to understand the effects of denaturants on proteins. Homopolypeptides like PLL are not complicated by the occurrence of a variety of secondary-structural interactions that are found in heteropolypeptides.

However, PLL, a homopolypeptide, may not be an ideal model for proteins, which are heteropolypeptides. Researchers have observed lower than expected FTIR secondary-structure frequencies for PLL, which may be due to its high degree of regularity compared to proteins (*55*). For example, the α-helical band for PLL absorbs at ~ 1638 cm^{-1}, whereas protein α-helix absorption is usually between 1650-1655 cm^{-1} (*32*). Homopolypeptides are more hydrated than heteropolypeptides, which may contribute to

the decrease in their FTIR amide I frequencies (*55*, *56*). Also, the mixture of amino acids in proteins alters the H-bonding strength within secondary structures, and disrupts inter- and intra-chain coupling which occurs with homopolypeptides (*55*).

PLL was also chosen as a model peptide to gain further insight on the interaction of GdnHCl with cytochrome c. As discussed in Chapter 4, cytochrome c contains more lysine (Lys) residues than any other amino acid. The primary sequences of horse and tuna cytochromes c are comprised of 18% and 16% Lys residues (Table 4.1), respectively (*57*, *58*).

2.2 EXPERIMENTAL PROCEDURES

2.2.1 Materials

Poly-L-lysine hydrobromide (PLL, M_r 53,500 and 34,300 Da, same product number: P2636) was purchased from Sigma and used without further purification. All of the results shown in this chapter were obtained using PLL with a M_r of 53,500, however preliminary experiments were performed using PLL with a M_r of 34,300. Both lots were assumed to have similar structures according to the FTIR spectra shown in Figure 2.2, where only a small shift of the amide I maxima is observed.

Guanidine hydrochloride (GdnHCl, 99+%, Sigma, FW 95.53), guanidine-d_5-deuteriochloride (Gdn-d_5-DCl, 98%D, Aldrich, FW 101.58) and ^{13}C-labeled GdnHCl (Gdn-^{13}C-HCl, 99%, Isotech Inc., FW 96.53) were used as chemical denaturants. Results with ^{13}C-labeled GdnHCl are not shown in this chapter. Phosphate buffers (pH and pD 7.0) were prepared by dissolving 100 mM phosphate salts ($Na_2HPO_4 \cdot 7H_2O$ and $NaH_2PO_4 \cdot H_2O$ from Fisher) in distilled H_2O with a specific resistance of 18.2 MΩ from

Barnsted nanopure system or in D_2O (99.9%, ICN Biomedicals). All solutions were prepared in a 100 mM sodium phosphate buffer. PLL stock solutions of known concentration were prepared by weight and diluted to the desired final concentration with buffer and the appropriate amount of denaturant.

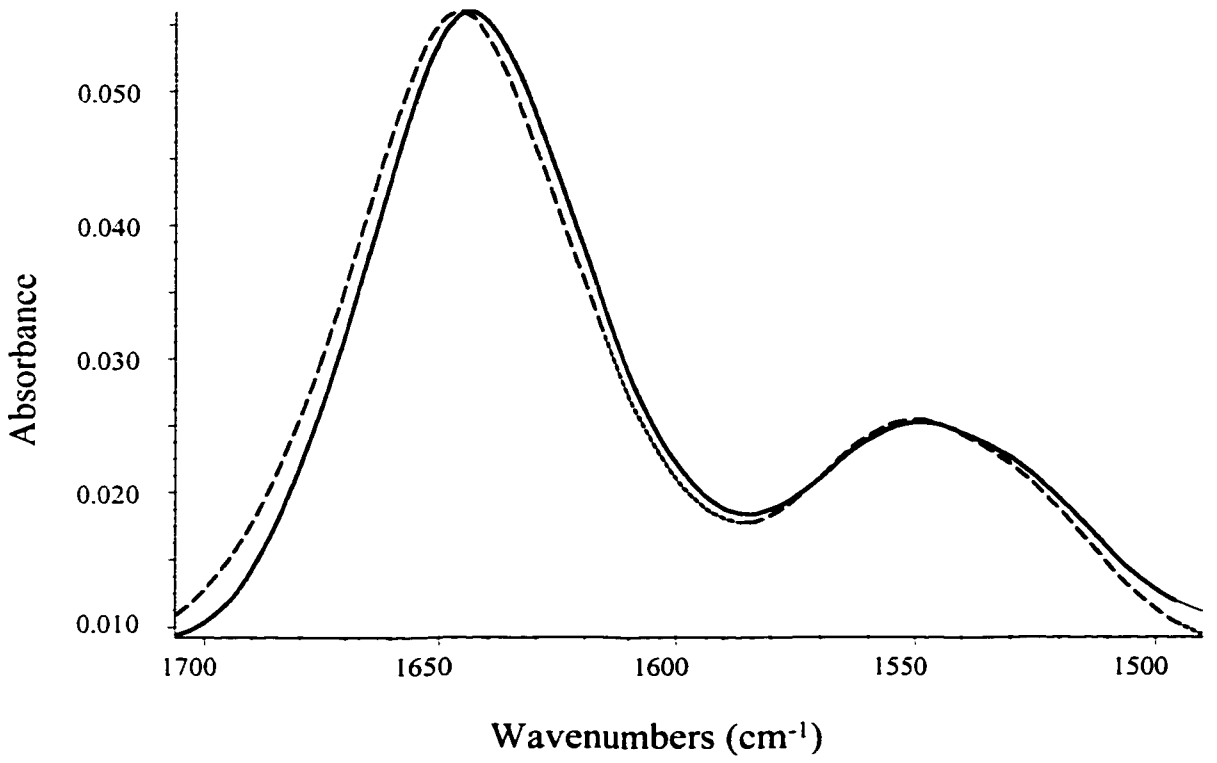

Figure 2.2 FTIR spectra of the amide I and II modes of 25 mg/mL PLL (in 100 mM NaPi buffer, pH 7, H_2O,) with a M_r of ~54 kDa (solid line) and ~34 kDa (dashed line). The FTIR spectra shown represent an average of 256 scans at a resolution of 2 cm^{-1}, acquired using CaF_2 windows with a 6-μM pathlength.

2.2.2 Methods

CD spectroscopy

CD experiments were performed on a Jasco 710 spectropolarimeter purged with nitrogen at a flow rate of ~5 L/min. All CD spectra recorded in the far-UV region (195-250 nm) were acquired using an *FTIR cell* mount thermostated at 25°C (as described in the FTIR section). Initially, baselines in the CD spectra were shifted slightly due to variation in the position of the FTIR cell in the CD instrument. This was solved by adding brackets in the CD instrument to fix the FTIR cell in place. The sampling conditions used with the FTIR cell (CaF_2 windows) are contrasted to those used with a conventional CD cell (fused quartz) in Table 2.1 below (*31, 44*). The use of an FTIR cell to acquire CD data is a novel technique, which has not been reported in the literature, and has several advantages. FTIR and CD are complementary techniques and the spectra can be recorded on the same day with the same sample, hence identical concentration and pathlength are used.

Table 2.1: Experimental conditions to acquire far-UV CD data with the FTIR *vs* CD cell

Type of cell	Concentration	Volume (μL)	Pathlength (cm)
CD cell	0.050 - 1.0 mg/mL (μM range)	200	0.01 - 0.1
FTIR cell	20 - 50 mg/mL (mM range)	7	0.006

Spectra were generated at a speed of 50 nm/min with a response time of 0.5 sec. All the CD spectra shown represent an average of 5 scans at a 0.2-nm resolution and a bandwidth of 1 nm. A PLL stock solution was diluted to 25 mg/mL (~0.5 M) with buffer and the desired amount of denaturant. Spectra were recorded using an FTIR cell, which

was assembled as described in Section 2.2.2. Absorption of the blank (GdnHCl in buffer) was subtracted from the PLL sample and the final spectra were smoothed with Jasco software. The observed ellipticity (θ, mdeg) was converted to molar ellipticity (*1*, *44*) using equation 2.1, where M_r is the molecular weight, [θ] the molar ellipticity ($deg \cdot cm^2 \cdot dmol^{-1}$), *c* the concentration and *l* the cell pathlength in cm.

$$[\theta] = \frac{Mr \bullet \theta}{10 \bullet l \bullet c} \qquad \textbf{2.1}$$

FTIR spectroscopy

FTIR spectra were recorded using a Nicolet Magna-IR 550 spectrophotometer Series II equipped with a deuterated triglycine sulfate (DTGS) detector purged with dry air from a Whatman model 75-52 FTIR purge-gas generator. Data were acquired and processed using Omnic software. Samples (7.0 μL) were placed in a thermostated FTIR cell mount (Harrick Inc.), in between two CaF_2 windows (13 x 2 mm, Wilmad Inc.) separated by a 6-μM Teflon spacer (Harrick Inc.). The FTIR cell was taken apart and reassembled for each use in order to clean the windows and add the new sample. A small pathlength was needed to maximize the energy through the sample due to high absorption from the background (H_2O and GdnHCl) (*40*). The FTIR cell temperature was maintained at 25°C by an Omega CN8500 temperature controller. It was critical to record the spectrum of the sample and background at the same temperature due to the strong dependence of H_2O absorption on temperature (*31*). All spectra represent an average of 256 scans recorded at a resolution of 2 cm^{-1} using Happ-Genzel apodization with an aperture of 69.

The final concentration of PLL in each sample was 25 mg/mL (~0.5 mM) diluted from a stock solution with buffer and the required amount of denaturant. Contributions from water and denaturant were removed from the raw spectrum using the subtraction procedure of Dong *et al.* (*40*, *41*) given below. This procedure was also used for experiments with isotopically labeled denaturants.

i. A background spectrum of GdnHCl in buffer was subtracted from that of the protein sample with the same concentration of GdnHCl, to obtain a straight baseline from 1750-2000 cm^{-1}.

ii. The subtraction factor in step (i) was adjusted using Omnic software to compensate for any changes in pathlength (e.g. the FTIR cell was reassembled after each use), such that a smooth amide I/II region was obtained with no discontinuities. It is critical to maintain the amide I/II peak heights for the denatured protein as close as possible to the ratio for the native form.

iii. A water vapor spectrum was subtracted from the result in step (i). This water vapor spectrum was generated by recording the FTIR spectrum of buffer twice (using the same sample). These two spectra (Ref-1 and Ref-2) should be identical except for small time-dependent changes in the water-vapor intensity that occur on continuous purging of the sample compartment with dry air. The resulting difference spectrum (Ref-1 – Ref-2) represents water vapor only.

iv. The resulting spectrum was smoothed with a nine-point Savitsky-Golay algorithm using Omnic software.

Careful subtraction of the water vapor is very important since if it is not performed correctly, artifacts may appear in the spectrum upon Fourier-self deconvolution or

derivative analysis (*40*). Over- and under-subtraction of the denaturant may affect the intensity and identity of the components in the amide I region.

2.3 RESULTS

2.3.1 FTIR background subtraction

Reliable subtraction of water (liquid and vapor) and GdnHCl background absorptions from the sample absorption is very important in the study of protein denaturation by FTIR spectroscopy. The subtraction steps and criteria used are outlined in Section 2.2.2. Intentional over- and under-subtraction of the denaturant from the protein was performed to observe the effects of incorrect background subtraction. Bowler *et al.* (*9*) performed a similar study and found that if background subtraction was not carried out correctly, a doubled peak in the amide I region would be observed, or one with a concave discontinuity. The effect of water vapor on the FTIR amide I spectrum was also examined here.

The first subtraction step involves removing the contribution of GdnHCl from the protein sample (with the same concentration of GdnHCl), while maintaining a straight baseline between 1750 – 2000 cm^{-1}. Figure 2.3 illustrates the effects of over- and under-subtraction of GdnHCl. Incorrect subtraction alters the baseline as well as the intensity of the amide bands. In frame A, an over-subtracted spectrum (dashed line) is compared to a correctly background-subtracted spectrum (solid line). As illustrated, over-subtraction of GdnHCl yields a non-linear, negative sloping baseline with a shifted amide I band maximum (*9*). In addition, the amide I/II ratio is lowered from ~1.8 to ~1.4, which is lower than the value for PLL in buffer (~2.0), and violates the criterion given in

step ii of Section 2.2.2. Under-subtraction, illustrated in frame B, results in the opposite effects, *i.e.* a positive baseline and a higher amide I/II ratio (~2.3). In addition, the amide I band is broader in the under-subtracted spectrum and the band maximum shifts from 1660 to 1667 cm^{-1}.

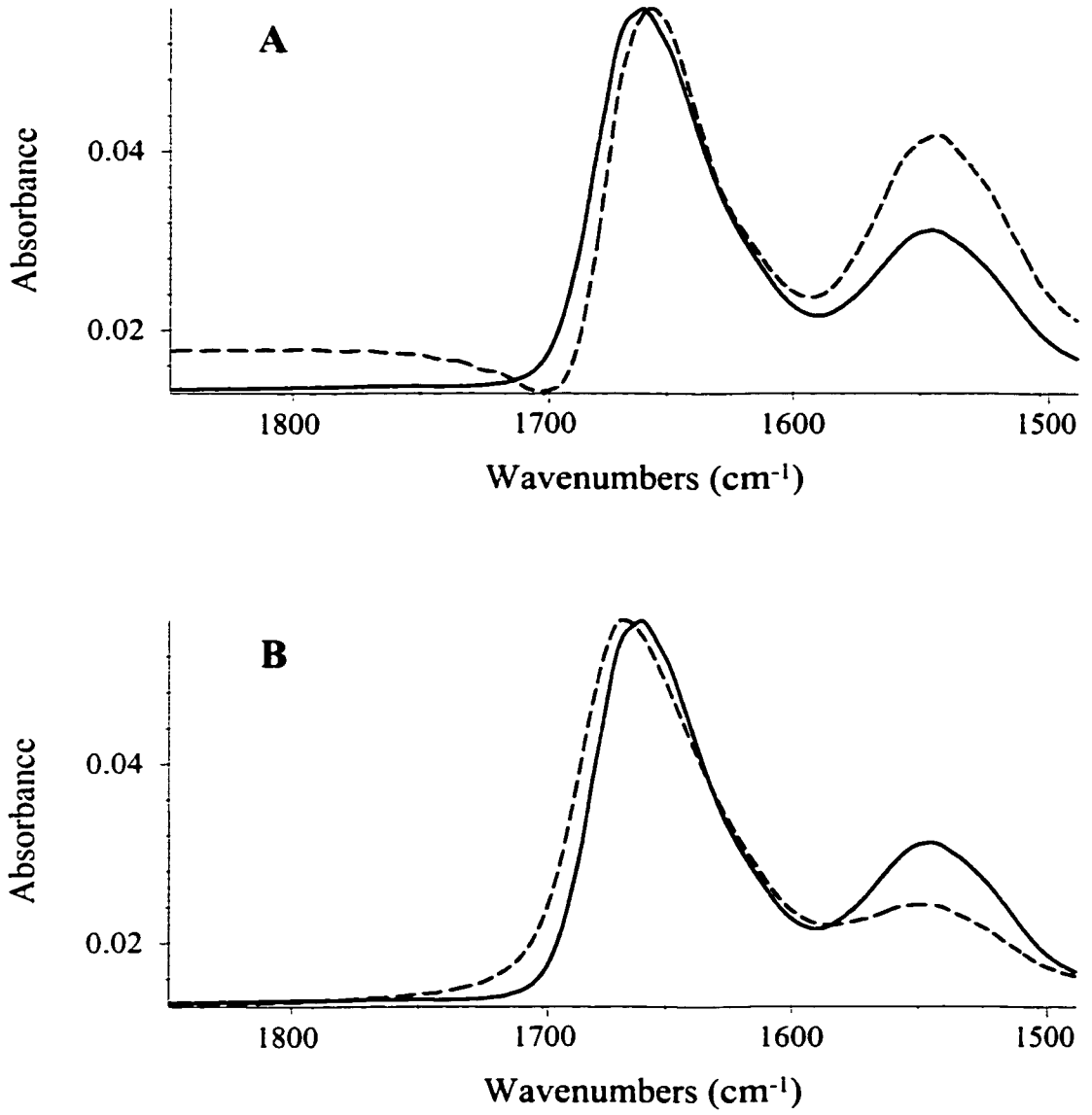

Figure 2.3 FTIR spectra of intentional (A) over- and (B) under-subtraction (dashed lines) of 3 M GdnHCl background from 25 mg/mL PLL in 3 M GdnHCl (in 100 mM NaPi buffer, pH 7, H_2O). These spectra are compared to correctly subtracted spectra (solid lines). The FTIR spectra shown represent an average of 256 scans at a resolution of 2 cm^{-1}, acquired using CaF_2 windows with a 6-μM pathlength.

Since the FTIR cell was disassembled and reassembled for filling (Section 2.2.2), the pathlength varied slightly for each sample. Adjustment of the subtraction factor (SF) using Omnic software compensated for pathlength differences between the sample and the background. For example, in Figure 2.3 frame A, the over-subtracted spectrum has an SF of 0.982, whereas the under-subtracted spectrum in frame B has an SF of 0.940. Thus, increasing the SF, or the degree of subtraction, produces a negative baseline, a red-shift in the amide I band maximum and a decrease in the amide I/II ratio.

Subtraction of water vapor is a key step, since incorrect subtraction may lead to artifacts and enhancement of spectral noise upon Fourier self-deconvolution (FSD) or second-derivative analysis (*31*, *40*). A spectrum can be judged to be virtually water-vapor free, if there are no sharp absorptions (spikes) between 1700 and 1800 cm^{-1} (*31*). For example, in Figure 2.4 frame A, the FTIR spectrum of PLL in buffer (after the buffer absorption has been subtracted out) is shown *prior* to water-vapor subtraction. As illustrated, if gaseous water is not removed, the resulting spectrum is noisy, and FSD or derivative analysis will not be possible. The spectrum of water vapor alone is presented in frame B. The spikes in the PLL spectrum in frame A line up with those in frame B. The smoothed spectrum *after* water-vapor subtraction (spectrum A – spectrum B) is shown in frame C.

The study of proteins and peptides in aqueous solutions is simplified by switching to D_2O and Gdn-d_5-DCl. This shifts the strong absorption of water and denaturant out of the amide I window, as explained in Section 1.2.1.

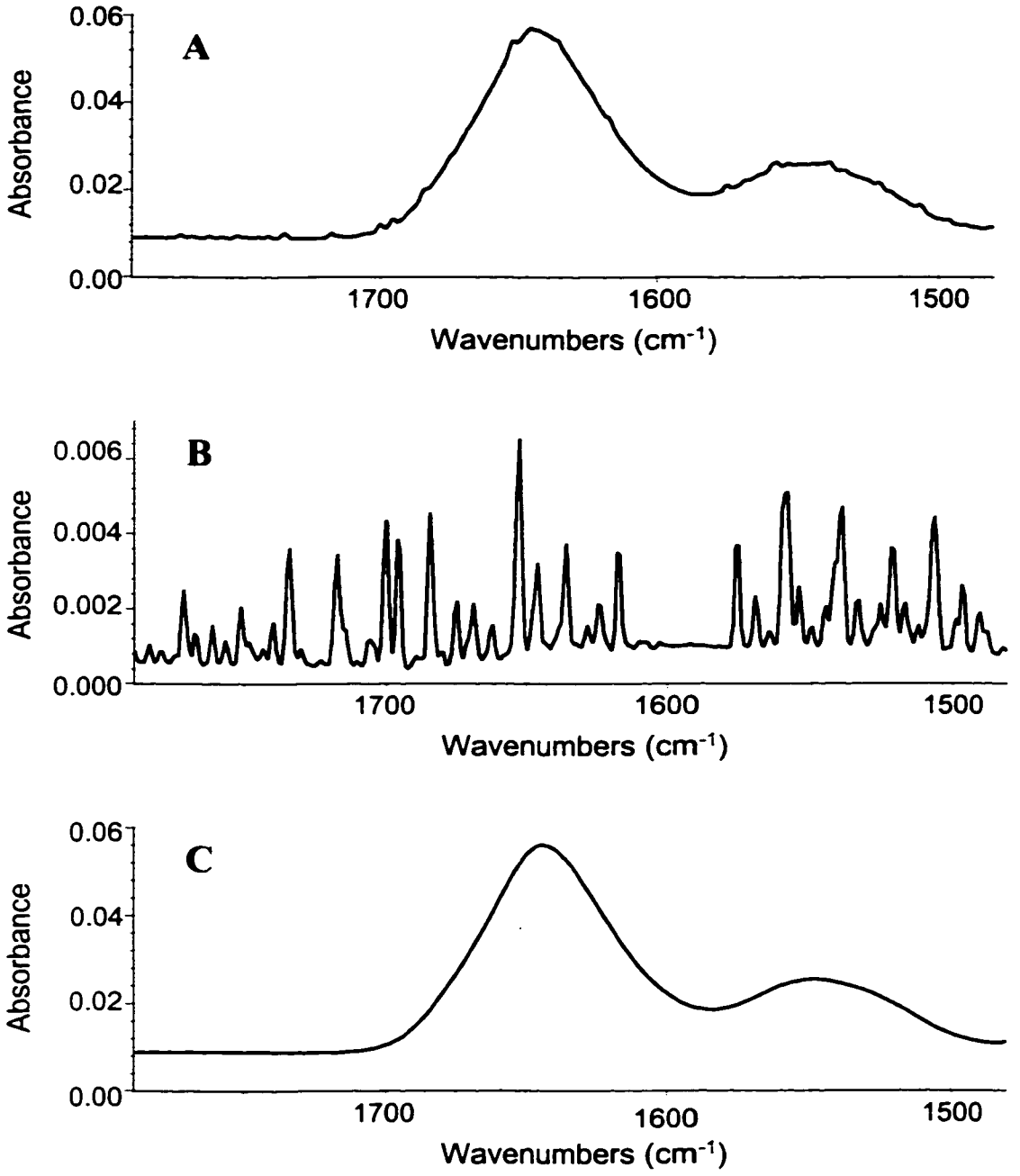

Figure 2.4 FTIR spectra to illustrate the effects of water vapor subtraction. The spectra represent an average of 256 scans at a resolution of 2 cm^{-1}, acquired using CaF_2 windows with a 6-μM pathlength. (A) 25 mg/mL PLL in 100 mM NaPi buffer (pH 7, H_2O) ***before*** water vapor subtraction, (B) water vapor spectrum (Ref-1 Ref-2, see Section 2.2.2) and (C) spectrum of PLL in buffer ***after*** water vapor subtraction, *i.e.* spectrum A spectrum B.

2.3.2 FTIR and CD analysis of the interaction of GdnHCl with PLL in H_2O

FTIR spectroscopy

PLL exists as a random coil in aqueous solution at neutral pH, and gives rise to an FTIR amide I absorption centered at 1644 cm^{-1}. Typically, random structures derived from proteins show an absorption maximum between 1640 and 1648 cm^{-1}. Any differences in absorption between proteins and PLL can be attributed to a higher degree of solvent-protein interaction or distortion of structural elements in homopolypeptides (*31*). The FTIR amide I spectra of PLL in buffer (pH 7) and in 3 M GdnHCl are presented in Figure 2.5. The sample absorbs at 1644 cm^{-1} in buffer, and at 1660 cm^{-1} in 3 M GdnHCl.

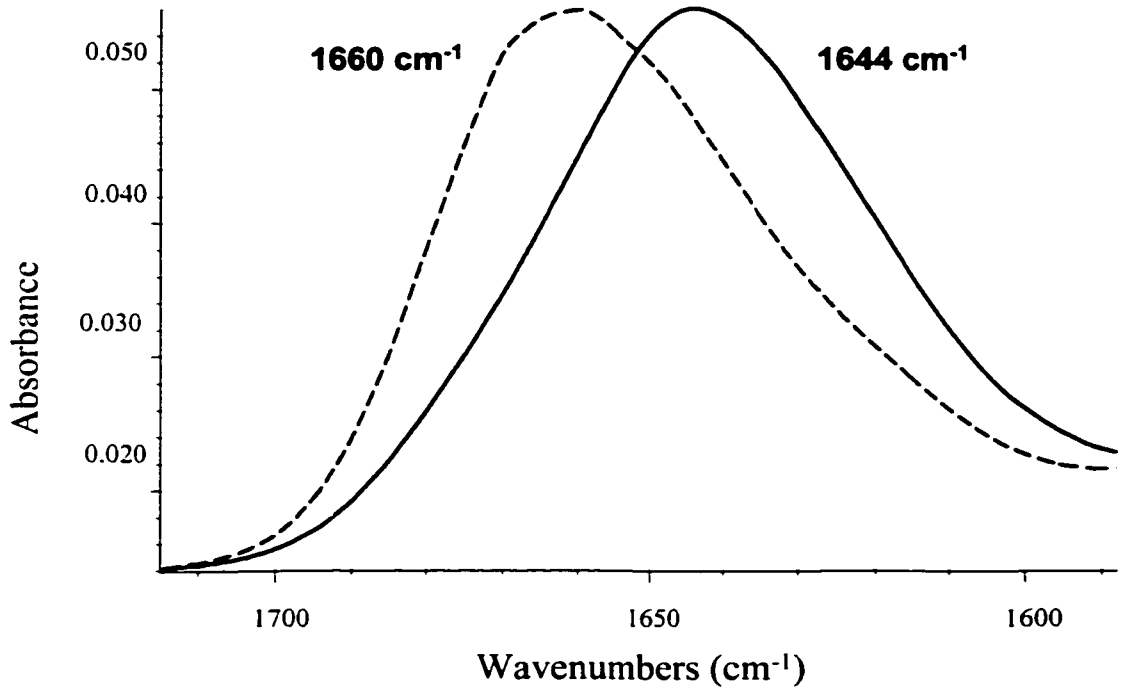

Figure 2.5 FTIR amide I region of 25 mg/mL PLL in 100 mM NaPi buffer, pH 7, H_2O (solid line) and in 3 M GdnHCl in buffer (dashed line). The FTIR spectra shown represent an average of 256 scans at a resolution of 2 cm^{-1}, acquired using CaF_2 windows with a 6-μM pathlength.

Stacked spectra of the FTIR amide I and II regions in 0-3 M GdnHCl are shown in Figure 2.6. As the concentration of GdnHCl increases, the absorption gradually blue-shifts from 1644 to 1660 cm^{-1}. In 1.0 and 1.5 M GdnHCl, the amide I is broad and asymmetric with maxima at ~1644 and 1675 cm^{-1}. In 2-3 M GdnHCl, the amide I band sharpens with a major absorption at 1660 cm^{-1}. As seen in Figure 1.4, GdnHCl absorbs at 1675 cm^{-1}; therefore, the band at 1660 cm^{-1} is an intermediate band between the absorptions of PLL (1644 cm^{-1}) and GdnHCl (1675 cm^{-1}). It is speculated that the 1660 cm^{-1} band contains absorption due to PLL-associated GdnHCl. GdnHCl from *bulk* solvent can be subtracted from the spectrum, but not when it is associated with the polypeptide.

Parameters (band maximum, integrated intensity, relative integrated intensity and half-width at half-height; HWHH) for the FTIR absorption in the amide I region *vs* GdnHCl concentration were measured using Omnic software, and listed in Table 2.2. The integrated intensities vary slightly with increasing concentration of GdnHCl, and appear to be less than in the native form. Generally, as the concentration of GdnHCl was increased, the HWHH increased as well. Therefore, the observed band broadening may be attributed to associated GdnHCl. The amide I band for PLL in 3 M GdnHCl appears sharper than in 1-2.5 M GdnHCl, which could suggest that changes in the PLL-GdnHCl interaction occur between 2.5 and 3 M GdnHCl. However, errors in bulk GdnHCl subtraction may attribute to the aforementioned observed spectral changes.

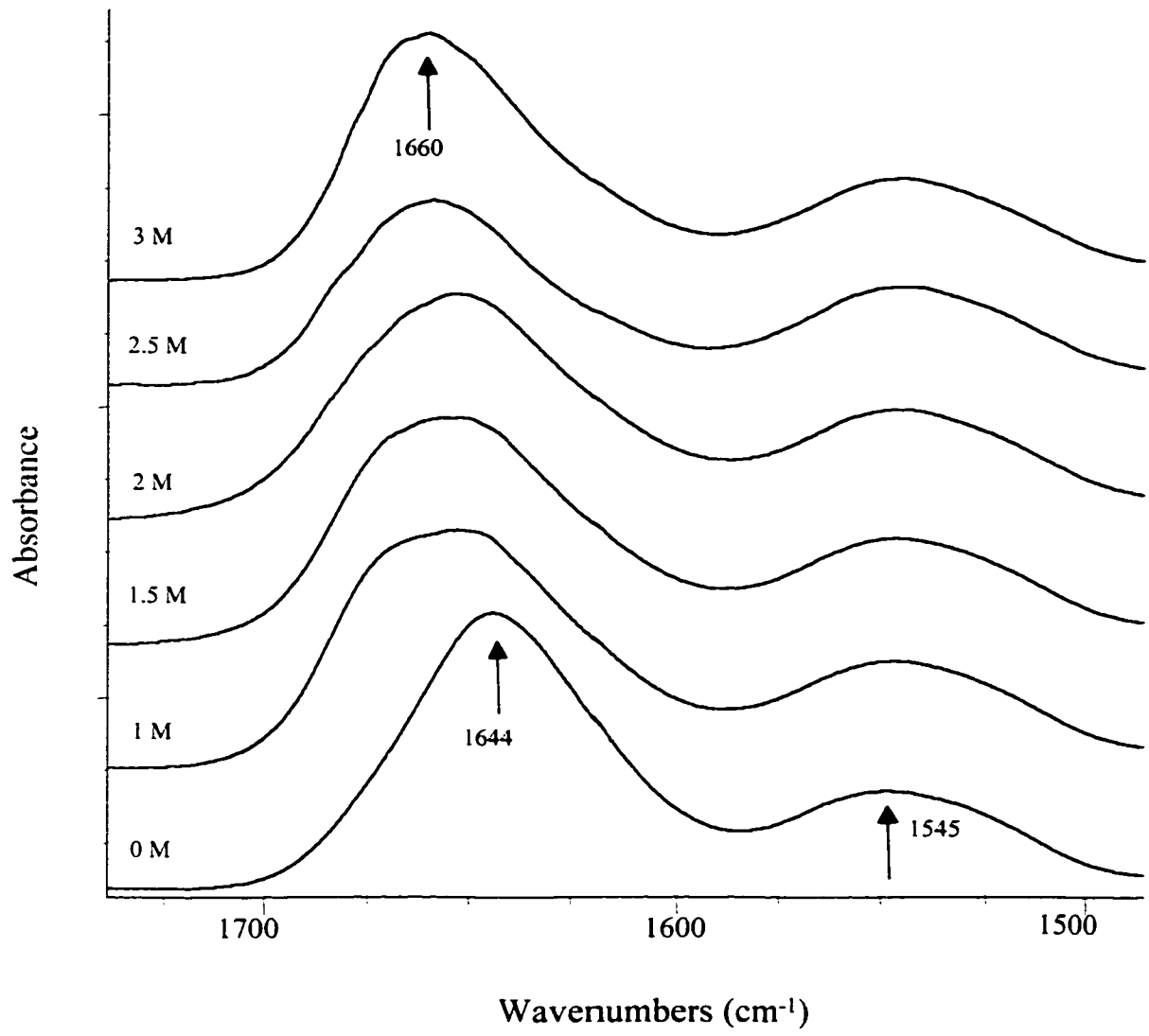

Figure 2.6 FTIR amide I and II modes of 25 mg/mL PLL in 0-3 M GdnHCl (in 100 mM NaPi buffer, pH 7, H_2O). The FTIR spectra shown represent an average of 256 scans at a resolution of 2 cm^{-1}, acquired using CaF_2 windows with a 6-μM pathlength.

Table 2.2: Parameters for FTIR absorption in the amide I region *vs* GdnHCl concentration

[GdnHCl] (M)	Amide I maximum (cm^{-1})	Integrated intensity	Relative integrated intensity (%)	HWHH (cm^{-1})
0	1644	2.19	100	25.1
1.0	1653 1668	2.21	101	34.7
1.5	1653 1668	2.08	95	35.2
2.0	1653	2.01	92	36.6
2.5	1660	1.87	85	37.6
3.0	1660	1.99	91	27.5

CD spectroscopy

The CD spectra of PLL in buffer (H_2O) and GdnHCl were also examined. PLL in the absence of denaturant gives rise to a negative CD band at 198 nm with a shoulder at 202 nm as illustrated in Figure 2.7. The empirical rules for random structure of proteins predict a large negative CD signal from 192 to 201 nm (*44*). The CD spectra of PLL in 3 and 4 M GdnHCl are also shown in Figure 2.7. A strong negative band is observed at 201 nm as well as a minor band at 205 nm in 3 M GdnHCl, while in 4 M GdnHCl, a broad band centered at 200 nm with a shoulder at 201 nm is observed.

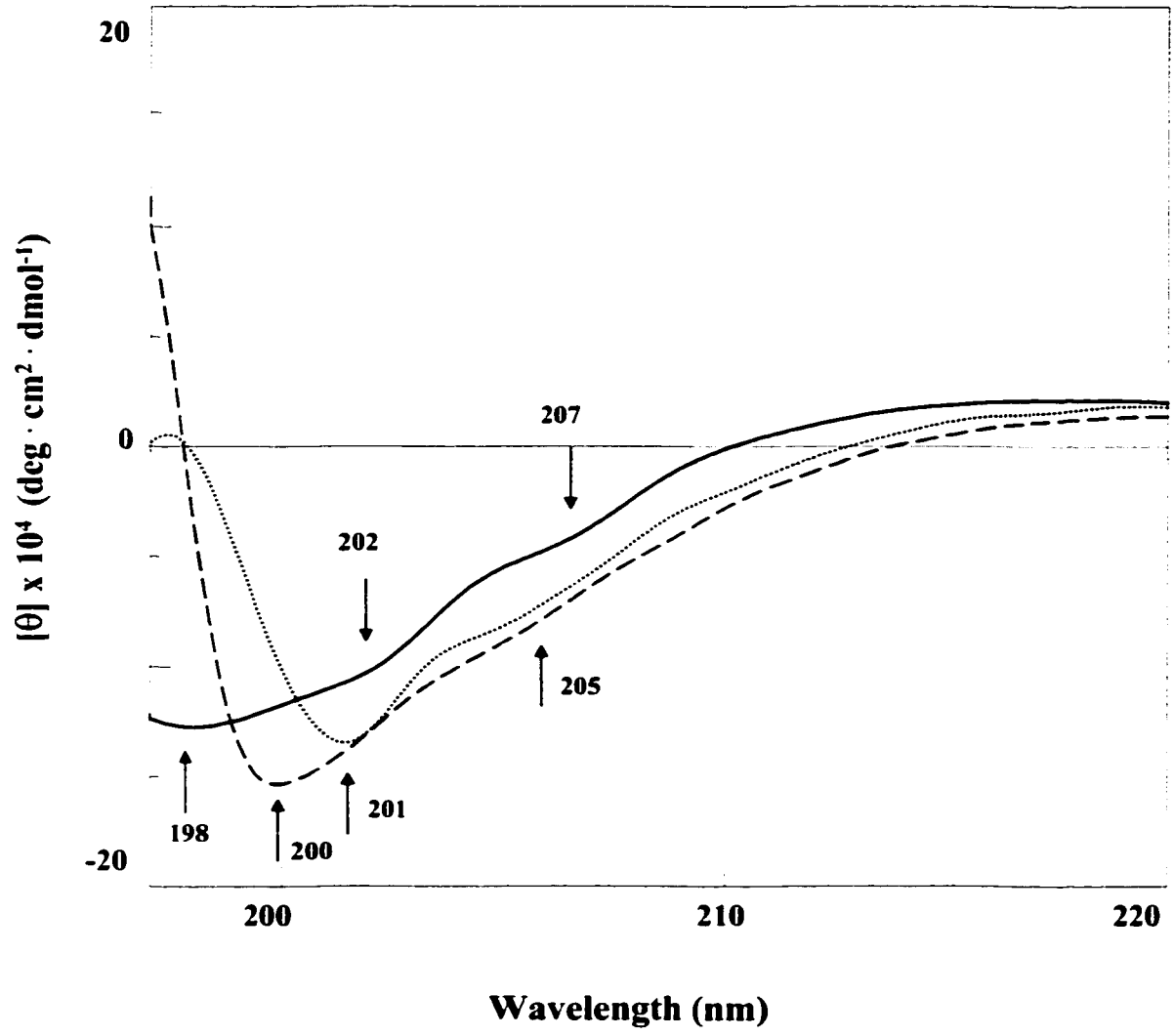

Figure 2.7 Far-UV CD spectra of 25 mg/mL PLL in 100 mM NaPi buffer, pH 7, H_2O (solid line), 3 M GdnHCl (dotted line) and 4 M GdnHCl (dashed line). The CD spectra represent an average of 5 scans at a resolution of 0.2-nm, recorded using an FTIR cell (6-μM pathlength) as described in Section 2.2.2.

Stacked CD spectra of PLL in GdnHCl are presented in Figure 2.8. These reveal that there is little change in the CD absorption in 0 – 2 M GdnHCl. However, between 2.5 and 4 M GdnHCl, the far-UV absorption varies significantly. The 198-nm band, which is present from 0 to 2.5 M GdnHCl, disappears in 3 M GdnHCl, and a 201-nm

band becomes prominent. A strong asymmetric band at 200 nm is observed for PLL in 4 M GdnHCl. Interestingly, this 200-nm band is coincident with the GdnHCl absorption band.

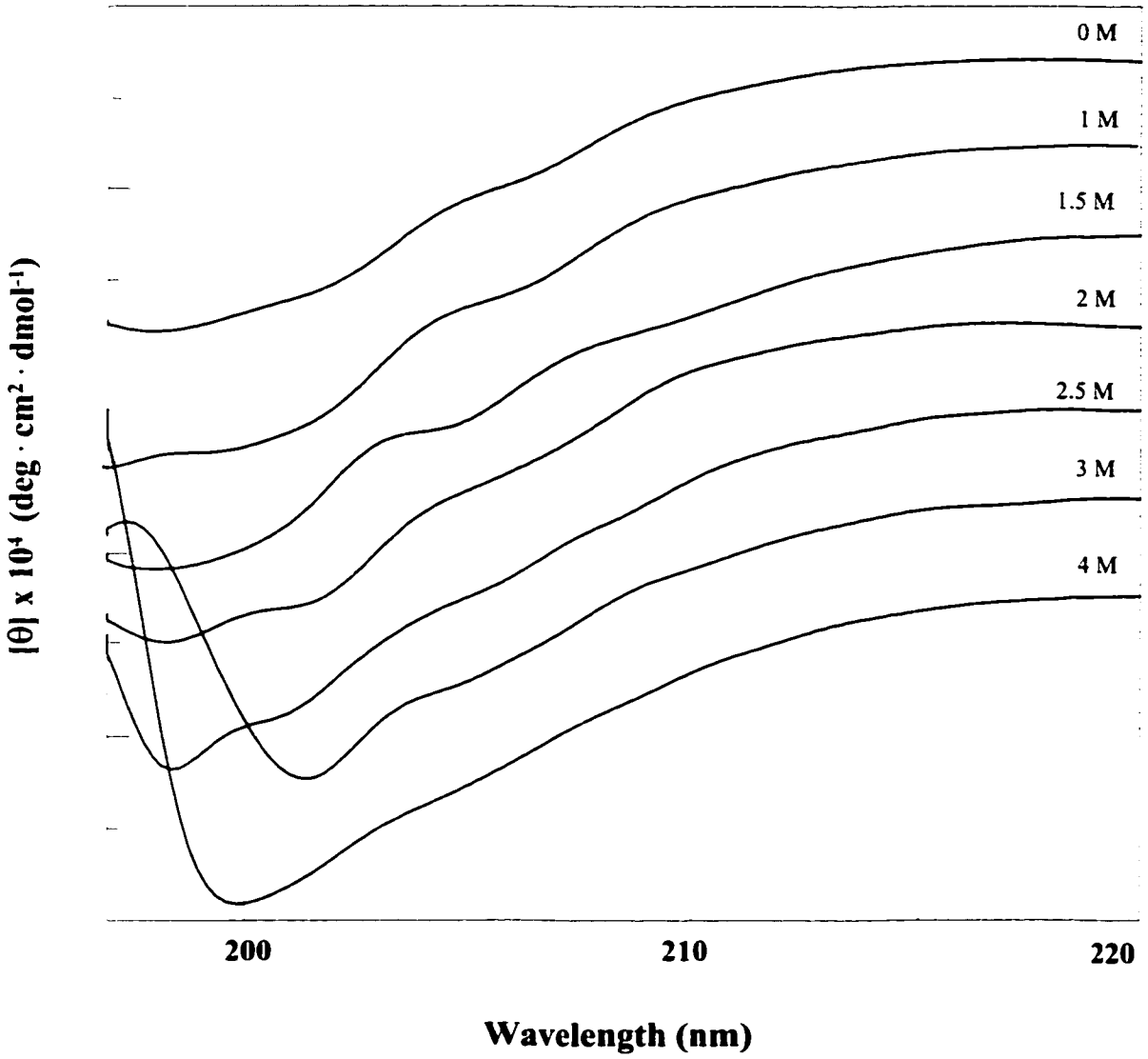

Figure 2.8 Far-UV CD stacked spectra of 25 mg/mL PLL in 0-4 M GdnHCl (in 100 mM NaPi buffer, pH 7, H_2O). The CD spectra represent an average of 5 scans at a resolution of 0.2-nm, recorded using an FTIR cell (6-μM pathlength) as described in Section 2.2.2.

2.3.3 FTIR and CD analysis of the interaction of Gdn-d_5-DCl with PLL in D_2O

FTIR spectroscopy

Both H_2O and GdnHCl (Figure 1.4) have strong absorptions in the amide I region with maxima at 1644 and 1675 cm^{-1}, respectively. If D_2O is used instead of H_2O, the water absorption is red-shifted from 1644 to 1200 cm^{-1}. Gdn-d_5-DCl (Figure 1.4) absorbs at 1600 cm^{-1}, which is at the red-limit of the amide I'. The FTIR spectra of PLL in buffer and in 3 M Gdn-d_5-DCl are presented in Figure 2.9. PLL in D_2O has the same absorption maximum (1644 cm^{-1}) as previously seen in H_2O, which is somewhat surprising given the expected red-shift in random-coil absorption in D_2O compared to H_2O (Section 1.2.1). The spectrum of PLL in 3 M Gdn-d_5-DCl reveals bands at 1644 and 1622 cm^{-1}.

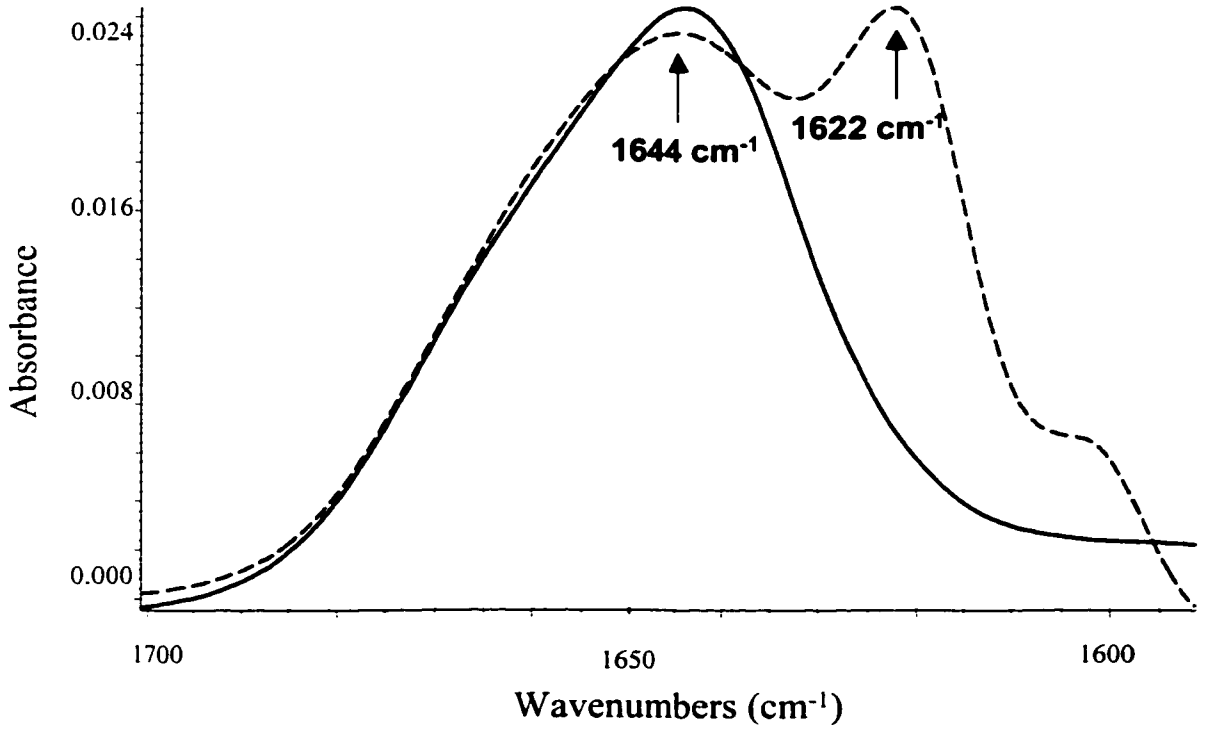

Figure 2.9 FTIR amide I' of 25 mg/mL PLL in 100 mM NaPi buffer, pD 7, D_2O (solid line) and in 3 M Gdn-d_5-DCl (dashed line). The FTIR spectra shown represent an average of 256 scans at a resolution of 2 cm^{-1}, acquired using CaF_2 windows with a 6-μM pathlength.

Stacked spectra of FTIR amide I' and II' modes of PLL in 0–3 M Gdn-d_5-DCl are shown in Figure 2.10. As the concentration of Gdn-d_5-DCl increases, the intensity of the amide band at 1622 cm^{-1} increases. Even in 1 M Gdn-d_5-DCl, a shoulder at 1622 cm^{-1} is observed.

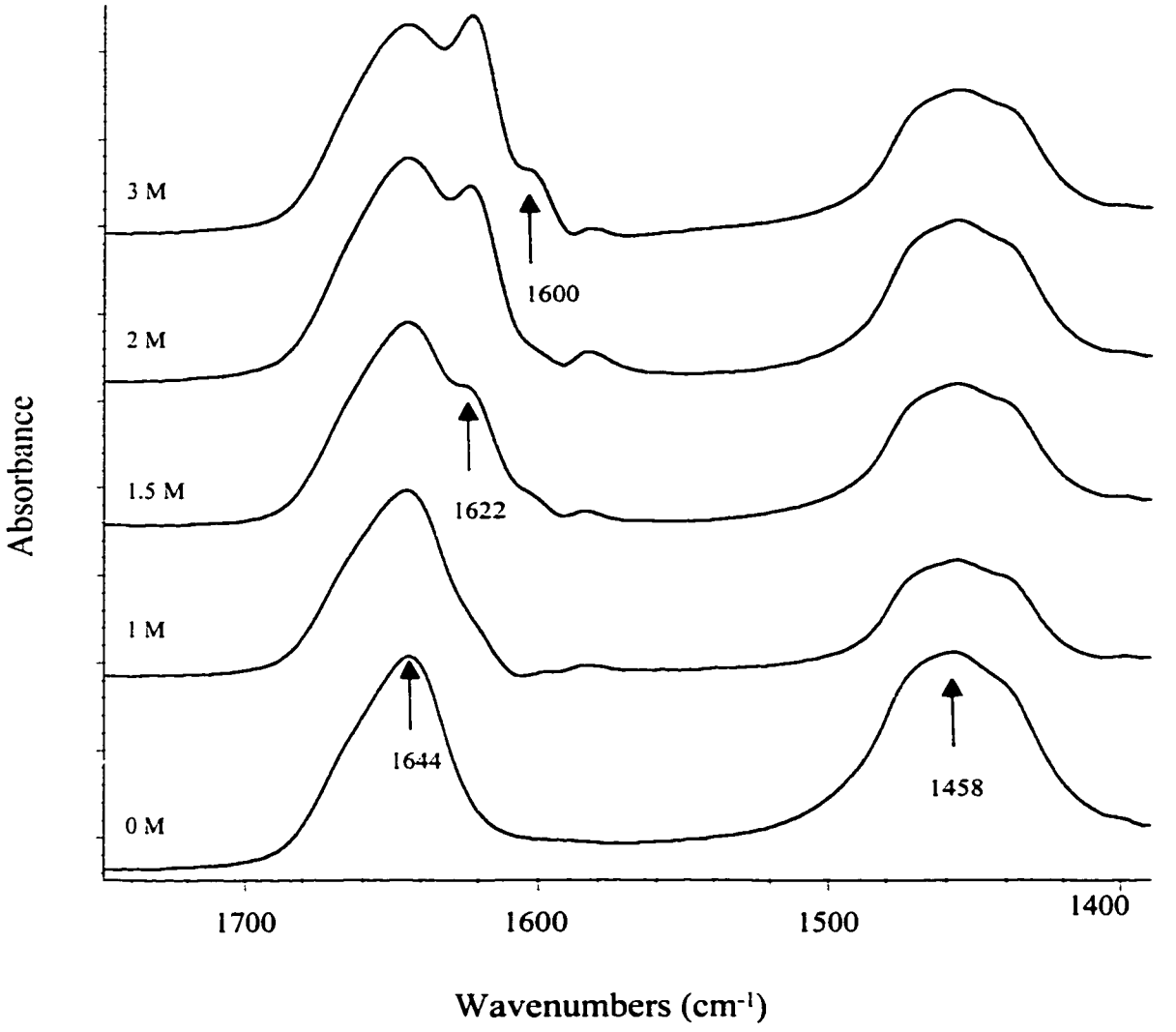

Figure 2.10 FTIR amide I' and II' modes of 25 mg/mL PLL in 0-3 M Gdn-d_5-DCl (in 100 mM NaPi buffer, pD 7, D_2O). The FTIR spectra shown represent an average of 256 scans at a resolution of 2 cm^{-1}, acquired using CaF_2 windows with a 6-μM pathlength.

Spectral parameters, *i.e.* band maximum, integrated intensity, relative integrated intensity and half-width at half-height (HWHH) for the FTIR absorptions in the amide I' region *vs* concentration of Gdn-d_5-DCl are listed in Table 2.3. As the concentration of Gdn-d_5-DCl is increased, the HWHH of the amide I' band increased as well. The total intensity in the amide I' region (1700-1600 cm^{-1}) was integrated using Omnic peak area tool. The area of PLL in buffer was assumed to be 100%, and the relative intensities in Gdn-d_5-DCl are tabulated below. The significant increase in area in 1.5 M Gdn-d_5-DCl is coincident with the appearance of a band at 1622 cm^{-1} in Figure 2.10. Overall, as the concentration of Gdn-d_5-DCl increases, so does the integrated amide I' intensity, which is consistent with the additional absorption observed in the FTIR spectra (Figure 2.10).

Table 2.3: Parameters for FTIR absorption in the amide I' region *vs* Gdn-d_5-DCl concentration

[Gdn-d_5-DCl (M)	Amide I' maximum (cm^{-1})	Integrated intensity	Relative integrated intensity (%)	HWHH (cm^{-1})
0	1644	0.849	100	18.8
1.0	1644	0.877	103	21.2
1.5	1644 1622	1.09	128	25.6
2.0	1644 1622	1.26	148	26.5
3.0	1644 1622	1.33	157	28.0

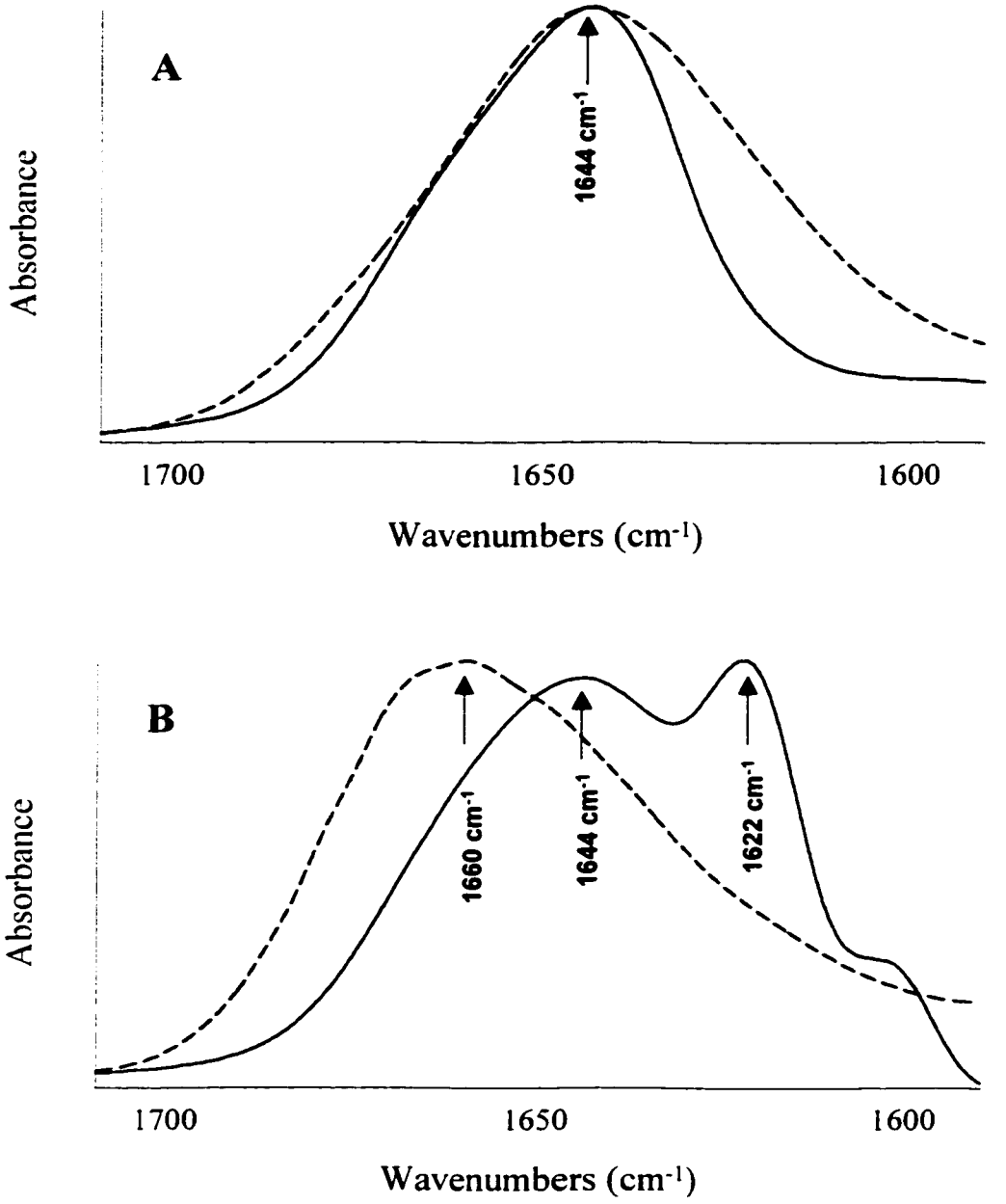

Figure 2.11 FTIR amide I and I' regions of 25 mg/mL PLL in (A) 100 mM NaPi buffer pH and pD 7; H_2O (dashed line) *vs* D_2O (solid line) and (B) 3 M GdnHCl (dashed line) *vs* 3 M Gdn-d_5-DCl (solid line). The FTIR spectra shown represent an average of 256 scans at a resolution of 2 cm^{-1}, acquired using CaF_2 windows with a 6-μM pathlength.

The FTIR amide I and I' regions of PLL in H_2O and D_2O are compared in Figure 2.11. In frame A, the FTIR spectra of PLL in buffer are overlaid. Although there is no *apparent* shift in the center of the amide band (~1644 cm^{-1}), considerable band broadening occurs in H_2O. This is due to red-shifting of main chain and side chain N-H bending absorptions below 1500 cm^{-1} in D_2O. In frame B, PLL in 3 M GdnHCl and 3 M Gdn-d_5-DCl are compared. In 3 M GdnHCl, a broad asymmetric band is apparent with a maximum at ~1660 cm^{-1}, while in 3 M Gdn-d_5-DCl, absorptions at 1644 and 1622 cm^{-1} are observed. These differences are further discussed in Section 2.4.

The FTIR amide I and I' region of PLL in H_2O and D_2O overlaid in Figure 2.11 (frame A), were curve-fitted in Figure 2.12 to resolve component bands under the broad amide envelopes. PLL in H_2O revealed bands at 1675, 1647 and 1621 cm^{-1}, while in D_2O bands at 1666 and 1644 cm^{-1} were observed. The curve-fitting parameters are found in Table 2.4. In H_2O, components were assigned to β-turns (1675 cm^{-1}, 9%), random structures (1647 cm^{-1}, 68%) and turns (1621 cm^{-1}, 23%). In D_2O, β-turns (1666 cm^{-1}, 24%) and random coils (1644 cm^{-1}, 76%) were detected.

Table 2.4: Curve-fitting parameters for amide I and I' bands of PLL in H_2O *vs* D_2O

	Frequency (cm^{-1})	**Secondary structure assignment**	**% Area**
H_2O	1675	β-turns	9
	1647	Random structures	68
	1620	Turns	23
D_2O	1666	β-turns	24
	1644	Random structures	76

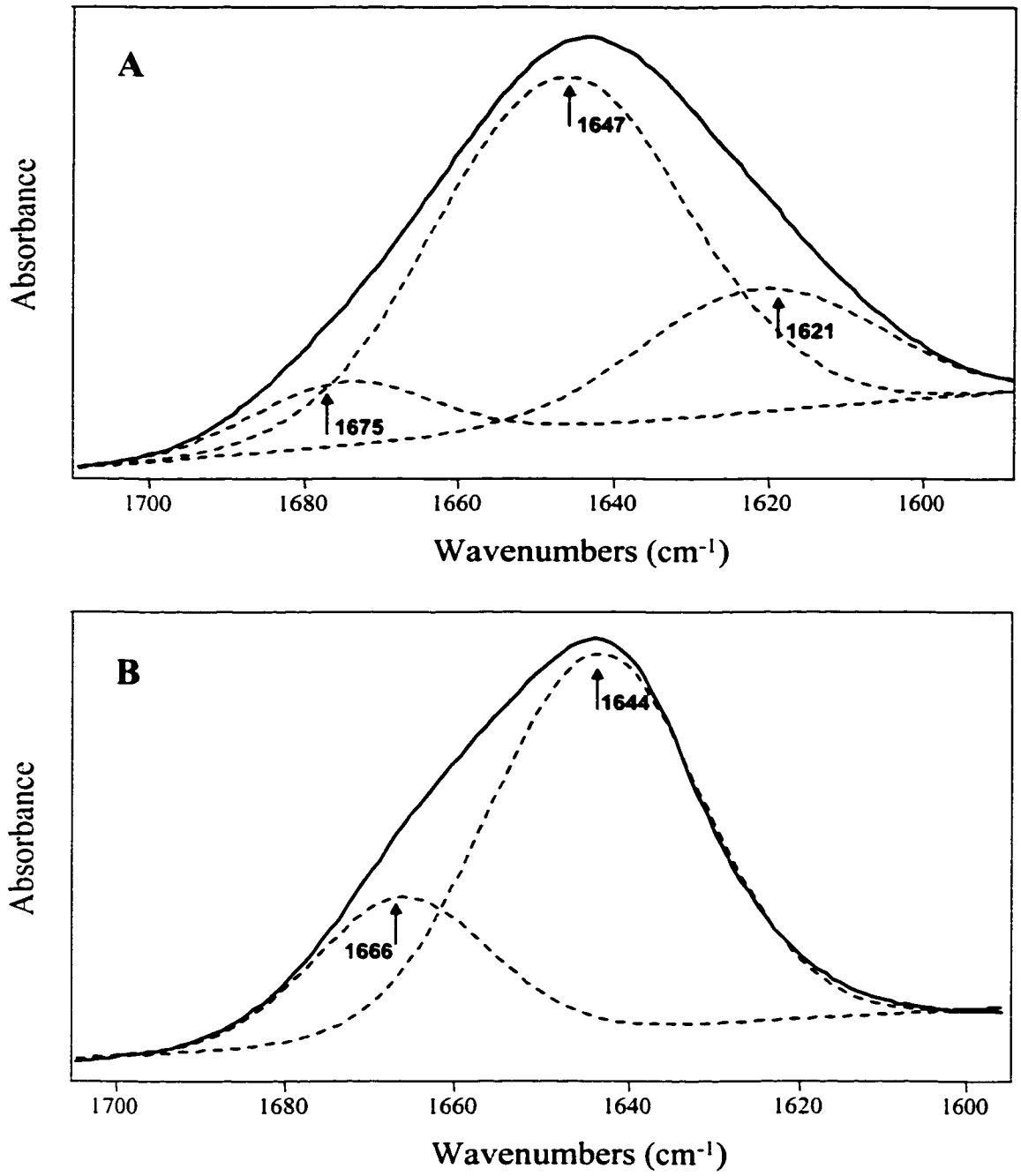

Figure 2.12 Curve-fitted FTIR amide I and I' of 25 mg/mL PLL in 100 mM NaPi buffer: (A) H_2O at pH 7 and (B) D_2O at pD 7. The original spectrum (solid line) was fitted using Galactic Peak Solve software and the bands (dashed lines) have Gaussian peak shapes.

The FTIR amide I' band of PLL in 3 M Gdn-d_5-DCl was curve-fitted as shown in Figure 2.13. Three bands were resolved and their curve-fitting parameters are listed in Table 2.5. The component are assigned to: random structures (1645 cm^{-1}, 80%), PLL-associated Gdn-d_5-DCl (1620 cm^{-1}, 15%) and residual Gdn-d_5-DCl (1602 cm^{-1}, 5%). Data in GdnHCl (H_2O) was not fitted due to uncertainties in the background subtraction.

Table 2.5: Curve-fitting parameters for amide I' bands of PLL in 3 M Gdn-d_5-DCl

Frequency (cm^{-1})	Secondary structure assignment	% Area
1645	Random structures	80
1620	PLL-associated Gdn-d_5-DCl	15
1602	Residual Gdn-d_5-DCl	5

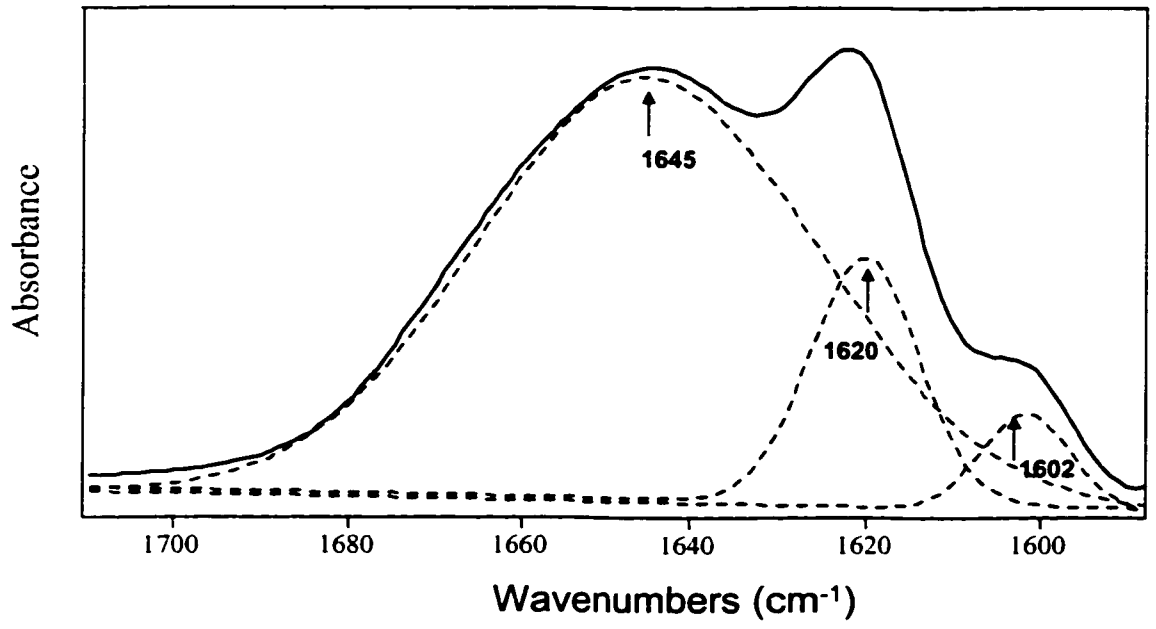

Figure 2.13 Curve-fitted FTIR amide I' of 25 mg/mL PLL in 3 M Gdn-d_5-DCl (in 100 mM NaPi buffer, pD 7, D_2O). The original spectrum (solid line) was fitted using Galactic Peak Solve software and the bands (dashed lines) have Gaussian peak shapes.

CD spectroscopy

The CD spectra of PLL in buffer, 3 and 4 M Gdn-d_5-DCl are shown in Figure 2.14. In buffer, a negative signal at 198 nm is observed as in H_2O. In 3 M Gdn-d_5-DCl, PLL exhibits a major band at 198 nm with a minor band at 201 nm, and in 4 M Gdn-d_5-DCl, a broad asymmetric band at 198 nm with a shoulder at 202 nm is observed.

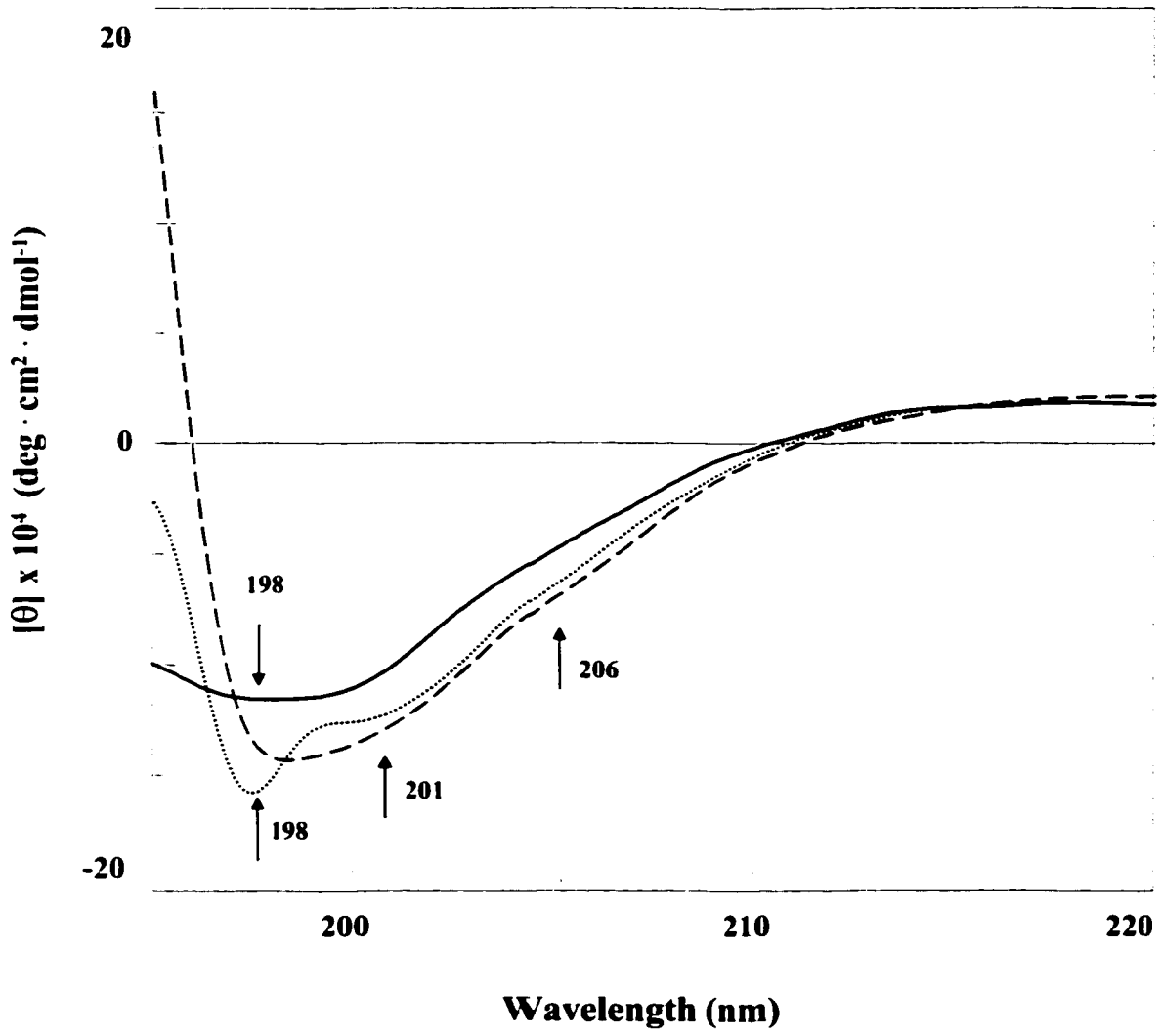

Figure 2.14 Far-UV CD spectra of 25 mg/mL PLL in 100 mM NaPi buffer, pD 7, D_2O, (solid line), 3 M Gdn-d_5-DCl (dotted line) and 4 M Gdn-d_5-DCl (dashed line). The CD spectra represent an average of 5 scans at a resolution of 0.2-nm, recorded using an FTIR cell (6-μM pathlength) as described in Section 2.2.2.

Stacked CD spectra of PLL in Gdn-d_5-DCl are presented in Figure 2.15. Little change is observed in 0–2 M Gdn-d_5-DCl, as is the case for PLL in 0–2 M GdnHCl. In 2.5-4 M Gdn-d_5-DCl, CD absorption varies significantly. As the concentration of Gdn-d_5-DCl is increased, the 201-nm band coincident with Gdn-d_5-DCl absorption becomes more prominent, which suggests association of Gdn-d_5-DCl with the polypeptide.

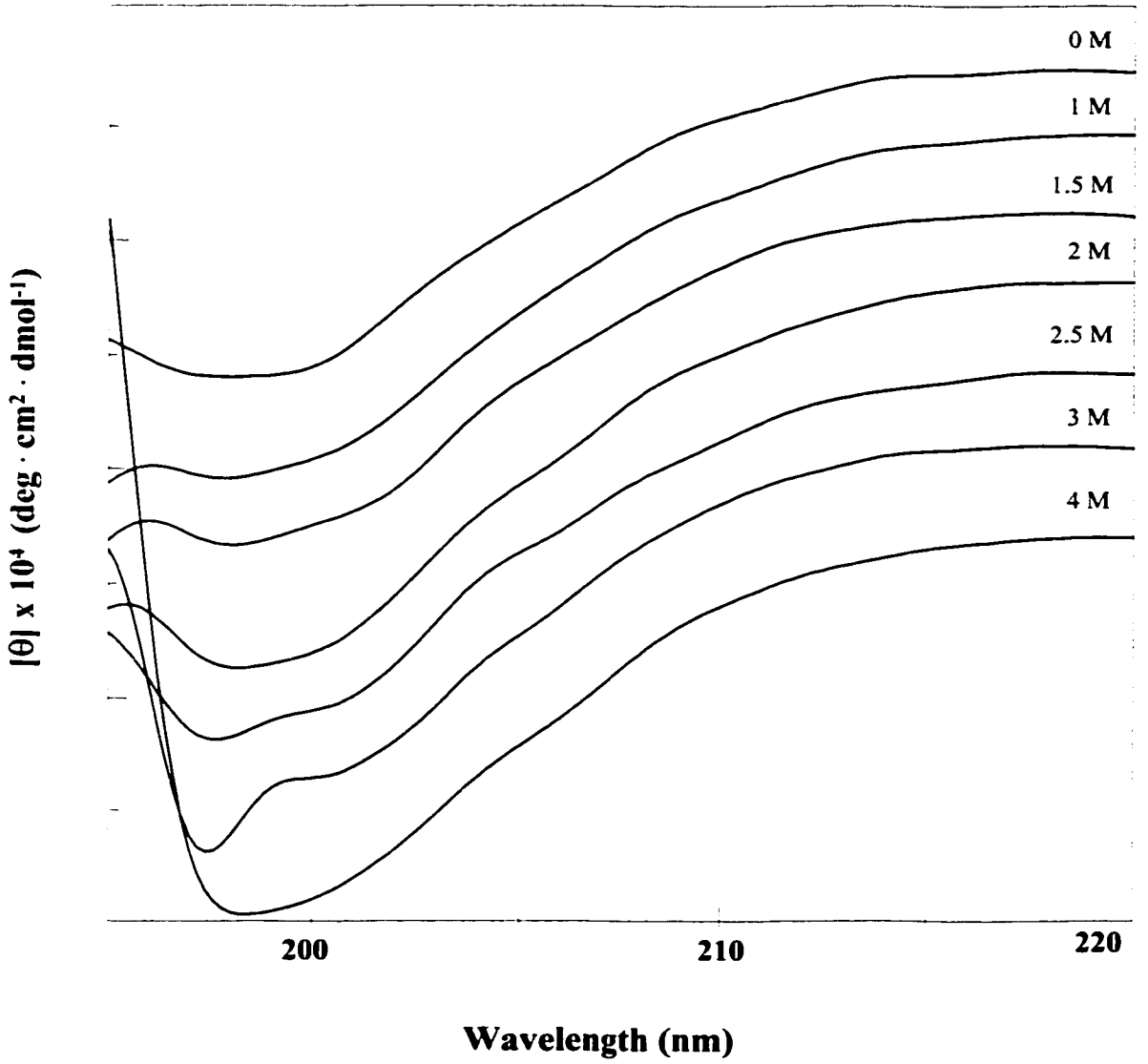

Figure 2.15 Far-UV CD stacked spectra of 25 mg/mL PLL in 0-4 M Gdn-d_5-DCl (in 100 mM NaPi buffer, pD 7, D_2O). The CD spectra represent an average of 5 scans at a resolution of 0.2-nm, recorded using an FTIR cell (6-μM pathlength) as described in Section 2.2.2.

2.4 DISCUSSION

FTIR and CD spectroscopies are complementary techniques. CD absorption is sensitive to asymmetry in the molecular environment of a chromophore and contributions from peptide bonds (180-240 nm) gives rise to a CD signal in the far-UV region (*1, 44*). FTIR, on the other hand, monitors H-bonding of the amide carbonyls (*31*).

FTIR results

At neutral pH, PLL exists as a random coil; therefore no *unfolding* should occur in GdnHCl. Since the surface of a random coil is the most hydrated of all the peptide secondary structures (*54*), it is not surprising that the FTIR spectrum of PLL in H_2O is different from that in 3 M GdnHCl, as shown in Figure 2.5. At high concentrations of GdnHCl, guanidine molecules populate the environment surrounding the peptide side chains, which may affect the interaction between the polypeptide backbone and the solvent molecules (H_2O *vs* GdnHCl). Most likely guanidine molecules bound to the polypeptide will exhibit different vibrational frequencies than free molecules (*9*).

Stacked FTIR amide I and II bands of PLL in varying amounts of denaturant (GdnHCl and Gdn-d_5-DCl) are shown in Figures 2.6 and 2.10. The criteria used for background subtraction are outlined in Section 2.2.2. In accordance with the criterion in step (ii), the target amide I/II ratios were ~2.0 and 1.5 for H_2O and D_2O data sets, respectively. These were the ratios reported for PLL in buffer (native form). It appears at first glance that PLL interacts differently with the denaturant in H_2O compared to D_2O. In H_2O, a *blue* shift of the absorbance in the amide I region is observed, whereas in D_2O, a new *red*-shifted band grows in. However, upon closer inspection, the bands at 1660

cm^{-1} (in H_2O) and 1622 cm^{-1} (in D_2O) are intermediate bands between the absorption of PLL (1644 cm^{-1}) and the denaturant (GdnHCl; 1675 cm^{-1} and Gdn-d_5-DCl; 1600 cm^{-1}). Vibrational coupling between guanidine and PLL may explain this newly formed population.

In H_2O, there are more uncertainties in the background subtraction due to strong absorption of water and denaturant in the amide I region. Upon comparison of the FTIR spectra of PLL in 0-3 M GdnHCl (H_2O, Figure 2.6), it appears that the nature of the PLL-GdnHCl interaction changes as the concentration of GdnHCl is increased, as judged by the blue-shift of the amide I. However, due to uncertainties in the subtraction, one can not rely on information derived from these spectra. Therefore, attention is focused on PLL in D_2O and Gdn-d_5-DCl, where there are less difficulties with background subtraction.

The 1644-cm^{-1} FTIR band assigned to the backbone absorption of PLL is present in 0-3 M Gdn-d_5-DCl. This implies that H-bonding of the PLL polypeptide backbone is only slightly disrupted, if at all. If the Gdn-d_5-DCl interacts with the PLL backbone, one would expect a shift in the 1644 cm^{-1} band. Since this is not observed, it is speculated that the Gdn-d_5-DCl interacts mainly with the lysyl side chains, and not with the peptide backbone. Since the lysyl side chains are long (see Figure 2.1) and flexible, preferential interaction of Gdn-d_5-DCl with the side chains of PLL is not expected to perturb the backbone amide I' absorption. As the concentration of denaturant increases, so does the integrated intensity of the amide I' band (Table 2.3), especially in 1.5 to 3.0 M Gdn-d_5-DCl. This is consistent with the presence of additional absorption under the amide I' window due to PLL-associated Gdn-d_5-DCl.

The FTIR amide I and I' regions of PLL in H_2O *vs* D_2O are compared in Figure 2.11, frame A. At first glance, it appears that the center of the amide bands absorb at the same frequency (~1644 cm^{-1}) for PLL in H_2O and D_2O. This was surprising since FTIR amide I bands in H_2O are generally red-shifted by ~5-10 cm^{-1} in D_2O (*31*). However, the amide I band in H_2O is considerably broader than the amide I' in D_2O, suggesting that differences in the spectra are not due to mass effects alone.

In order to gain further insight on the differences in structure of PLL in H_2O *vs* D_2O, the FTIR amide I and I' modes were curve-fitted as shown in Figure 2.12. In H_2O (frame A), the FTIR amide I envelope is resolved to 3 bands at 1675, 1647 and 1621 cm^{-1}, while in D_2O (frame B), only 2 bands were observed at 1666 and 1644 cm^{-1}. As expected, the major band assigned to random coil was red-shifted (~3 cm^{-1}) in D_2O. PLL in H_2O exhibited a greater contribution due to turns (~32%) than in D_2O (~24%). In H_2O, the absorption due to turns is split into high and low frequency components. In D_2O on the other hand, only one band due to turns was detected at the high-frequency end of the amide I' region. Therefore, differences in structure of PLL in H_2O *vs* D_2O at neutral pH are attributed to the presence of turns, as reported by FTIR spectroscopy.

The amide I' region of PLL in 3 M Gdn-d_5-DCl (D_2O) was curve-fitted using Gaussian bands (Figure 2.13). Bands at 1645, 1620 and 1602 cm^{-1} are assigned to random coil (80%), PLL-associated Gdn-d_5-DCl (15%) and residual denaturant (5%), respectively. Most of the absorption of Gdn-d_5-DCl (~1602 cm^{-1}) from bulk solvent can be subtracted out, but not when it is associated with PLL since this band is not present in the background spectrum. Since the new 1620-cm^{-1} absorption signals the presence of PLL-associated Gdn-d_5-DCl, it is important for the understanding protein denaturation to

determine the nature of this association. As previously stated, the absorption at 1645 cm^{-1} of PLL in 3 M Gdn-d_5-DCl is assigned to the polypeptide backbone which appears to be relatively unperturbed. Therefore, the presence of the 1620-cm^{-1} band is likely due to the association of Gdn-d_5-DCl with the lysyl side chains.

CD results

It is evident from Figures 2.7 and 2.14 that the CD spectra of PLL in buffer are different from those in 3–4 M GdnHCl and Gdn-d_5-DCl. The native form of PLL generates a strong negative CD signal at 198 nm in H_2O and D_2O. This absorption agrees with empirical rules for a random coil (Table 1.3). However, the far-UV CD bands observed for PLL in H_2O and D_2O have slightly different shapes, suggesting that the hydration of the polypeptide chain is not the same in the two solvents.

Differences in the CD spectra in 3 and 4 M GdnHCl and Gdn-d_5-DCl suggest that the solvation of the PLL chain is dependent on the concentration of the denaturant. In 3 M GdnHCl (H_2O), a strong negative CD signal at 201 nm coincident with GdnHCl absorption is observed, as well as a minor band at 205 nm. Similarly, in 3 M Gdn-d_5-DCl, a strong negative band at 198 nm with a minor band at 201 nm are observed. Common features in the CD spectra suggest that the asymmetry of the chromophore (peptide bond) is the same in 3 M GdnHCl and Gdn-d_5-DCl. However, the solvation is assumed to be different as evidenced by a shift in wavelength of ~3-4 nm. When the concentration of denaturant is increased from 3 M to 4 M, dramatic differences are observed in the CD spectra. In 4 M GdnHCl (H_2O), a broad negative CD band at 200 nm with a shoulder at 201 nm is detected. Likewise, PLL in 4 M Gdn-d_5-DCl exhibits a

broad negative band at 198 nm with a shoulder at 202 nm. Therefore, CD data suggest that solvation is not the same in 3 and 4 M GdnHCl and Gdn-d_5-DCl.

FTIR results in D_2O (Figure 2.10) suggest that Gdn-d_5-DCl associates with PLL. The denaturant seems to interact preferentially with the lysyl side chains as manifested by the lack of perturbation of the amide I' band and the formation of a new population in the amide I' region. As the concentration of Gdn-d_5-DCl increases, so does the degree of Gdn-d_5-DCl–PLL association as evidenced from the growth of the 1622 cm^{-1} band in Figure 2.10. The presence of immobilized Gdn-d_5-DCl is also expected to perturb the CD spectra. If Gdn-d_5-DCl molecules associate with the lysyl side chains, then the asymmetry of their molecular environment should be increased relative to free Gdn-d_5-DCl. CD absorption at the wavelength expected for Gdn-d_5-DCl is observed (Figure 1.5), which corroborates this hypothesis. The stacked CD spectra in Figure 2.15 reveal that as the concentration of Gdn-d_5-DCl is increased, so does the intensity of the 198-nm band. Between 2 and 3 M Gdn-d_5-DCl, a large change in the CD spectra (Figure 2.15) is observed which parallels the major increase in the FTIR 1622-cm^{-1} intensity (Figure 2.10).

It is noteworthy that the signature α-helical band at 222 nm is not detected in any of the CD spectra under the solution conditions studied. This reveals that PLL does not convert from a random coil to an α-helical conformation in denaturant. Therefore, any observed changes in the CD spectra may be attributed to differences in solvation or asymmetry of the peptide bonds upon association with Gdn-d_5-DCl.

2.5 CONCLUSIONS

The CD and FTIR data in H_2O and D_2O reveal that the solvation of PLL in a random coil conformation is different in water *vs* GdnHCl and Gdn-d_5-DCl. Since there are fewer uncertainties in the FTIR background subtraction in D_2O, attention was focussed on these data.

At first glance, it appeared that the structures of PLL were the same in H_2O and D_2O, since the center of the FTIR amide bands absorbed at the same frequency (~1644 cm^{-1}). Therefore, the structure of PLL in H_2O *vs* D_2O was investigated by curve-fitting the FTIR amide I and I' modes. Differences in the structures were detected, along with a high content of turns.

Spectral perturbations provide strong evidence that the denaturant associates with PLL. According to Denisov *et al.* (*27*), internal water sites and secondary structure are lost simultaneously, accompanied by an influx of external solvent, in this case GdnHCl/Gdn-d_5-DCl. Therefore, if more GdnHCl or Gdn-d_5-DCl molecules populate the environment surrounding the polypeptide, then the likelihood of association of with PLL is increased. The random-coil band at 1644 cm^{-1} due to PLL backbone absorption is relatively insensitive to the denaturant, while additional absorption at 1622 cm^{-1} grows in with increasing concentration of Gdn-d_5-DCl. This suggests that association occurs between the Gdn-d_5-DCl and the lysyl side chains.

Denaturation potency of the guanidinium salt is affected by the nature of the anion according to the Hofmeister series (*16*). For example, GdnSCN is a more potent denaturant relative to GdnHCl. This indicates that the counter ion plays a role in the

destabilizing action of guanidinium. A schematic of the interaction of the guanidinium ion with the lysyl side chain is proposed and shown in Figure 2.16 below.

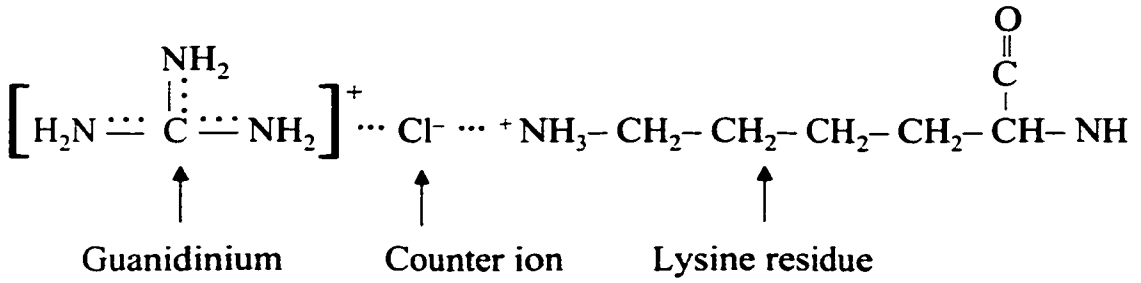

Figure 2.16 Interaction of GdnHCl with Lysine residue.

It is also evident from the CD data that the solvation of PLL changes as denaturant is added. A major change in CD absorption is observed at ~ 2.5 M GdnHCl/Gdn-d_5-DCl, which is attributed to the association of guanidinium ions with the lysyl side chain. Therefore, immobilized GdnHCl/Gdn-d_5-DCl perturbs the CD spectra, hence generates a signal resulting from an increase in the asymmetry of molecular environment of the peptide bonds.

CHAPTER 3: INVESTIGATION OF THE GdnHCl-DENATURED STATE OF HRP AND HRP-CN VIA FTIR, CD AND FLUORESCENCE SPECTROSCOPIES

3.1 INTRODUCTION

Spectroscopic tools were used to characterize the difference between the GdnHCl-denatured states of horseradish peroxidase C (HRP) and its cyanide ligated form (HRP-CN). Initially, HRP was chosen as a model system to study chemical denaturation by FTIR spectroscopy. However, the FTIR results revealed complex time-dependent changes in the denatured states of HRP and HRP-CN that were difficult to interpret. Probing the GdnHCl-denatured states of proteins via FTIR is a relatively novel technique, which has only recently been reported. Therefore, HRP is not an ideal model system for the development of this technique since it contains calcium ions, disulfide bridges and heterogeneously glycosylated sites that may complicate the results. In addition, it is possible that excess CN^- will break disulfide bonds and further obscure the data interpretation. Therefore, cytochrome c was chosen as a simpler system devoid of the aforementioned structural elements, and will be discussed in Chapter 4. The results for HRP and HRP-CN are presented briefly in this chapter.

HRP isoenzyme C is the most studied heme peroxidase (*59*). It consists of a single polypeptide chain of 308 amino acids, with a molecular weight of 44 kDa (*60*). Characteristic structural features include: an iron (III) protoporphyrin IX, 8 heterogeneously-glycosylated carbohydrate chains, 4 disulfide bridges and 2 calcium binding sites (*59*). Its known function is to catalyze the oxidation of a variety of aromatic

substrates by hydrogen peroxide (*61*). Its catalytic mechanism involves two intermediates known as compound I and II (*47*).

HRP is a class III peroxidase belonging to the plant extracellular family, and its crystal structure has been recently solved to 2.15-Å resolution (*62*). A unique feature to this class is a 34-residue insertion between two helices, which serves as a substrate access channel. In addition, HRP has three aromatic residues (Phe142, Phe68 and Phe179) which guard the entrance to the exposed-heme edge (*62*). The heme active center has two key catalytic residues (His170 and His 42) that mediate peroxide reactivity and compound I formation (*62*). The heme is located between a proximal His170, which is covalently bound to the iron, and a distal His42. The Fe(III) ion of resting HRP is in a 5-coordinate high-spin state, as determined by resonance Raman spectroscopy (*62*).

The 8 N-linked glycans account for about 22-27 % of the protein's molecular weight, but do not interfere with substrate access, binding or catalysis (*61*). Most of the glycosylation sites are positioned in loop regions, which are evenly distributed throughout the protein's surface and point away from the molecule (*62*). It was speculated by Gajhede *et al.* that the purpose of the glycans was to increase the enzyme's solubility in aqueous solution and provide resistance to free-radical protein crosslinking (*62*).

The C_α backbone of HRP is presented in Figure 3.1, and from this it can be seen that the secondary structure is predominately α-helical (~30%) with very little β-sheet (*59, 62, 63*). There are 10 prominent α-helices (helix A to J), as well as 13 structurally conserved regions found in all members of the plant peroxidase family (*62*).

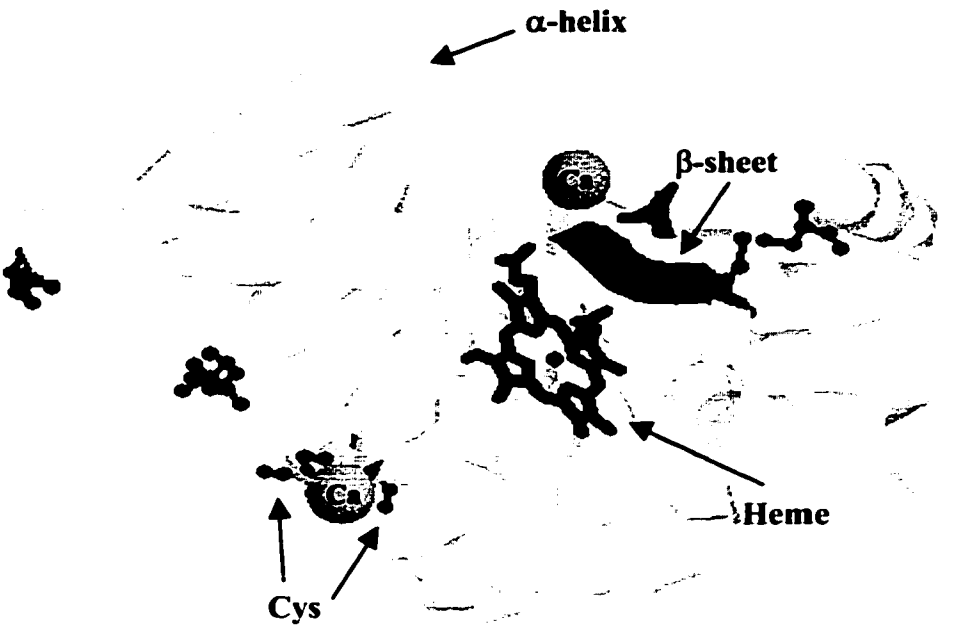

Figure 3.1 C_α backbone of horseradish peroxidase C showing the heme, α-helices, β-sheets, Trp, Cys residues and 2 Ca^{+2} ions. The protein coordinates were obtained from the Pubmed NCBI website (www.ncbi.nlm.nih.gov/Pubmed/medline.html), and the figure was generated by Rasmol software.

The calcium ions and disulfide bridges in HRP are major stabilizing elements (*64*). Calcium ions are required to maintain the structural environment of the heme, and their removal alters the position of the distal His and the enzyme activity (*62*). Tsaprailis *et al.* performed fluorescence studies on EDTA-treated HRP, where EDTA chelated the bound calcium ions, and the protein was found to be more sensitive to denaturation in GdnHCl (*64*). In the same study, HRP was also treated with dithiothrietol (DTT), which reduced the disulfide bonds. Calcium ions were found to have a greater effect on the overall stability of the protein than the disulfide bonds. Removing both calcium ions and reducing the disulfide bridges dramatically decreased the kinetic stability of HRP. The

half-life for unfolding of the EDTA- and DTT-modified protein was 0.4 s compared to 519 s for the unmodified form (*64*).

Thermal denaturation of EDTA- and DTT-treated HRP was studied by Chattopadhyay and Mazumdar (*63*). They also found that depletion of Ca^{2+} decreased the stability of the enzyme, such that loss of secondary structure was observed at 61°C instead of 74°C (*63*). In addition, reduction of the disulfide bonds had a marked effect on the stability of the protein, as judged by a large decrease in the T_m value (midpoint of unfolding transition).

The cyanide adduct is produced by adding a small amount of KCN to HRP. The CN^- ligand binds reversibly to the ferric iron of the heme (*65*), and binding appears to have a stabilizing effect in solutions containing less than 1 M GdnHCl. This may be attributed to a more stable heme cavity as a result of extended distal H-bonding involving the CN^- ligand (*66*). Low concentrations of KCN (~100 μM) should be used since disulfide bonds may be cleaved by excess CN^- nucleophile (*16*):

$$\text{R-S-S-R} + \text{CN}^- \rightleftharpoons \text{RS}^- + \text{RSCN} \qquad \textbf{3.1}$$

Denaturation studies by Tsaprailis *et al.* (*66*) revealed that the cyanide-ligated form unfolds five times faster ($t_{1/2}$ = 93.9 s) in 6 M GdnHCl than the unligated form ($t_{1/2}$ = 519 s). Therefore, HRP-CN appears to be less resistant to denaturation compared to the unligated HRP. Only 30% of HRP-CN refolds in the presence of ~1 mM KCN, and it is speculated that excess free CN^- breaks disulfide bonds (equation 3.1) that are essential for the proper refolding of HRP. Fluorescence data indicate that HRP-CN exhibits greater steady-state fluorescence intensity than HRP at pH >10.5 (*47*).

Fluorescence-decay studies revealed a Trp117 picosecond lifetime component of 58 ps for HRP-CN and 45 ps for HRP (*47*). The *m* values, which are a measure of the solvent-exposed surface area between native and denatured states (*8*), were found to be 2.0 kcal/mol and 3.8 kcal/mol for HRP and HRP-CN, respectively (*66*). This implies that HRP-CN should unfold about two times more cooperatively than HRP.

In the present study, fluorescence spectroscopy was used to compare the global unfolding of HRP and HRP-CN in 0-6 M GdnHCl. In addition, percent relative fluorescence ($\%F_{350}$) *vs* time was monitored for HRP and HRP-CN in 1 M and 6 M GdnHCl. This was done to compare time-dependent changes in the structure of the ligated and unligated forms in denaturant.

3.2 EXPERIMENTAL PROCEDURES

3.2.1 Materials

Lyophilized, salt-free horseradish peroxidase isoenzyme C (Grade I, M_r = 44 kDa) was obtained from Boehringer Mannheim and used without further purification. Guanidine hydrochloride (GdnHCl, 99+%, FW 95.53), N-acetyl-L-tryptophanamide (NATA, FW 245.3) and N-acetyl-L-tyrosinamide (NAYA, FW 222.2) were purchased from Sigma. The source of the cyanide ligand was KCN (FW 65.12) from BDH chemicals. The Phosphate buffer (pH 7.0) was prepared by dissolving 100 mM phosphate salts ($Na_2HPO_4 \cdot 7H_2O$ and $NaH_2PO_4 \cdot H_2O$) from Fisher in distilled H_2O with a specific resistance of 18.2 MΩ from Barnsted nanopure system. All solutions were prepared in a 100 mM sodium phosphate buffer.

3.2.2 Methods

The concentration of horseradish peroxidase (ε_{403} = 102 $mM^{-1}cm^{-1}$) (*82*) stock solution was determined spectrophotometrically using a Hewlett-Packard 8451A diode array spectrophotometer. The protein stock solution was diluted to the desired final concentration with buffer and the appropriate amount of denaturant. A small amount of KCN solution (0.1 mM), was added to the final HRP solution to form the HRP-CN complex.

Fluorescence spectroscopy

Fluorescence spectra were recorded on an Aminco-Bowman Series 2 spectrofluorimeter. The final concentration of HRP used in these experiments was 2.0 μM. Fluorescence intensities were standardized (100% fluorescence) relative to 2.0 μM NATA (HRP has 1 Trp) and 10.0 μM NAYA (HRP has 5 Tyr). The concentrations of NATA (ε_{280} = 5.69 $mM^{-1}cm^{-1}$) and NAYA (ε_{276} = 1.49 $mM^{-1}cm^{-1}$) (*67*) fluorescence standards were determined spectrophotometrically. The structures of NATA, NAYA, Trp and Tyr are shown in Figure 3.2.

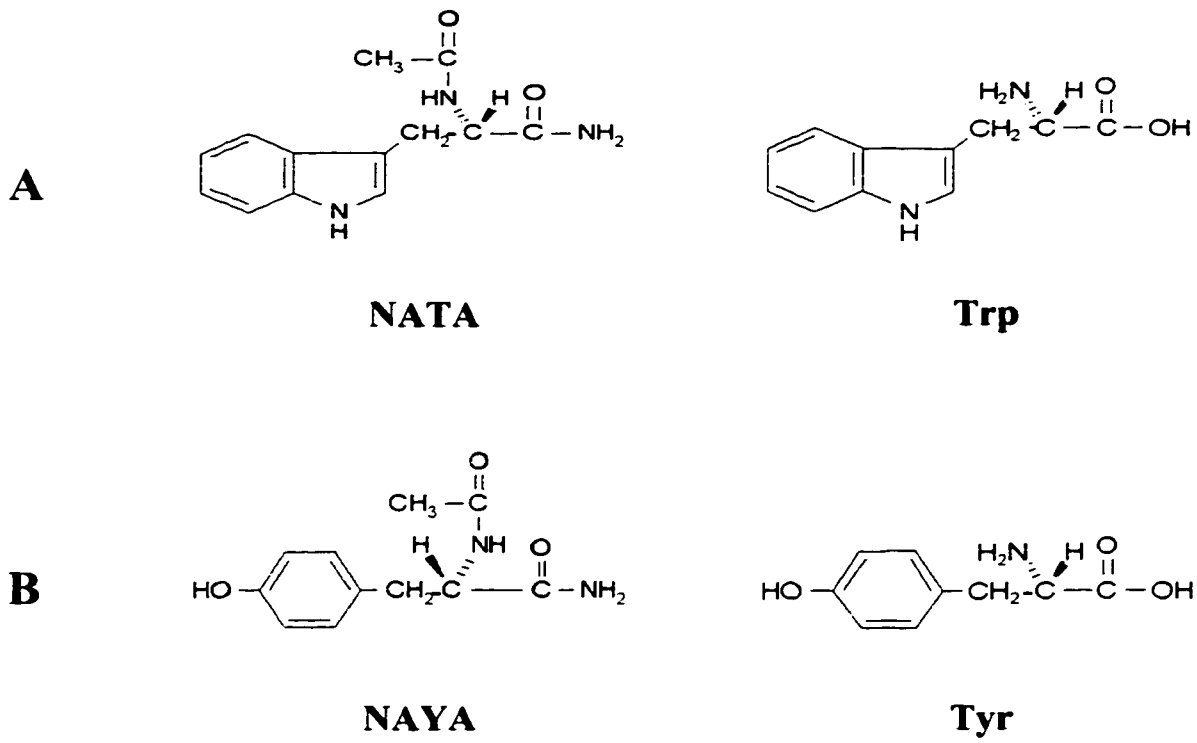

Figure 3.2 Structures of (A) NATA & Trp and (B) NAYA & Tyr.

Emission of the blank (1 and 6 M GdnHCl) was subtracted from the appropriate protein and standard samples. Percent relative fluorescence at 350 nm ($\%F_{350}$) was calculated using equation 3.2.

$$\%F_{350} = \frac{F_{350}(\text{sample}) - F_{350}(\text{blank})}{F_{350}(\text{standard}) - F_{350}(\text{blank})} \times 100 \qquad \textbf{3.2}$$

The protein samples were allowed to denature for ~24 h at room temperature prior to recording fluorescence spectra to ensure equilibrium was reached. Tryptophan was excited at 280 nm and its emission scanned from 300 to 450 nm at a rate of 1.00 nm/s,

with slit widths of 4 nm. The sample holder was thermostated to 25°C using a VWR water bath, Model 1162.

CD spectroscopy

CD experiments were performed as described in Section 2.2.2. The stock solution of HRP was diluted to 2.0 mM with buffer and the corresponding concentration of denaturant. Samples were incubated for 3 h and CD spectra were recorded every hour over a 12-h period. Samples were then placed in the FTIR cell fitted with a 6-μM Teflon spacer as described in Section 2.2.2. Absorption of the blank (GdnHCl in buffer) was subtracted from the HRP sample and the final spectra were smoothed using the Jasco software. The observed ellipticity was converted to molar ellipticity using equation 2.1.

FTIR spectroscopy

FTIR spectra were recorded as described in Section 2.2.2. The final concentration of HRP in each sample was 2.0 mM diluted from the stock solutions with buffer with the required amount of denaturant. Contributions from water and denaturant were removed from the raw spectrum as outlined in Section 2.2.2. Fourier transform self-deconvolution (FSD) of the broad amide I envelope allowed resolution of the component bands and assignment of secondary structural elements. Deconvolution parameters used were half-width at half-height (HWHH) of 20 cm^{-1} and an enhancement (K factor) of 1.5.

3.3 RESULTS

3.3.1 Time-dependent fluorescence changes in GdnHCl

Fluorescence spectroscopy was used to monitor the global unfolding of HRP and its cyanide ligated form, HRP-CN. Trp117 was used as a built-in fluorescent probe, which reports on its microenvironment and is sensitive to the overall protein conformation. A Trp residue in an aqueous environment fluoresces maximally at a wavelength of 350 nm, whereas a Trp that is buried within a protein core emits at $\lesssim$ 330 nm (*16*).

Fluorescence spectra of HRP and HRP-CN in 0-6 M GdnHCl are presented in Figure 3.3. Samples were incubated in GdnHCl for 24 h prior to data acquisition. As shown, Trp fluorescence intensifies with increasing concentration of GdnHCl due to relief of heme quenching by increased separation between Trp and heme. At neutral pH, Trp117 and the heme are ~1.2 nm apart (*47*). As expected, emission maxima are red shifted upon denaturation, which is indicative of a change in the Trp environment from hydrophobic (protein interior) to hydrophilic (solvent exposed).

The fluorescence spectra of unligated HRP in 0-6 M GdnHCl are shown in Figure 3.3, frame A. As the concentration of GdnHCl increases, so does the fluorescence intensity, which appears proportional to the concentration of denaturant. Since the intensity has not leveled off, the unfolding of HRP in 6 M GdnHCl may not be complete. The fluorescence spectra for HRP-CN in 0-6 M GdnHCl are shown in Figure 3.3 frame B. In 0-2 M GdnHCl, the fluorescence signal increases proportionally with denaturant concentration. Between 2 and 2.5 M GdnHCl, a dramatic increase in the fluorescence intensity is observed, indicative of a major loss of tertiary structure. In 2.5-6 M GdnHCl,

HRP-CN appears to fluoresce maximally, with only a slight change in the fluorescence signal with increasing concentration of GdnHCl, suggesting that protein unfolding is complete. From these data, it appears that HRP-CN is less stable than the unligated HRP in GdnHCl.

Loss of tertiary structure with respect to time (from 0 to 24 h) of HRP and HRP-CN in 1 and 6 M GdnHCl was also probed by fluorescence spectroscopy. According to Pappa and Cass (*23*), minimal unfolding of the protein backbone occurs in 1 M GdnHCl and the heme site remains intact. In 6 M GdnHCl however, the backbone is completely unfolded and the heme is no longer bound to the protein. Percent relative fluorescence ($\%F_{350}$) *vs* time is plotted in Figure 3.4 for HRP and HRP-CN in 1 and 6 M GdnHCl. The $\%F_{350}$ values were computed using equation 3.2, and the fluorescence of NATA and NAYA standards (Figure 3.2) were assumed to be 100%.

In 1 M GdnHCl after 24 h, the $\%F_{350}$ values were greater for HRP (9.3%) than HRP-CN (7.1%). Conversely, in 6 M GdnHCl after 24 h, the opposite trend was observed since the $\%F_{350}$ values for HRP and HRP-CN were 55.0 and 65.1%, respectively. Cyanide binding appears to have a stabilizing effect on HRP in 1 M GdnHCl, but not as the concentration of GdnHCl is increased above 1.5 M. According to the graph in Figure 3.4 frame B, $\%F_{350}$ values were relatively constant between 18-24 h. After 48 h (data not shown), global unfolding was assumed to be complete since HRP and HRP-CN have the same $\%F_{350}$ value of 65.5%.

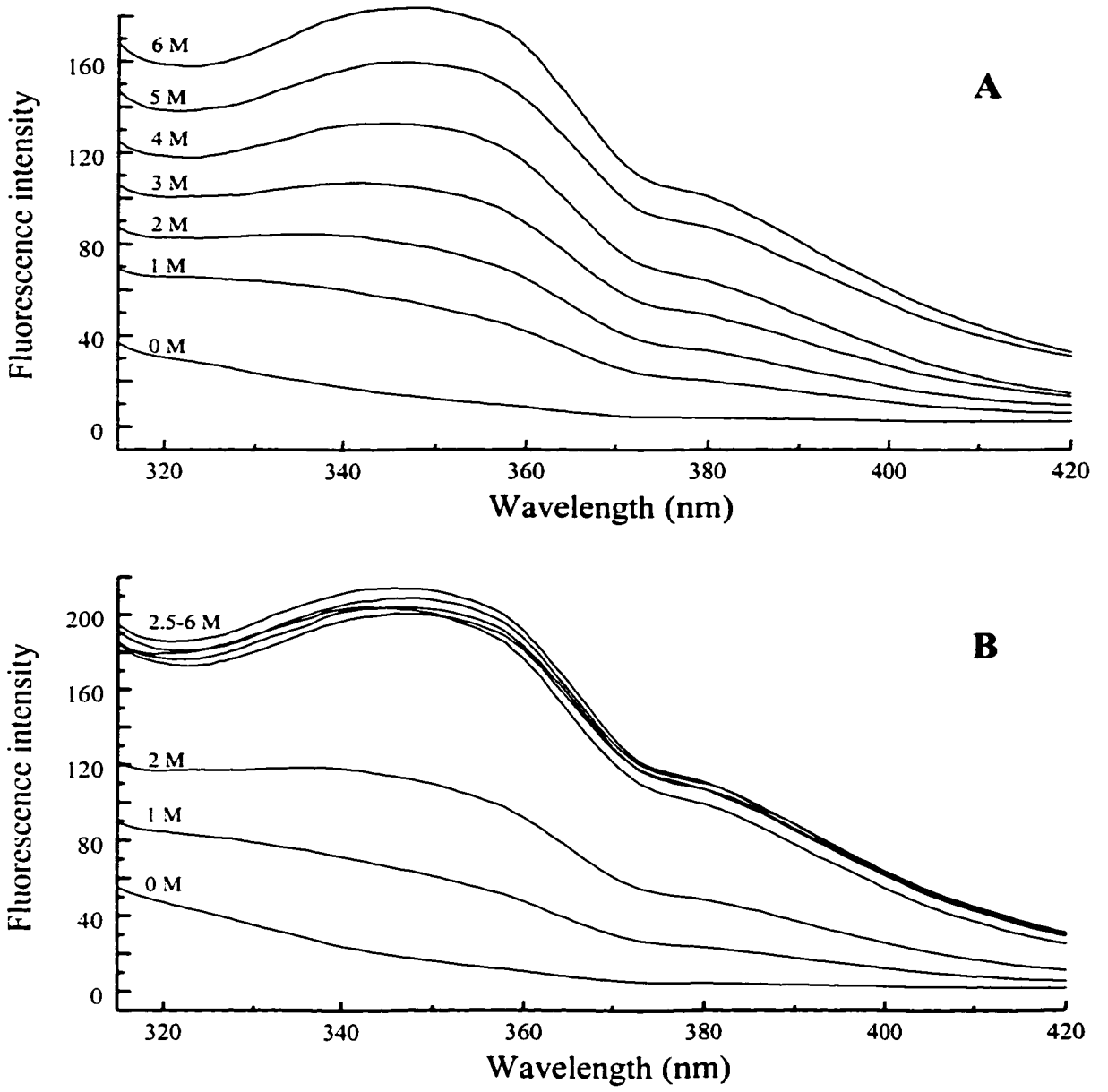

Figure 3.3 Tryptophan fluorescence spectra (λ_{ex} = 280 nm) of 2 μM (A) HRP and (B) HRP-CN in 0-6 M GdnHCl (in 100 mM NaPi buffer, pH 7, H_2O). The proteins were incubated in GdnHCl for ~24 h. The cyanide-ligated form was prepared by adding excess KCN (100 μM) to HRP.

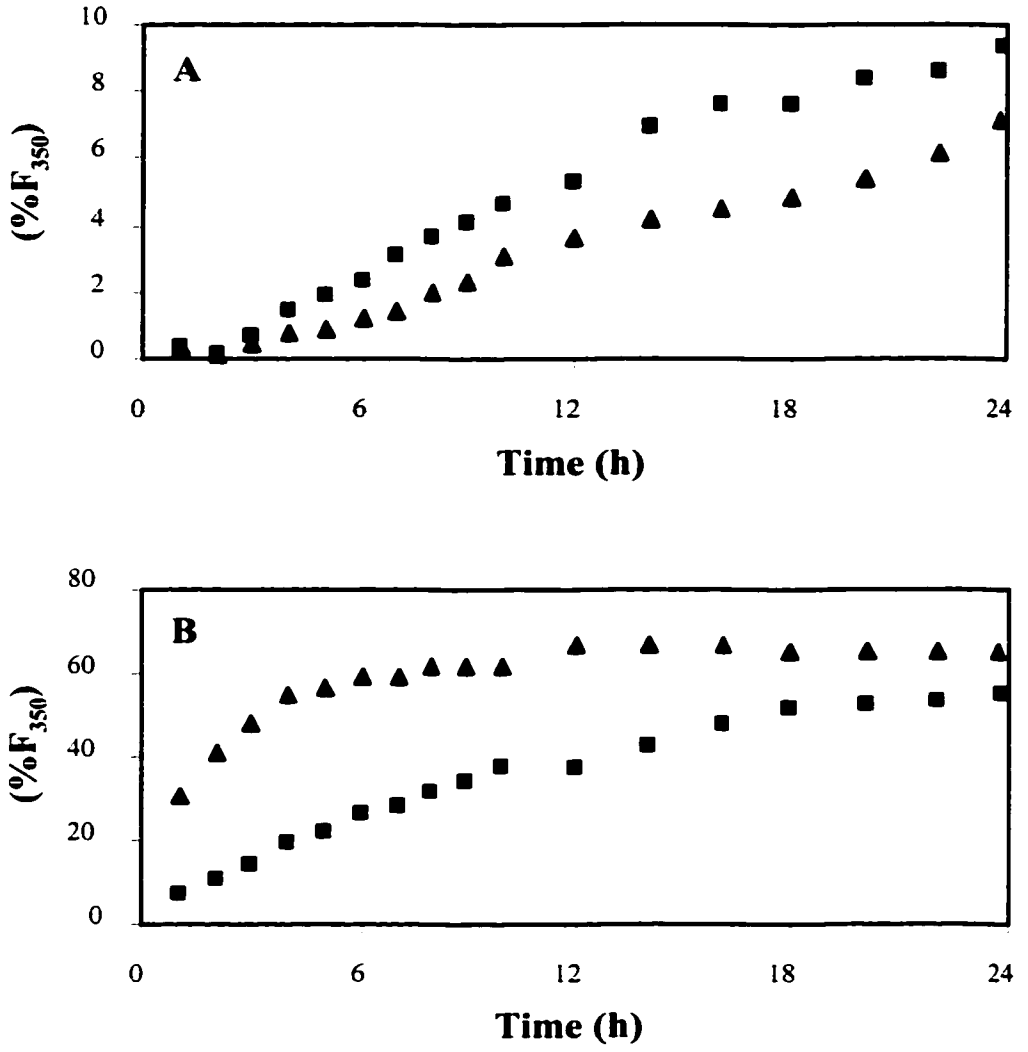

Figure 3.4 Percent relative fluorescence ($\%F_{350}$) *vs* time (0-24 h) for 2 μM HRP (squares) and HRP-CN (triangles) in 1 M GdnHCl (frame A) and 6 M GdnHCl (frame B). HRP-CN was formed by adding excess KCN (100 μM) to HRP. All solutions were prepared in 100 mM NaPi buffer, pH 7, H_2O.

3.3.2 Time-dependent CD changes in 1 M GdnHCl

CD spectroscopy was utilized to study time-dependent variations in the α-helical content of HRP and HRP-CN in 1 M GdnHCl. Changes in α-helicity were probed via the characteristic double minima at 209 and 222 nm. Samples of HRP and HRP-CN were incubated for 3 h in 1 M GdnHCl, and CD spectra were recorded every hour (up to 12 h).

Figure 3.5 depicts changes in the α-helical content of HRP and HRP-CN 1 M GdnHCl at 2-h time intervals from 3 to 11 h. Not much change in the α-helicity is observed over this time period for HRP, except for a slight negative increase in the CD signal after 9 and 11 h. The CD spectra of HRP-CN revealed greater changes in the α-helicity compared to HRP. A dramatic increase in the negative ellipticity is observed for the α-helical bands of HRP-CN after 9-h incubation in 1 M GdnHCl. Further increase occurs after 11 h, indicating that HRP-CN has not reached a stable conformation in 1 M GdnHCl at this time. This increase in negative ellipticity with time suggests that cyanide binding to HRP has a stabilizing effect in 1 M GdnHCl, which was also noticed in the fluorescence results in Section 3.3.1.

In Figure 3.6, the far-UV CD spectra of HRP and HRP-CN are compared at the beginning (3 h, frame A) and end (12 h, frame B) of the incubation period in 1 M GdnHCl. After 3 h, the α-helical CD signal for HRP is more intense than that for HRP-CN, which suggests that HRP has a greater α-helical content at that time. Conversely, after 12 h, the CD signal is more intense for HRP-CN relative to HRP. In addition, the double negative features in the CD spectrum for HRP-CN are not as pronounced after 12 h incubation in 1 M GdnHCl.

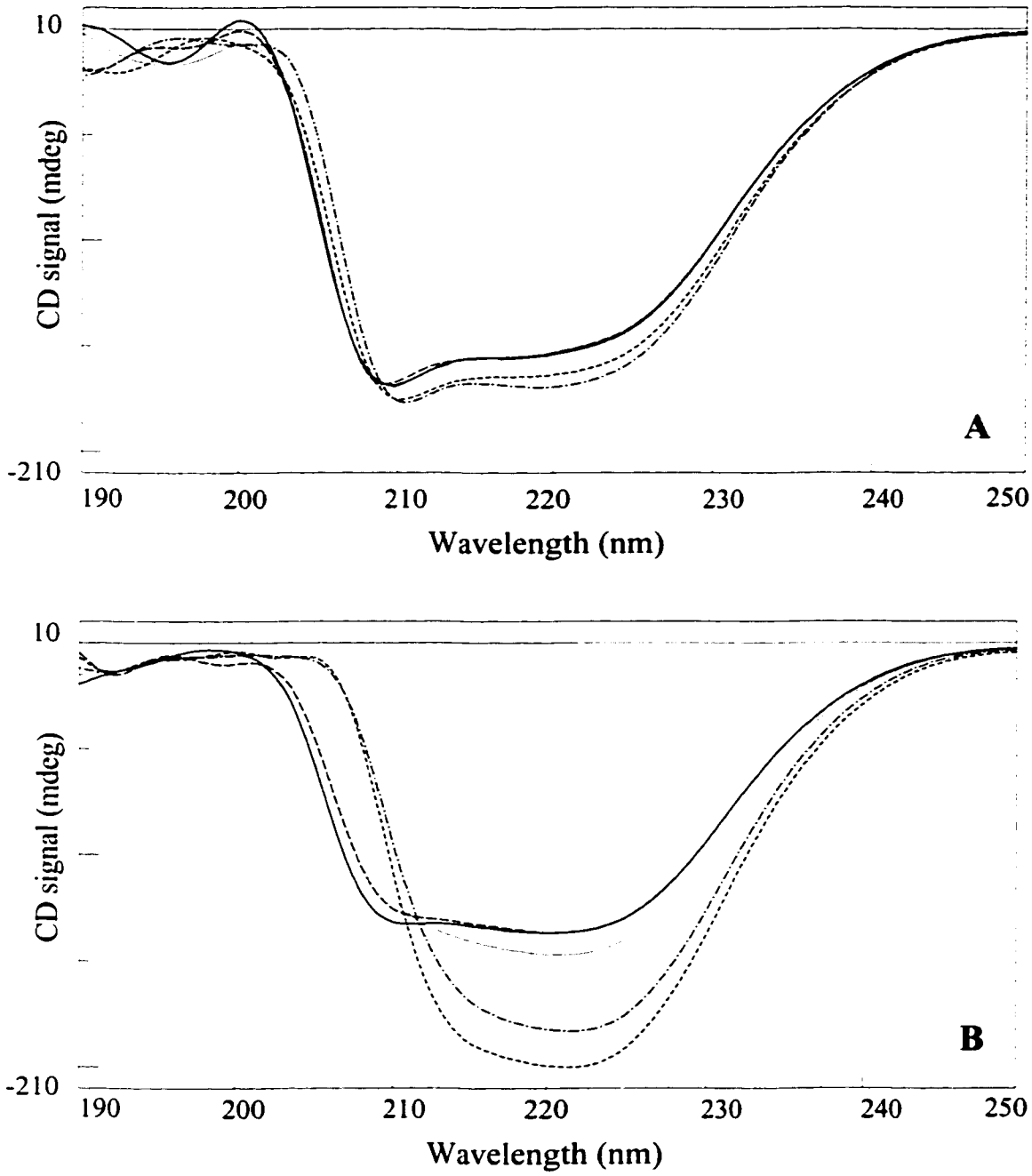

Figure 3.5 Far-UV CD spectra of the α-helical band of 2 mM (A) HRP and (B) HRP-CN in 1 M GdnHCl (in 100 mM NaPi buffer, pH 7, H_2O) *vs* time: 3 h (solid line), 5 h (long dashed line), 7 h (dotted line), 9 h (mixed dashed & dotted line) and 11 h (short dashed line). The cyanide-ligated form was prepared by adding excess KCN (100 μM) to HRP. The CD spectra represent an average of 5 scans at a resolution of 0.2-nm, recorded using an FTIR cell with a 6-μM pathlength as described in Section 2.2.2.

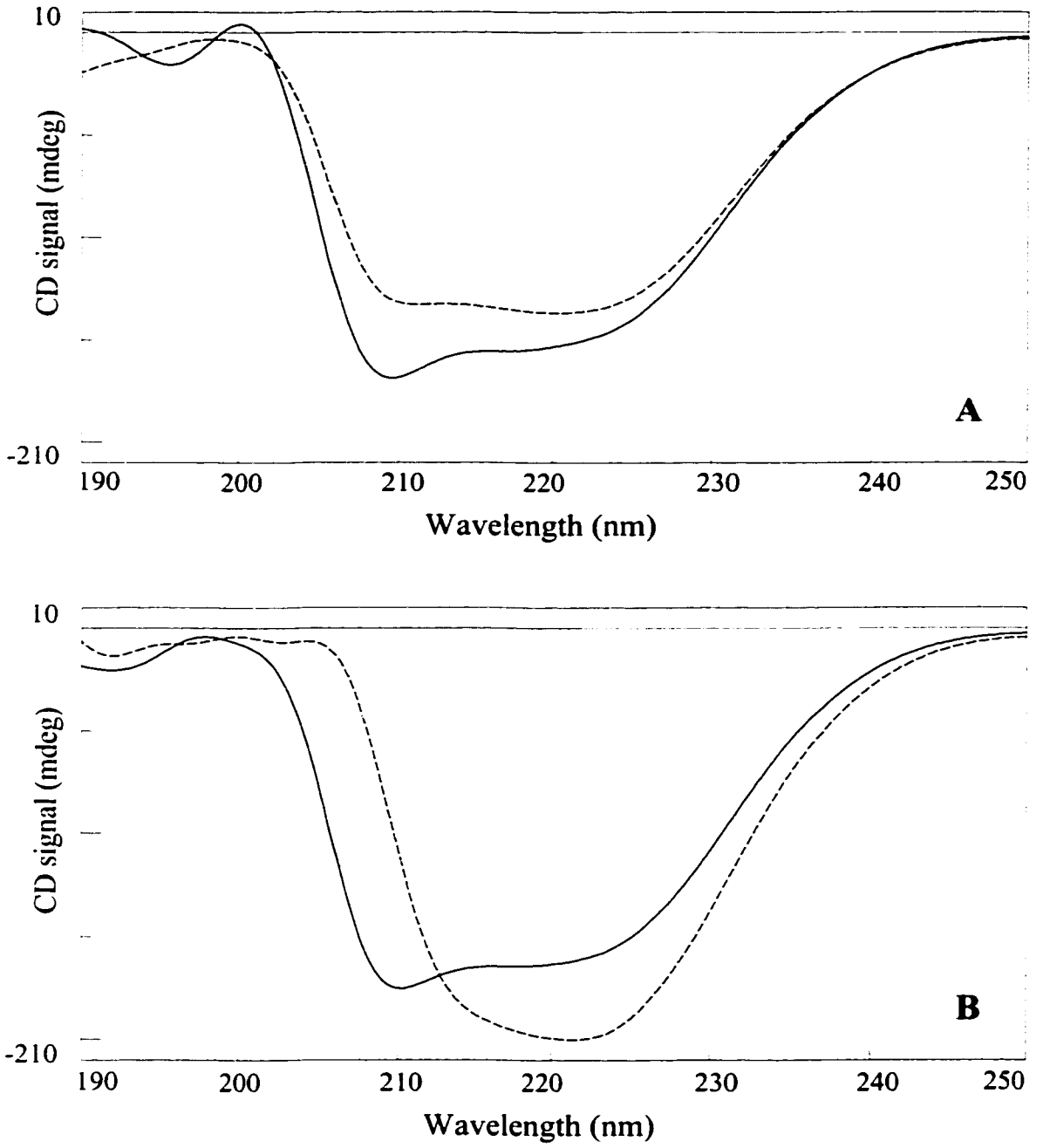

Figure 3.6 Far-UV CD spectra of the α-helical band of 2 mM HRP (solid line) and HRP-CN (dashed line) incubated for 3 h (frame A) and 12 h (frame B) in 1 M GdnHCl (in 100 mM NaPi buffer, pH 7, H_2O). The cyanide-ligated form was prepared by adding excess KCN (100 μM) to HRP. The CD spectra represent an average of 5 scans at a resolution of 0.2-nm, recorded using an FTIR cell with a 6-μM pathlength as described in Section 2.2.2.

3.3.3 Changes in secondary structure monitored by FTIR spectroscopy

The structure-sensitive FTIR amide I region (1700–1600 cm^{-1}) was utilized to monitor changes in the secondary structures of HRP and HRP-CN in the presence of 1 M GdnHCl, with respect to time. Samples were incubated for 3 h in 1 M GdnHCl and FTIR spectra were recorded every hour (up to 12 h).

The deconvolved FTIR amide I spectra of HRP in 1 M GdnHCl vs time are plotted in Figure 3.7, frame A. Upon deconvolution, bands at 1678, 1657, 1645 and 1615 cm^{-1} are resolved. According to the empirical rules (Table 1.1) and amino-acid side-chain absorptions (Table 1.2), these frequencies can be assigned to antiparallel β-sheets, α-helices, unordered structures and Arg residues, respectively. After 5 h, a band at 1622 cm^{-1} grows in which may be due to β-sheets. Between 7-11 h, the random-structure band gradually shifts to 1642 cm^{-1}. The time dependent changes observed are difficult to interpret and will be further analyzed in the discussion (Section 3.4).

Deconvolved FTIR amide I spectra of HRP-CN in 1 M GdnHCl vs time are plotted in Figure 3.7, frame B. Upon deconvolution, bands at 1679, 1657, 1645 and 1623 cm^{-1} are resolved, and are assigned to antiparallel β-sheets, α-helices, unordered structures and β-sheets according to the empirical rules (Table 1.1). Arg residues may also absorb at the same frequency as the β-sheet band. The intensities of all of the HRP-CN amide I components increase with time, however the 1623-cm^{-1} band exhibits the most pronounced growth.

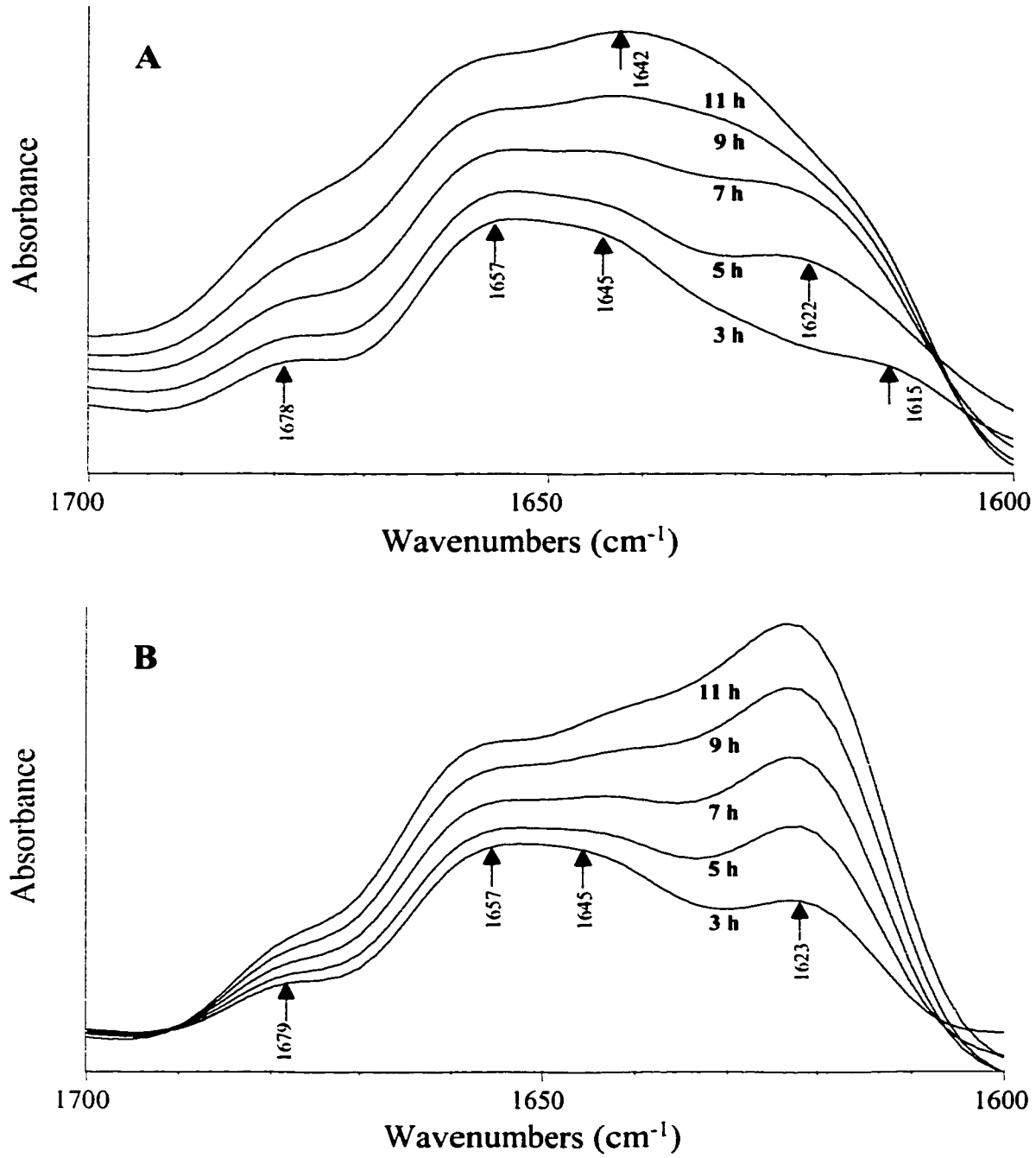

Figure 3.7 Stacked deconvolved FTIR amide I spectra of 2 mM (A) HRP and (B) HRP-CN in 1 M GdnHCl (in 100 mM NaPi buffer, pH 7, H_2O) *vs* time (3-, 5-, 7-, 9- and 11-h intervals). The cyanide-ligated form was prepared by adding KCN (0.1 mM) to HRP. The FTIR spectra represent an average of 256 scans at a resolution of 2 cm^{-1}, acquired using CaF_2 windows with a 6-μM pathlength.

3.4 DISCUSSION

HRP is one of the most widely studied heme peroxidases, which was the reason it was initially chosen as a model system for this work. However, as illustrated by the results, HRP is not an ideal model to study protein chemical denaturation by FTIR spectroscopy. Examining the GdnHCl-denatured states of proteins by FTIR is a novel technique that has only recently been reported; therefore, a simpler protein model system was required. HRP contains structural elements such as calcium ions, disulfide bridges and heterogeneously glycosylated sites that may contribute to spectral perturbations.

The FTIR results revealed complex time-dependent spectral changes for HRP and its CN^- adduct (HRP-CN) over the first 24 h in 1 M GdnHCl. In addition, these time-dependent spectral changes rendered subtraction of background absorption difficult. In order for subtraction to be reliable, it must be performed on high quality, reproducible data. It is hypothesized that time-dependent changes in HRP-CN are enhanced by cleavage of disulfide bridges in the protein by excess CN^- nucleophile. Fluorescence studies performed by Tsaprailis *et al.* (*64*) on DTT- and EDTA-treated HRP revealed half-lives of unfolding of only ~0.4 s for the modified protein, and 519 s for the untreated protein. DTT reduces the disulfide bridges and EDTA chelates the calcium ions, which are clearly necessary for the conformational stability of HRP. It is speculated that HRP-CN is less stable than HRP due to cyanide-induced cleavage of one or more of the 4 disulfide bridges in the protein. Cleavage of the Cys11-Cys91 disulfide is the most likely since it is the most solvent-exposed (*66*).

From the fluorescence results in Figure 3.3, it is obvious that the global unfolding of HRP and HRP-CN in GdnHCl is very different. It appears that HRP-CN undergoes

complete unfolding in 2.5 M GdnHCl, since no significant change in fluorescence intensity is observed from 2.5-6 M GdnHCl. HRP, on the other hand, seems to unfold more gradually and may not be fully unfolded in 6 M GdnHCl after 24 h. As expected, the fluorescence intensity increases due to the relief of heme quenching of Trp fluorescence as the concentration of GdnHCl increases. In addition, the emission maximum red-shifts to 350 nm, indicating that Trp117 is in a solvent-exposed environment and not buried within the protein core.

Time-dependent changes in HRP and HRP-CN under mild (1 M GdnHCl) and strong (6 M GdnHCl) denaturing conditions were probed via fluorescence spectroscopy. The onset of denaturation was slow in 1 M GdnHCl (Figure 3.4), and even after 24 h the $\%F_{350}$ values are less than 10%, suggesting that the tertiary structures are slightly disrupted. In 6 M GdnHCl (Figure 3.4), significant loss of tertiary structure is observed for HRP and HRP-CN after 18 h. Surprisingly, $\%F_{350}$ data exhibited opposite trends in 1 and 6 M GdnHCl. After 24 h, the $\%F_{350}$ value was 2% greater for HRP than HRP-CN in 1 M GdnHCl, while in 6 M GdnHCl, the $\%F_{350}$ value for HRP was ~10% less than for HRP-CN. Cyanide binding appears to have a stabilizing effect on HRP in 1 M GdnHCl. A more stable heme cavity as a result of a stronger distal H-bonding network on CN^- binding may account for the decreased sensitivity to low concentrations of GdnHCl of HRP-CN relative to HRP (*66*). However, in 6 M GdnHCl the opposite is true, which may be because this denatured form is more susceptible to cleavage of its disulfide bridges by CN^-. After 48 h in 6 M GdnHCl (data not shown), unfolding appeared to be almost complete, and both proteins have a $\%F_{350}$ value of ~65.5%. Pappa and Cass (*23*) performed fluorescence and CD experiments, and found that below 1 M GdnHCl the

heme is intact and loss of heme is only observed at concentrations of GdnHCl greater than 5 M.

CD spectroscopy was employed to monitor changes in the α-helical content of HRP and HRP-CN with respect to time. The CD spectra reveal that the α-helical signal for HRP remains relatively constant over 3-12 h incubation in 1 M GdnHCl. HRP-CN, on the other hand, exhibits more pronounced time-dependent changes in its α-helical absorption band. The helical signal for HRP-CN becomes increasingly negative between 3 and 12 h, suggesting that cyanide binding to HRP has a slightly stabilizing effect in 1 M GdnHCl (see previous paragraph), which was also observed by fluorescence spectroscopy.

The structure-sensitive FTIR amide I mode was used to monitor the loss of secondary structure during the onset of chemical denaturation. As judged by the spectra in Figure 3.7, it is evident that HRP and HRP-CN do not have identical secondary structures after 3-h incubation in 1 M GdnHCl. In addition, HRP and HRP-CN undergo very different time-dependent spectral changes under these mildly denaturing conditions. In the FTIR spectra of HRP in 1 M GdnHCl (Figure 3.7 frame A), the most remarkable change is the increased absorption at ~1642 cm^{-1} with time. This intensification in the region of random coil absorption (Table 1.1) suggests that a time-dependent loss of secondary structure occurs in 1 M GdnHCl. In Figure 3.7 frame B on the other hand, the component bands for HRP-CN absorb at the same frequencies, however absorption increases proportionally with time. A major increase in the 1623 cm^{-1} band occurs, which was assigned to β-sheets according to the empirical rules (Table 1.1).

In addition, the FTIR spectra in Figure 3.7 provide no evidence to suggest that GdnHCl associates with HRP or HRP-CN. As illustrated in Section 2.3.2, associated GdnHCl absorbs at the high frequency end of the FTIR amide I region (~1660-1668 cm^{-1}). It is important to note that the FTIR data presented in this chapter were of HRP and HRP-CN in 1 M GdnHCl, which may not be a high enough concentration to observe GdnHCl association. In Chapter 2 (Section 2.4), it was speculated that GdnHCl interacted preferentially with the lysyl side chains of PLL, and only ~2% of HRP's amino acid composition is due to Lys residues (*60*).

3.5 CONCLUSION

The complex time-dependent changes observed in the FTIR and CD spectra of HRP and HRP-CN are difficult to interpret, therefore HRP is not a good model system to study chemical denaturation. Since the use of FTIR to study protein chemical denaturation is a novel technique, cytochrome c was chosen as a simpler model and the results are presented in Chapter 4.

CHAPTER 4: INVESTIGATION OF THE GdnHCl-DENATURED STATE OF CYTOCHROME C VIA FTIR, CD AND FLUORESCENCE SPECTROSCOPIES

4.1 INTRODUCTION

Spectroscopic tools were utilized to probe the guanidine hydrochloride (GdnHCl) denatured states of ferricytochromes c (Fe^{III}) from horse and tuna. Cytochrome c was chosen as a model system for numerous reasons. It is stable, readily available in highly purified forms from commercial sources, has been studied extensively in the literature and its crystal structure has been solved.

Cytochrome c is a small electron-transfer protein with a M_r ~12,500 Da, containing 103-113 amino acids depending on the species from which it is derived. It is a member of the mitochondrial respiratory chain found in eukaryotes, and is located in the intermembrane space of the mitochondria (*57*). Its primary role is as an electron carrier between cytochrome c reductase and cytochrome c oxidase in the respiratory chain. During this process, the heme iron is cycled between Fe^{II} and Fe^{III} oxidation states (*40*).

Cytochrome c is made up of a single polypeptide chain bound to a protoporphyrin IX heme prosthetic group, which is important for the protein's function as an electron carrier (*68*). The heme moiety is covalently bound to the peptide backbone through thioether linkages with Cys14 and Cys17 residues. The iron center is coordinated by two axial ligands, His18 and Met80 and adopts a low-spin configuration (*69*). The prosthetic group is almost completely buried, with 7.5% of the heme surface exposed to the external environment (*58*). The linkages between the heme and the protein moiety, the H-bonding network and intramolecular linking between His18 and Met80 contribute to the overall

stability of cytochrome c (*68*). The structure of cytochrome c with important secondary structural elements and residues is shown in Figure 4.1.

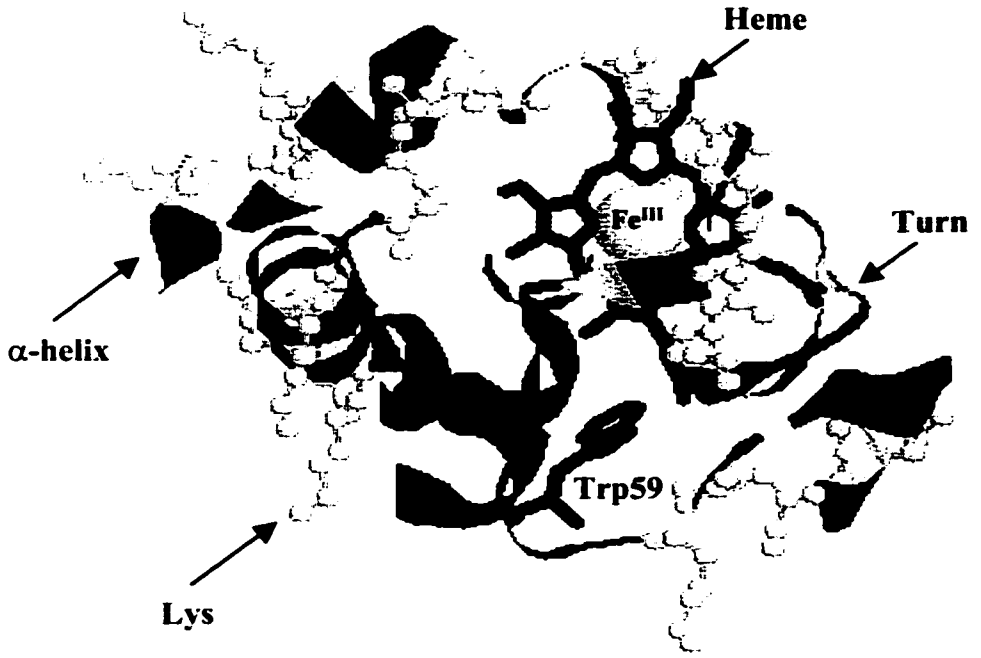

Figure 4.1 C_α backbone of horse cytochrome c showing the heme group, α-helices, β-turns, Trp59 and Lys residues. Tuna cytochrome c has similar structure, therefore is not shown here. The protein coordinates were obtained from the Pubmed NCBI website (www.ncbi.nlm.nih.gov/Pubmed/medline.html) and the figure was generated by Rasmol software.

As can be seen from Figure 4.1, cytochrome c is predominately α-helical with a significant contribution from β-turns. There are 3 major α-helices (C-terminus, N-terminus and 60's) as well as 2 minor α-helices (50's and 70's), which represent ~45% of the protein's secondary structure (*58*). The 5 helices are interconnected by strands of polypeptide chain and folded into a globular shape, within which the heme

pocket is formed. There are two type III β-turns (~8%) and four type II β-turns (~14%), such that β-turns represent 22% of the overall secondary structure of the protein.

Pairing of the N- and C-terminal α-helices in a perpendicular arrangement is a structural motif that is conserved in all cytochromes c (*48*). Packing of the two helices from opposite ends of the polypeptide chain is important for the stability of the protein, and kinetic studies revealed that pairing of these helices is the earliest detectable structural event during folding (*48*). The helix-helix interface is flexible and contains a bulky hydrophobic residue (Leu94), which is important for the stability of the protein (*48*).

There exists a wide range of homologous cytochromes c that can be used to study structure-function relationships (*57*). Therefore, subtle differences between homologous cytochromes c, such as horse and tuna species can be investigated. Some features found in all cytochromes c include: covalent linkages between the heme group and the polypeptide, axial ligands to the heme iron (His18 and Met80), pairing of the N- and C-terminal α-helices and a cluster of three helices around the heme edge (60's, N- and C-terminal) (*48*).

Horse and tuna cytochromes c have almost identical main-chain folds despite the fact that their sequence differs by 19 amino acids as shown in Figure 4.2 (*57, 58*). Of the 19 substitutions, 2 involve aromatic residues, 11 involve aliphatic residues charged at pH 7 and the remaining 6 represent uncharged aliphatic residues (*70*). There are two main regions where substitutions occur: residues 44-47 where all but Gly45 are replaced; and residues 58-62 where all but Trp 59 are replaced. Conversely, there is a large stretch from Thr63 to Lys88 (26 residues) where no substitutions occur (*57*).

	1 10	20	30
Horse	GDV**E**KGKK**I**F	VQKCAQCHTV	E**K**GGKHK**T**GP
Tuna	GDV**A**KGKK**T**F	VQKCAQCHTV	E**N**GGKHK**V**GP

	40	50	60
Horse	NL**H**GLFGRKT	GQA**P**G**F**TYTD	ANK**N**KGI**T**W**K**
Tuna	NL**W**GLFGRKT	GQA**E**G**Y**SYTD	ANK**S**KGI**V**W**N**

	70	80	90
Horse	**EE**TLMEYLEN	PKKYIPGTKM	IFAGIKKK**T**E
Tuna	**ND**TLMEYLEN	PKKYIPGTKM	IFAGIKKK**G**E

	100	104
Horse	R**E**DL**I**AYLK**K**	AT**NE**
Tuna	R**Q**DL**V**AYLK**S**	AT**S**

Figure 4.2 Sequence alignment of horse and tuna cytochromes c. Single letter codes are used for amino acid residues. The non-conserved amino acid residues are underlined and in **boldface** type.

The amino acid composition of horse and tuna cytochromes c is given in Table 4.1 (*71*). The FTIR frequencies for the amino acid side chains are listed in Table 1.2. Lysine (K) is the most abundant amino acid found in both proteins, with 19 and 16 residues for horse and tuna cytochromes c, respectively. This was another reason why poly-L-lysine (PLL) was chosen as a model; to study the interaction of guanidinium ions with the Lys-rich regions of cytochrome c. The interactions of GdnHCl and Gdn-d_5-DCl with PLL are discussed in Chapter 2.

Table 4.1: Amino acid composition for horse and tuna cytochromes c

Amino acid name	Letter symbol	Horse cyt c	Tuna cyt c	Characteristic of amino acid at pH 7
Glycine	G	12	13	simplest, aliphatic, optically inactive
Alanine	A	6	7	aliphatic
Valine	V	3	6	aliphatic, hydrophobic
Leucine	L	6	6	aliphatic, hydrophobic
Isoleucine	I	6	4	aliphatic, hydrophobic
Serine	S	-	4	aliphatic, OH-containing
Cysteine	C	2	2	S-containing, hydrophilic, pK_a 8.5
Threonine	T	10	7	aliphatic, OH-containing
Methionine	M	2	2	S-containing, hydrophobic
Phenylalanine	F	4	3	aromatic, very hydrophobic
Tyrosine	Y	4	5	aromatic, very hydrophobic, pK_a 10
Tryptophan	W	1	2	aromatic, hydrophobic
Proline	P	4	3	aliphatic, cyclic structure
Histidine	H	3	2	hydrophilic, uncharged or (+)ve, pK_a 6.5
Lysine	**K**	**19**	**16**	basic, hydrophilic, (+)ve, pK_a 10
Arginine	R	2	2	basic, hydrophilic, (+)ve, pK_a 12
Aspartic acid	D	3	4	acidic, (-)ve, pK_a 4.4
Glutamic acid	E	9	5	acidic, (-)ve, pK_a 4.4
Asparagine	N	5	6	acidic, uncharged
Glutamine	Q	3	4	acidic, uncharged

Most of the substitutions of horse and tuna cytochromes c occur on the molecular surface of the protein. NMR studies were used to monitor the effects of sequence changes on the chemical shifts of NH and $C_\alpha H$ protons (*57*). The largest difference in proton shifts was observed in the 60's helix involving residues 60-62. However, NMR

data revealed that the backbone conformations and the H-bonding networks are very similar despite these amino acid substitutions. Both proteins are highly charged at pH 7.0, with a net charge of +8 (*57*). Their structures about the heme group were also found to be almost identical based on NMR shifts (*70*). Five water molecules at conserved positions were identified, which play an important role in the mechanism of action and stability of the protein (*58*). It would appear that the sequence changes for horse and tuna cytochromes c have either compensatory or no effects on the native structure. This, as well as the denatured state will be further investigated using the spectroscopic probes discussed in Chapter 1. Results from chemical and thermal denaturation will be compared in Section 4.4.

4.2 EXPERIMENTAL PROCEDURES

4.2.1 Materials

Lyophilized ferricytochrome c (Fe^{III}) from horse heart (Type VI, M_r 12,384) and tuna heart (Type XI, M_r 12,170) were obtained from Sigma and used without further purification. Other reagents, *i.e.* NATA, GdnHCl and Gdn-d_5-DCl were obtained from the suppliers listed in Sections 2.2.1 and 3.2.1. Sodium phosphate buffers (100 mM) were prepared as described in Section 2.2.1. The concentration of cytochrome c (ε_{410} = 106.1 $mM^{-1}cm^{-1}$) (*72*) stock solutions were determined spectrophotometrically using a Hewlett-Packard 8451A diode array spectrophotometer. Protein stock solutions were diluted to the desired concentrations with buffer and the appropriate amount of denaturant. The concentration of NATA (ε_{280} = 5.69 $mM^{-1}cm^{-1}$) (*67*) fluorescence standard was also determined spectrophotometrically.

4.2.2 Methods

Fluorescence spectroscopy

Fluorescence experiments were performed as described in Section 3.2.2. The final concentration of horse and tuna cytochrome c in each sample was 2.0 μM. Fluorescence intensities were standardized (100% fluorescence) relative to 2.0 μM NATA for horse and 4.0 μM NATA for tuna. Standardization was required since horse c contains one Trp, while tuna c has two. Emission of the blank (0-5 M GdnHCl in buffer) was subtracted from the protein and standard samples. Percent relative fluorescence ($\%F_{350}$) was calculated using equation 3.2. The protein samples were allowed to denature (~24 h) at room temperature prior to recording the fluorescence spectra to ensure equilibrium conditions were reached.

CD spectroscopy

CD experiments were performed as described in Section 2.2.2. Advantages on the use of an FTIR cell to acquire CD data were discussed in Section 2.2.2. The stock solution of horse and tuna cytochromes c were diluted to 2.0 mM (~25 mg/mL) with buffer and the required amount of denaturant. Absorption of the blank (GdnHCl in buffer) was subtracted from the protein sample and the final spectra were smoothed with Jasco software. The observed ellipticity was converted to molar ellipticity (I) using equation 2.1.

FTIR spectroscopy

FTIR spectra were recorded as described in Section 2.2.2. The final concentration of horse and tuna cytochrome c in each sample was 2.0 mM (~25 mg/mL) diluted from the stock solutions with buffer and a suitable amount of denaturant. Contributions from water and denaturant were removed from the raw spectrum via the subtraction procedure of Dong *et al.* (*40*) outlined in Section 2.2.2. Fourier transform self-deconvolution (FSD) of the broad amide I envelope allowed resolution of the component bands and assignment of secondary structural elements. Deconvolution parameters used were HWHH of 15 cm^{-1} and an enhancement (K factor) of 1.8.

4.3 RESULTS

4.3.1 Cytochrome c denaturation as monitored by fluorescence spectroscopy

Fluorescence spectroscopy was used to monitor the global unfolding of the polypeptide backbone of cytochromes c from horse and tuna in the presence of GdnHCl (H_2O). Trp was used as a built-in fluorescent probe, which is sensitive to the overall conformation of the protein moiety during unfolding. Horse c has one tryptophan (Trp59), while tuna c has two (Trp33 and Trp59) (*57*). As mentioned in Section 3.3.1, intrinsic fluorescence from Trp reports on the surrounding microenvironment, and a Trp residue exposed to water fluoresces at 350 nm, whereas a Trp that is buried emits at ~330 nm (*16*).

Fluorescence intensities were compared to the NATA standard (Figure 3.2) under the same experimental conditions. NATA resembles a solvent-exposed Trp in solution, and is assumed to fluoresce at 100%. The percent relative fluorescence ($\%F_{350}$) of the

cytochrome c samples were computed using equation 3.1. The $\%F_{350}$ values vs concentration of GdnHCl are plotted in Figure 4.3 for both horse and tuna c.

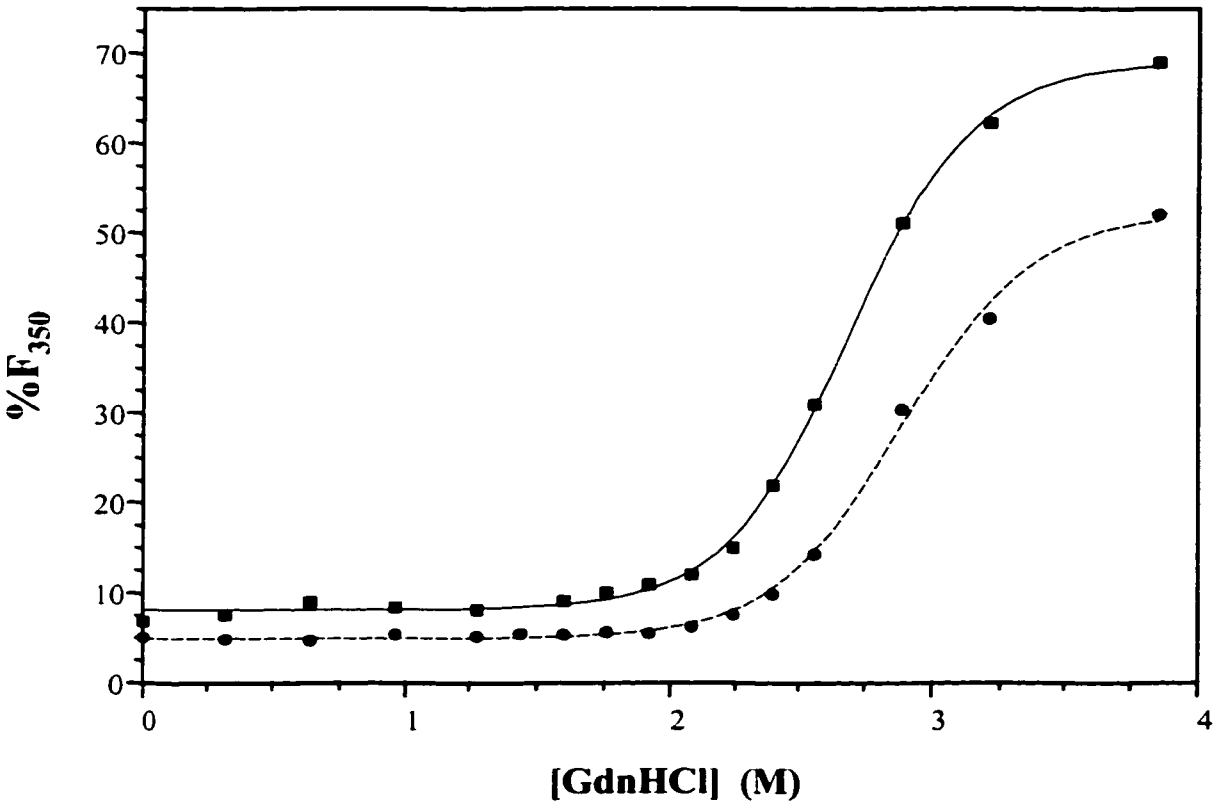

Figure 4.3 Percent relative fluorescence ($\%F_{350}$) vs [GdnHCl] (in 100 mM NaPi buffer, pH 7, H_2O) for 2 μM horse (solid line & squares) and tuna (dashed line & circles) cytochromes c. Experimental conditions given in Section 4.2.2.

The curves shown in Figure 4.3 have approximately the same sigmoidal shape assuming an $N \rightleftharpoons D$ transition, which implies that horse and tuna c have similar cooperativities of unfolding in the presence of GdnHCl (*4*). The $[GdnHCl]_{1/2}$ values, computed by Origin software (sigmoidal fit) represent the concentration of GdnHCl at

which 50% of the protein's molecules have unfolded. The $[GdnHCl]_{1/2}$ values were 2.7 and 2.9 M for horse and tuna c, respectively, when the excitation wavelength was fixed at 280 nm. These results are consistent with the literature values, i.e. 2.5-3.0 M for horse c (*48*, *73*, *49*, *17*) and 2.6-3.0 M for tuna c (*73*). The $[GdnHCl]_{1/2}$ values from this study and the literature consistently show that $[GdnHCl]_{1/2}$ is greater for tuna compared to horse c.

Tryptophan was excited at 280 and 295 nm, while emission was scanned from 300 to 450 nm. When the excitation wavelength is set at 280 nm, both Trp and Tyr are excited, therefore the fluorescence signal is stronger, whereas at 295 nm only Trp is excited (*16*). Fluorescence spectra recorded at 295 nm (data not shown), yielded essentially identical band shapes and $[GdnHCl]_{1/2}$ values to those obtained at 280 nm. For example, the $[GdnHCl]_{1/2}$ values for horse c were 2.69 and 2.65 M at λ_{ex} of 280 and 295 nm, respectively. Similarly for tuna cyt c, the $[GdnHCl]_{1/2}$ values were 2.89 and 2.88 M at λ_{ex} of 280 and 295 nm. Thus, the contribution of Tyr emission to the 280-nm excitation spectra appears to be negligible.

Fluorescence spectra of horse and tuna c in 0-4 M GdnHCl are presented in Figure 4.4. Trp fluorescence intensifies with increasing concentration of GdnHCl due to relief of heme quenching on fluorescence. This is due to the increased separation between the Trp fluorescent donor and the heme acceptor. As expected, the emission maxima for horse and tuna c in GdnHCl are red-shifted, which is indicative of a change in the Trp environment from hydrophobic (protein interior) to hydrophilic (solvent exposed).

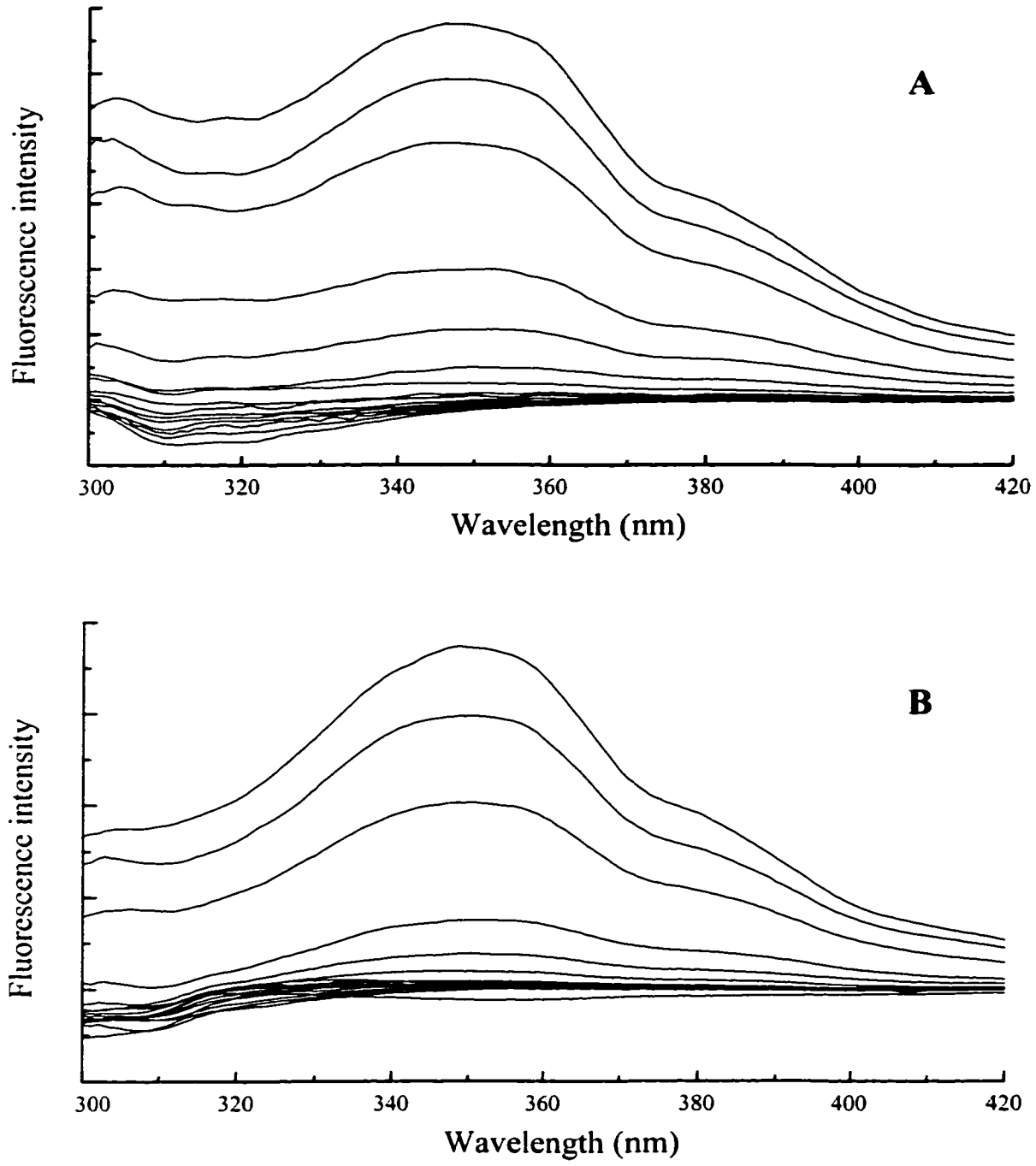

Figure 4.4 Stacked fluorescence spectra (λ_{ex} = 280 nm) of 2 μM (A) horse and (B) tuna cytochromes c in 0-4 M GdnHCl (in 100 mM NaPi buffer, pH 7, H_2O). Spectra are stacked from bottom to top in order of increasing concentration of GdnHCl.

4.3.2 Secondary structure changes in GdnHCl as monitored by far-UV CD spectroscopy

CD spectroscopy was used to monitor the α-helical content of horse and tuna c in GdnHCl. Changes in the characteristic strong negative α-helical bands at 209 and 222 nm were observed. As discussed previously (Section 1.2.1), CD and FTIR are complementary techniques and CD is sensitive to α-helices, while FTIR is preferred for the study of turns and sheets (*35*). Since cytochrome c is predominately α-helical (Figure 4.1), CD spectroscopy was used to aid in the interpretation of the FTIR results shown in Section 4.3.3.

The far-UV CD region of horse and tuna c in buffer is shown in Figure 4.5. This amide region is dominated by contributions from peptide bonds and is used to report on protein secondary structure, in particular α-helices (*1*). The presence of an intense double minima at 209 and 222 nm is consistent with a high α-helical content in both proteins. However, the CD spectra of horse and tuna c are not superimposable, suggesting that slight differences exist between their native α-helical structures. Tuna c has a stronger negative signal, especially in its 209-nm band. The positive feature at 196 nm can be assigned to the presence of β-turns according to the empirical rules given in Table 1.3.

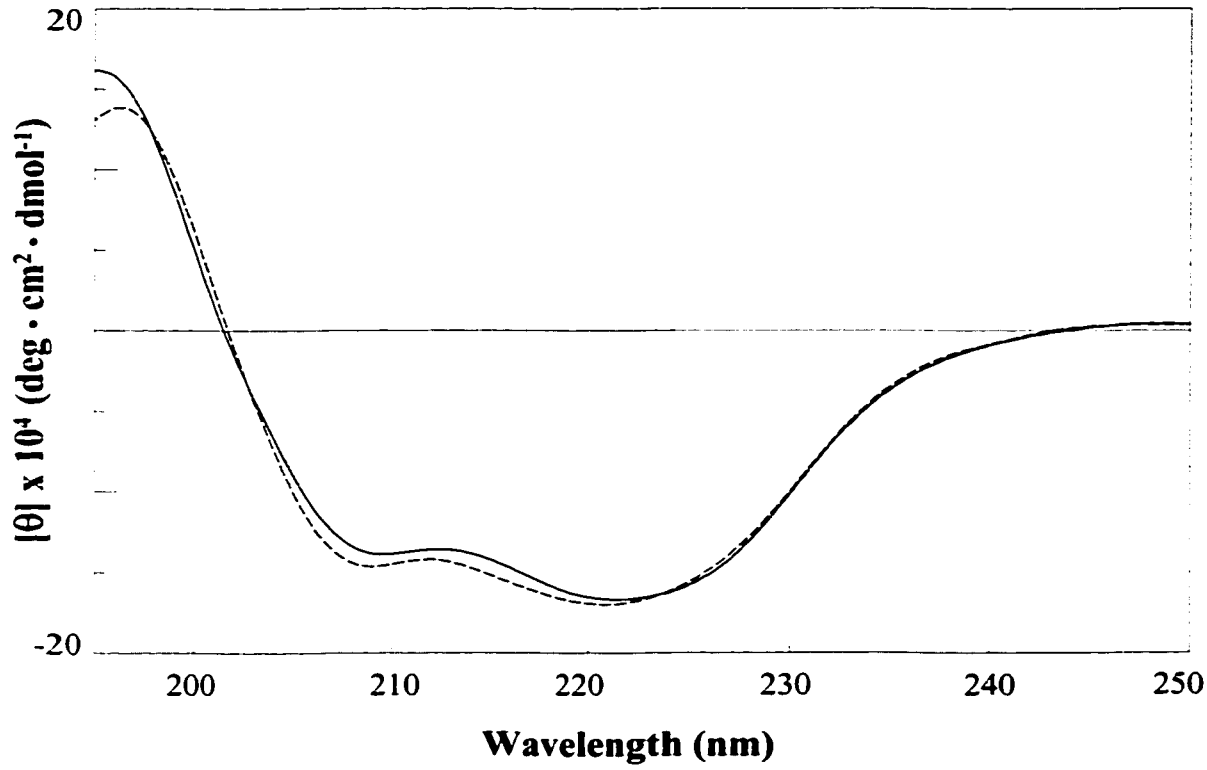

Figure 4.5 Overlaid far-UV CD spectra of 2 mM horse (solid line) and tuna (dashed line) cytochromes c in 100 mM NaPi buffer, pH 7, H_2O. The spectra represent an average of 5 scans at a resolution of 0.2-nm recorded using an FTIR cell with a pathlength of 6-μM as described in Section 2.2.2.

The CD amide region of horse and tuna cytochromes c in 3 M GdnHCl is presented in Figure 4.6. Although most of their α-helical structure is lost, horse and tuna c do not adopt similar conformations in 3 M GdnHCl. The CD signal generated by horse c is much more intense than that of tuna c. Horse c has a positive band at 197 nm that can be assigned to turns, negative bands at 201 and 206 nm which absorb in the random-coil region, as well as a minor absorption at 222 nm due to the presence of residual helical structure. The CD spectrum of tuna c reveals a positive feature at 197 nm due to turns, a single broad band at 205 nm from random structures and a small absorption at 222 nm due to residual helical structure.

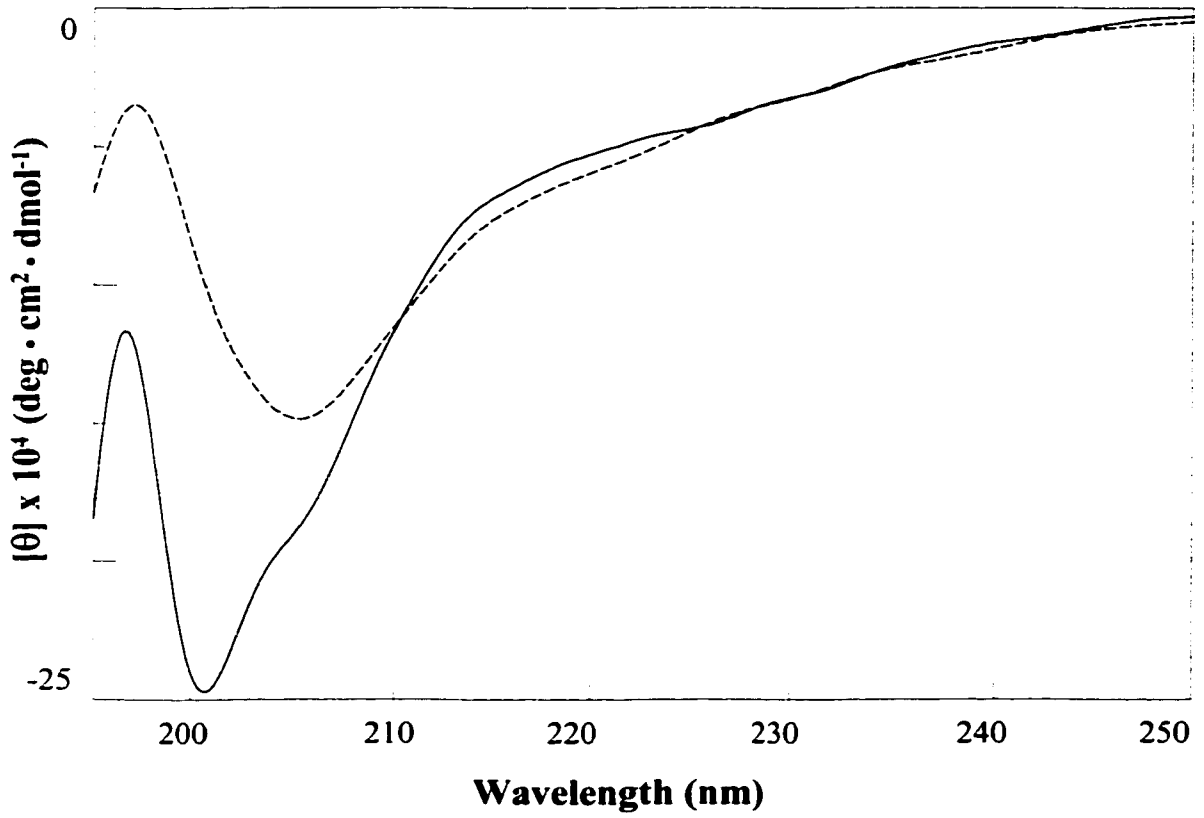

Figure 4.6 Overlaid far-UV CD spectra of 2 mM horse (solid line) and tuna (dashed line) cytochromes c in 3 M GdnHCl (in 100 mM NaPi buffer, pH 7, H_2O). The spectra represent an average of 5 scans at a resolution of 0.2-nm recorded using an FTIR cell with a pathlength of 6-μM as described in Section 2.2.2.

The CD amide region of horse and tuna cytochromes c in 5 M GdnHCl is presented in Figure 4.7. There is no absorption at 222 nm indicting total loss of helical structure in 5 M GdnHCl. Nonetheless, both cytochromes c exhibit different far-UV CD profiles. The spectrum of horse c reveals a predominant negative broad band centered at 201 nm. The spectrum of tuna c in 5 M GdnHCl resembles that of horse c in 3 M GdnHCl (Figure 4.6) with a positive band at 197 nm assigned to turns, which are common features of denatured proteins (*9*). In addition, tuna c has a sharp negative band

at 202 with a shoulder at 206 nm, which are assigned to random structures according to empirical rules (Table 1.3).

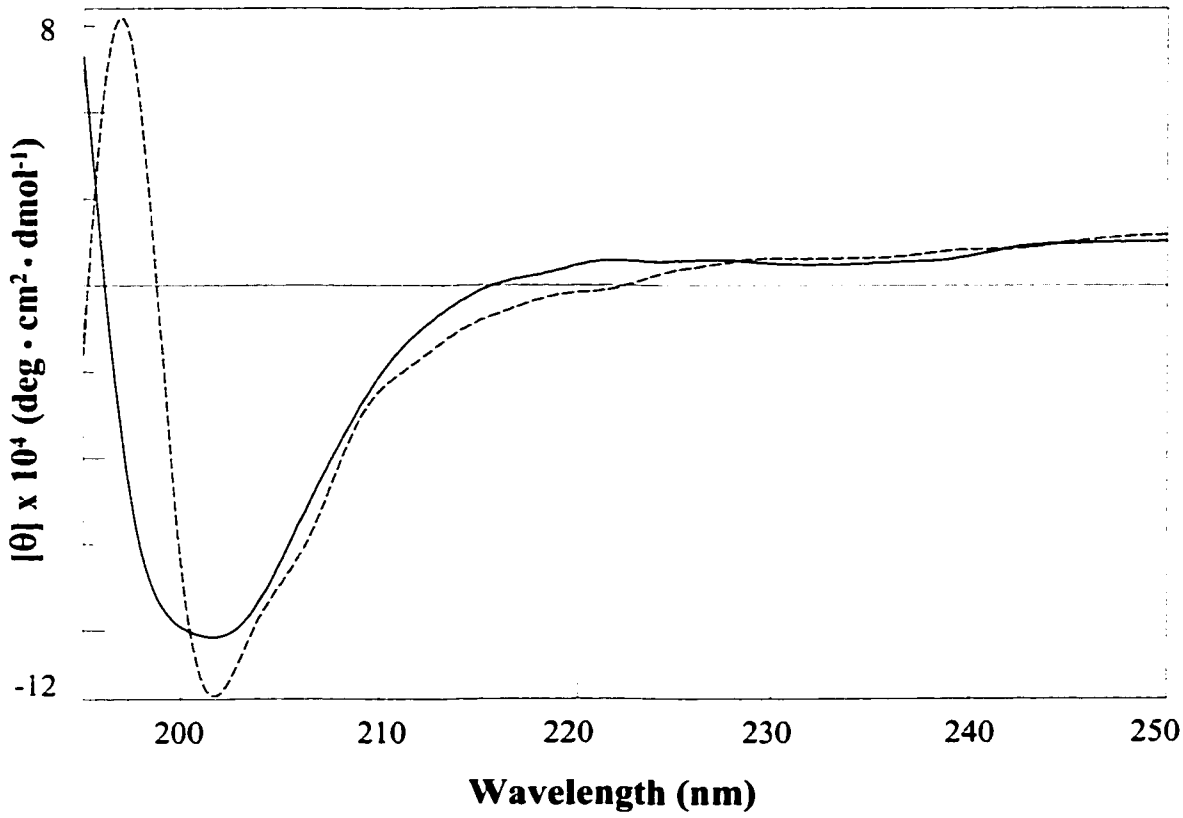

Figure 4.7 Overlaid far-UV CD spectra of 2 mM horse (solid line) and tuna (dashed line) cytochromes c in 5 M GdnHCl (in 100 mM NaPi buffer, pH 7, H_2O). The spectra represent an average of 5 scans at a resolution of 0.2-nm recorded using an FTIR cell with a pathlength of 6-μM as described in Section 2.2.2.

Overlaid CD spectra of horse cytochrome c in 0-4 M GdnHCl are presented in Figure 4.8. The spectra of horse c in 0-2 M GdnHCl are shown in frame A. The spectra in buffer and 1 M GdnHCl are very similar, except that the α-helical signal is more intense in buffer. In 1.5 and 2 M GdnHCl, a positive feature at 197 nm assigned to turns begins to grow in. Even though there are slight differences in the spectra from 0-2 M

GdnHCl, it appears that the α-helicity is not disrupted. In frame B, the CD spectra of horse c in 2.5-4 M GdnHCl are shown. As illustrated, a dramatic change from 2-2.5 M GdnHCl occurs, where most of the α-helical signal is lost. In 2.5 M GdnHCl, ~50% of the α-helicity is observed, accompanied by negative bands at 198 and 205 nm assigned to random structures. Horse c in 3 M GdnHCl was previously analyzed in Figure 4.6. Horse c in 4 M GdnHCl appears to possess mainly random structures, as does horse c in 5 M GdnHCl (Figure 4.7).

Overlaid CD spectra of tuna cytochrome c in 0-4 M GdnHCl are presented in Figure 4.9. In frame A, the spectra of tuna c in 0-2 M GdnHCl are shown. The spectra of tuna c in buffer, 1 M and 1.5 M GdnHCl are similar. Slight differences are observed in 1.5 M GdnHCl, where the positive band at 197 nm due to turns intensifies and the α-helical signal at 209 nm diminishes. In 2 M GdnHCl, the α-helical signal appears to be increasingly negative and the band due to turns is decreased. Even though there are slight differences in the spectra from 0-2 M GdnHCl, it appears that the α-helicity is not disrupted. In frame B, the CD spectra of tuna c in 2.5-4 M GdnHCl are presented. A dramatic change from 2-2.5 M GdnHCl occurs, resulting in the loss of most of the α-helical signal, which was also observed for horse c (Figure 4.8). In 2.5 M GdnHCl, ~50% of the α-helicity is detected, along with bands at 199 and 206 nm due to random structures. Tuna c in 3 M and 5 M GdnHCl was previously analyzed from Figure 4.6 and 4.7, respectively. Tuna c in 4 M GdnHCl exhibited random structural features, which are different from those observed for horse c in 4 M GdnHCl.

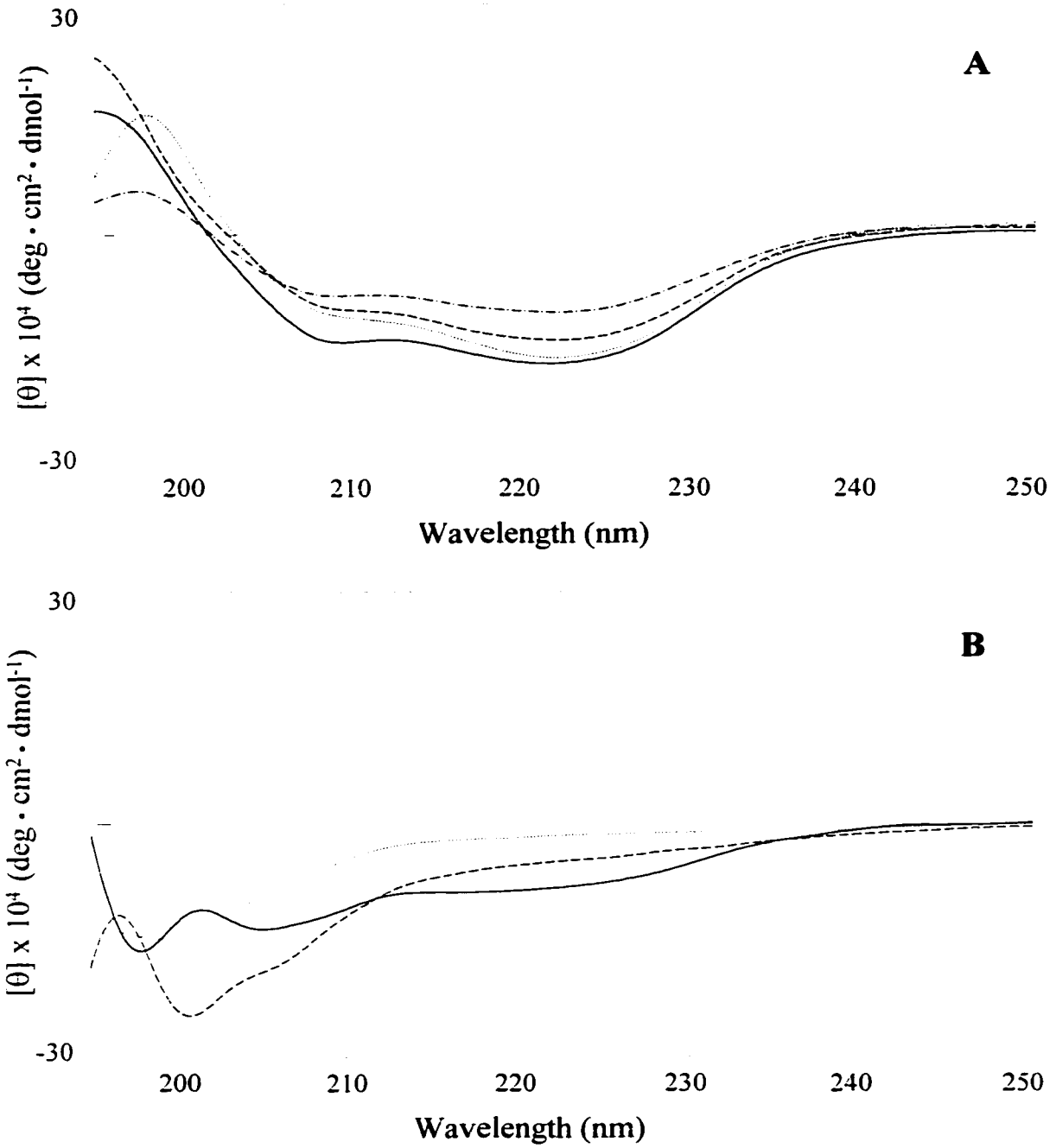

Figure 4.8 Overlaid far-UV CD spectra of 2 mM **horse** cytochrome c in 0-4 M GdnHCl (in 100 mM NaPi buffer, pH 7, H_2O). In frame A (0-2 M): 0 M (solid), 1 M (dashed), 1.5 M (dotted) and 2 M (mixed dashed/dotted) spectra are plotted. In frame B (2.5-4 M): 2.5 M (solid), 3 M (dashed) and 4 M (dotted) spectra are shown. The spectra represent an average of 5 scans at a resolution of 0.2-nm recorded using an FTIR cell with a pathlength of 6-μM as described in Section 2.2.2.

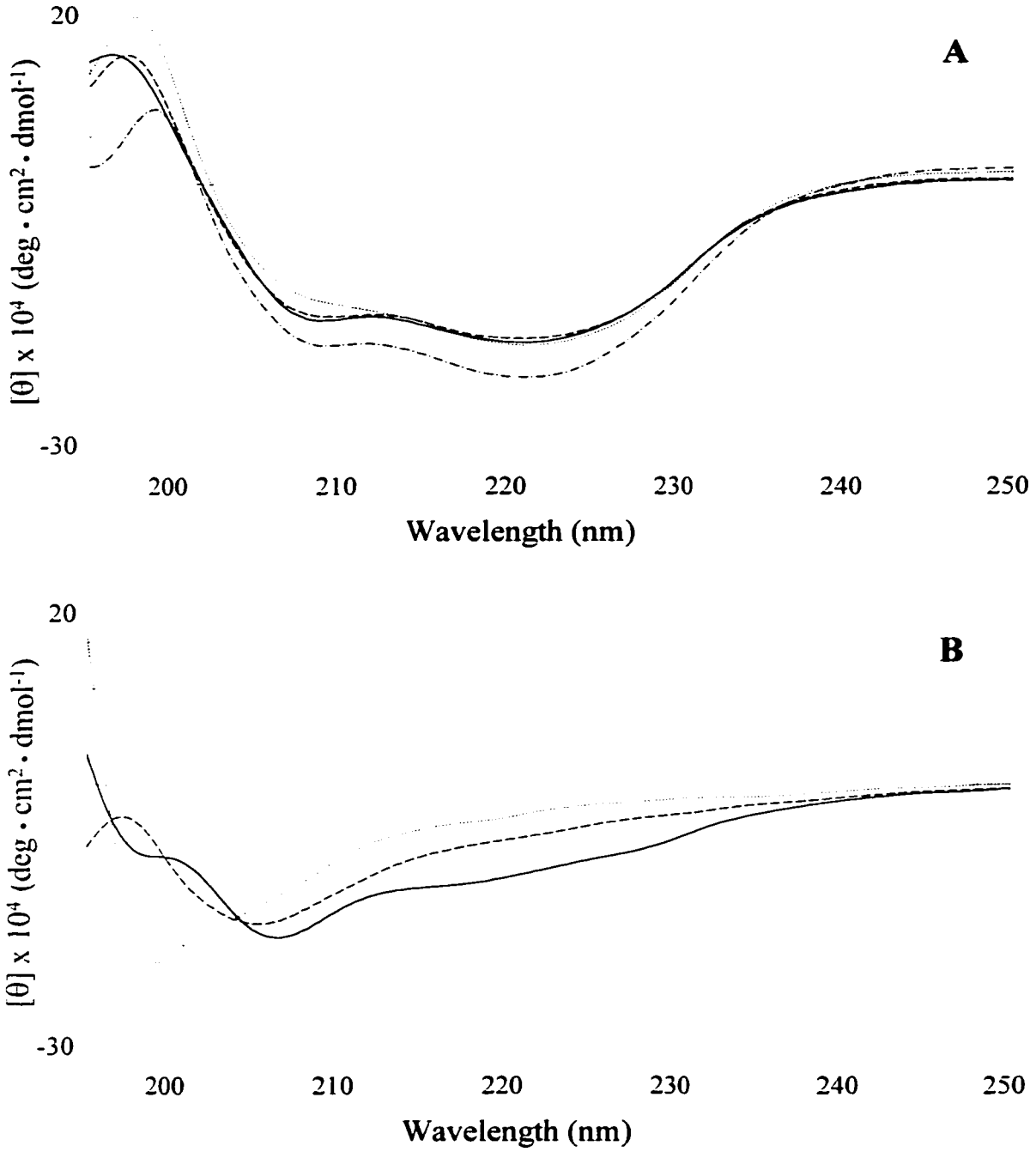

Figure 4.9 Overlaid far-UV CD spectra of 2 mM **tuna** cytochrome c in 0-4 M GdnHCl (in 100 mM NaPi buffer, pH 7, H_2O). In frame A (0-2 M): 0 M (solid), 1 M (dashed), 1.5 M (dotted) and 2 M (mixed dashed/dotted) spectra are plotted. In frame B (2.5-4 M): 2.5 M (solid), 3 M (dashed) and 4 M (dotted) spectra are shown. The spectra represent an average of 5 scans at a resolution of 0.2-nm recorded using an FTIR cell with a pathlength of 6-μM as described in Section 2.2.2.

Since cytochrome c is predominately α-helical, changes in the helical signal in the presence of denaturants is of interest. The lost of α-helical intensity in increasing concentrations of GdnHCl was monitored at 222 nm. The molar ellipticity at 222 nm, $[\theta]_{222}$, *vs* GdnHCl concentration is plotted in Figure 4.10.

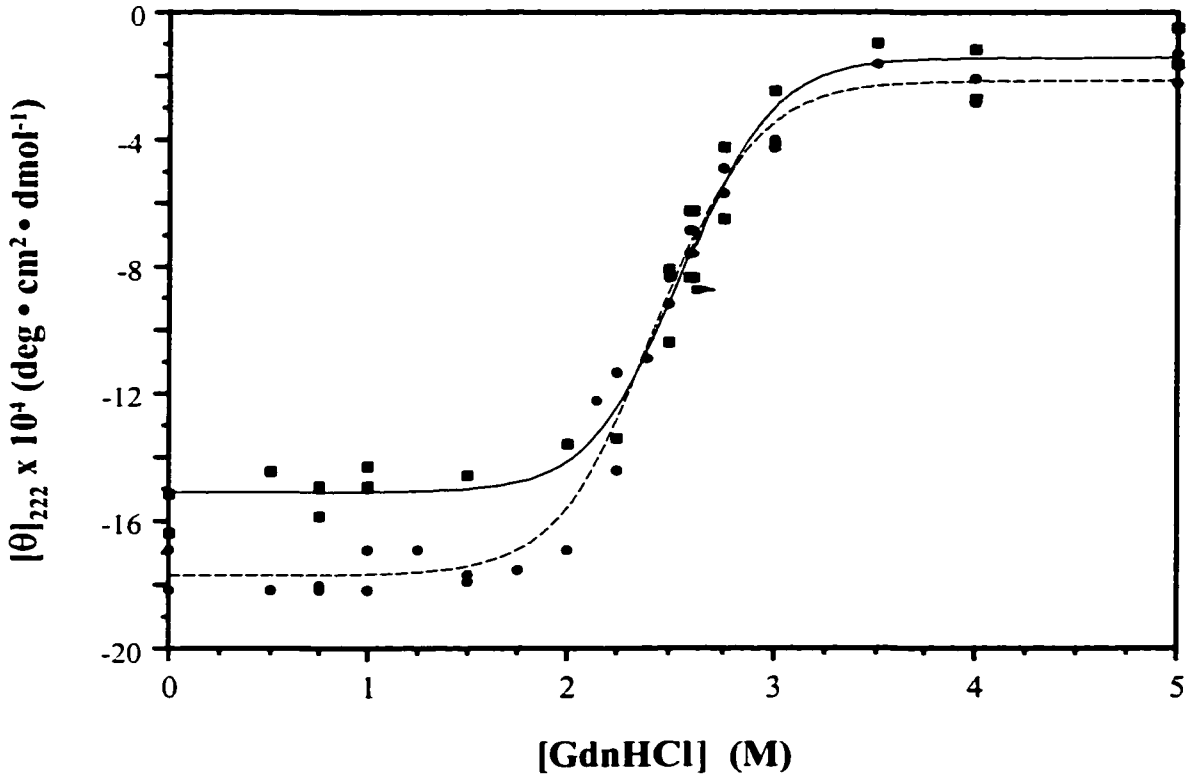

Figure 4.10 Molar ellipticity at 222 nm, $[\theta]_{222}$ *vs* [GdnHCl] (in 100 mM NaPi buffer, pH 7, H_2O) for 2 mM horse (solid line & squares) and tuna (dashed line & circles) cytochromes c. Experimental conditions given in captions of Figures 4.8 and 4.9.

The curves in Figure 4.10 have a similar sigmoidal shape. The $[GdnHCl]_{1/2}$ values computed by Origin software (sigmoidal fit), which represent the concentration of GdnHCl at which 50% of the α-helical signal is lost, are 2.6 and 2.4 M for horse and tuna

cytochromes c, respectively. This is consistent with literature $[GdnHCl]_{1/2}$ value for horse c of 2.5 M GdnHCl (*20*). It is also evident from CD spectra in Figures 4.8 and 4.9, that 50% of the 222-nm α-helical band is lost in ~2.5 M GdnHCl.

4.3.3 Secondary structure changes in GdnHCl and Gdn-d_5-DCl as monitored by FTIR spectroscopy

FTIR spectroscopy was utilized to monitor secondary structural changes in the native and denatured states of horse and tuna cytochromes c in GdnHCl and Gdn-d_5-DCl. Horse and tuna cytochromes c are structurally homologous, *i.e.* their crystal structures are almost identical, despite 19 amino acid substitutions.

Cytochrome c in GdnHCl (H_2O)

The deconvolved FTIR amide I (1700-1600 cm^{-1}) region of horse and tuna cytochromes c in buffer is presented in Figure 4.11. As shown, the deconvolved spectrum for horse c contains 4 distinct bands in the amide I region, while tuna c exhibits 5 bands. The frequencies of the bands for horse c are: 1679, 1657, 1633 and 1618 cm^{-1}. The spectrum for tuna c in buffer contains the same bands with an additional absorption at 1650 cm^{-1}. Assignment of these bands to secondary structures are based on empirical rules listed in Table 1.1 (*31*, *36*). In horse c, the high frequency band 1679 cm^{-1} is attributed to the presence of antiparallel β-turns, while the band at 1633 cm^{-1} is due to β-turns. The major absorption at 1657 cm^{-1} is assigned to α-helices, which is the predominant secondary structure, and the minor band at 1618 cm^{-1} is due to absorption of Arg and Lys side chains in cytochrome c (*74*). In tuna c, the additional band at 1650 cm^{-1} represents a splitting of the α-helical absorption into 2 components. The higher

frequency band (1657 cm^{-1}) represents more ordered and less solvent exposed α-helices, while the lower frequency band (1650 cm^{-1}) is due to more disordered and solvent exposed helices. These findings are consistent with FTIR studies by Filosa *et al.* (*74*), who assigned the amide I intensity for native horse c as follows: 23% turns (1670 & 1680 cm^{-1}), 47% α-helices (1657 cm^{-1}), 7% random structures (1646 cm^{-1}) and 21% β-extended chains (1636 cm^{-1}). Their assignments for tuna c are: 26% turns (1671 & 1682 cm^{-1}), 46% α-helices (1649 & 1659 cm^{-1}), 8% random structures (1649 cm^{-1}) and 18% β-extended chains (1635 cm^{-1}).

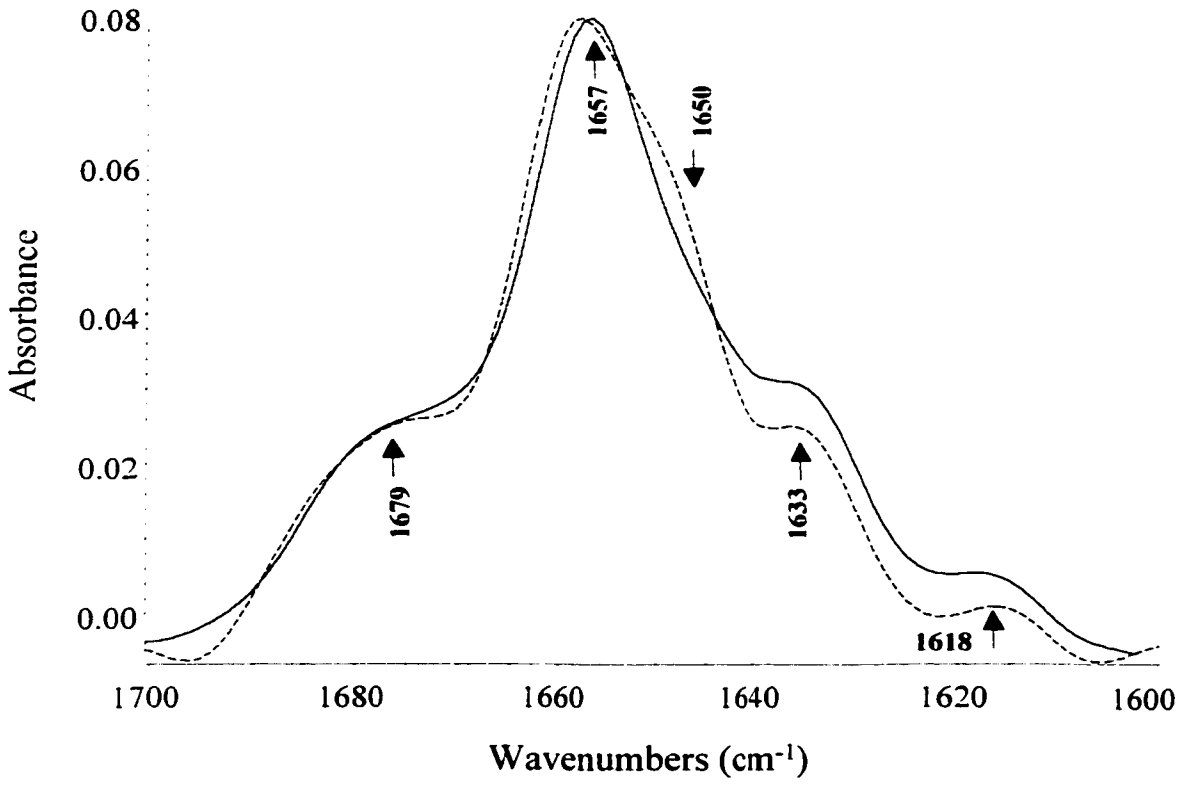

Figure 4.11 Deconvolved FTIR amide I spectra of 2 mM horse (solid line) and tuna (dashed line) cytochromes c in 100 mM NaPi buffer (pH 7, H_2O). The FTIR spectra shown represent an average of 256 scans at a resolution of 2 cm^{-1}, acquired using CaF_2 windows with a 6-μM pathlength.

The deconvolved FTIR amide I region of horse and tuna cytochromes c in 3 M GdnHCl is presented in Figure 4.12. A dramatic difference between the two spectra is observed, with the amide I of horse c being much broader than that of tuna c. For horse c, bands at 1675, 1658, 1653 and 1616 cm^{-1} are tentatively assigned to turns and loops, residual helical structure, random structure and Arg residues, respectively. For tuna c, bands at 1682, 1657, 1634 and 1616 cm^{-1} are speculated to result from turns and loops, residual helical and/or random structures, turns and Arg residues, respectively.

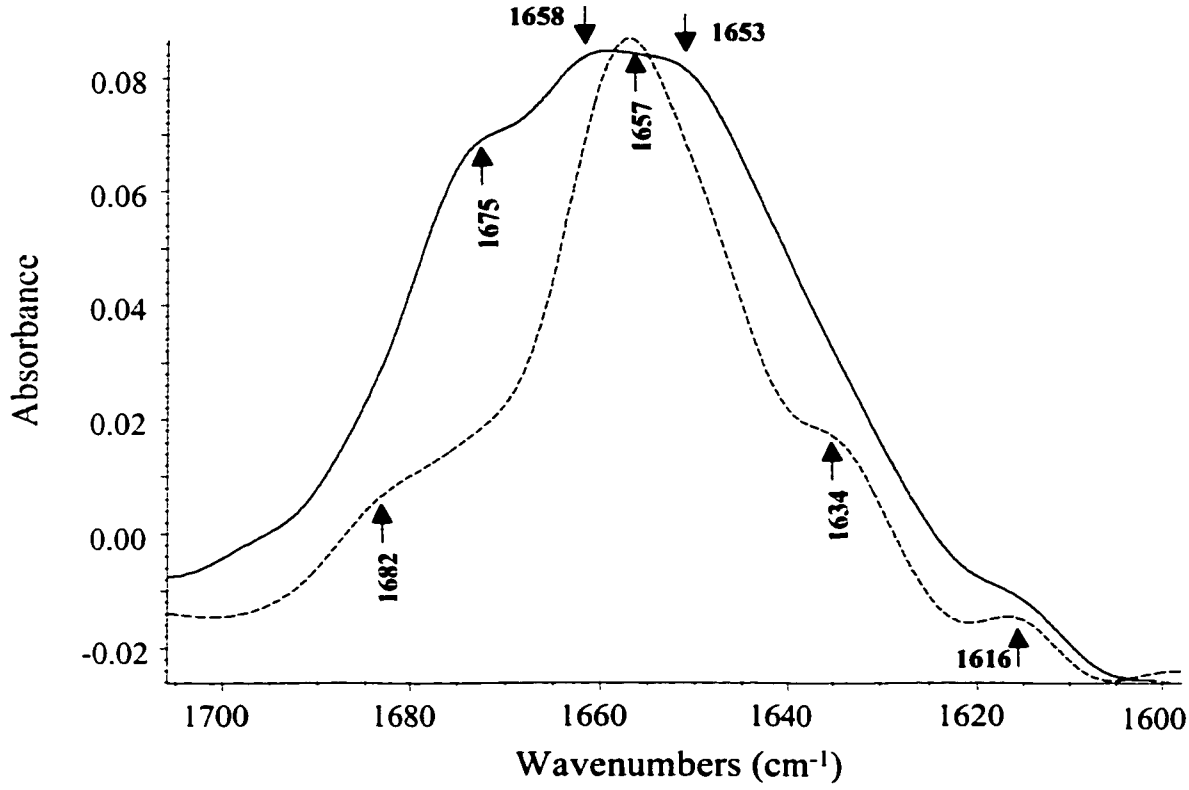

Figure 4.12 Deconvolved FTIR amide I spectra of 2 mM horse (solid line) and tuna (dashed line) cytochromes c in 3 M GdnHCl (in 100 mM NaPi buffer, pH 7, H_2O). The FTIR spectra shown represent an average of 256 scans at a resolution of 2 cm^{-1}, acquired using CaF_2 windows with a 6-μM pathlength.

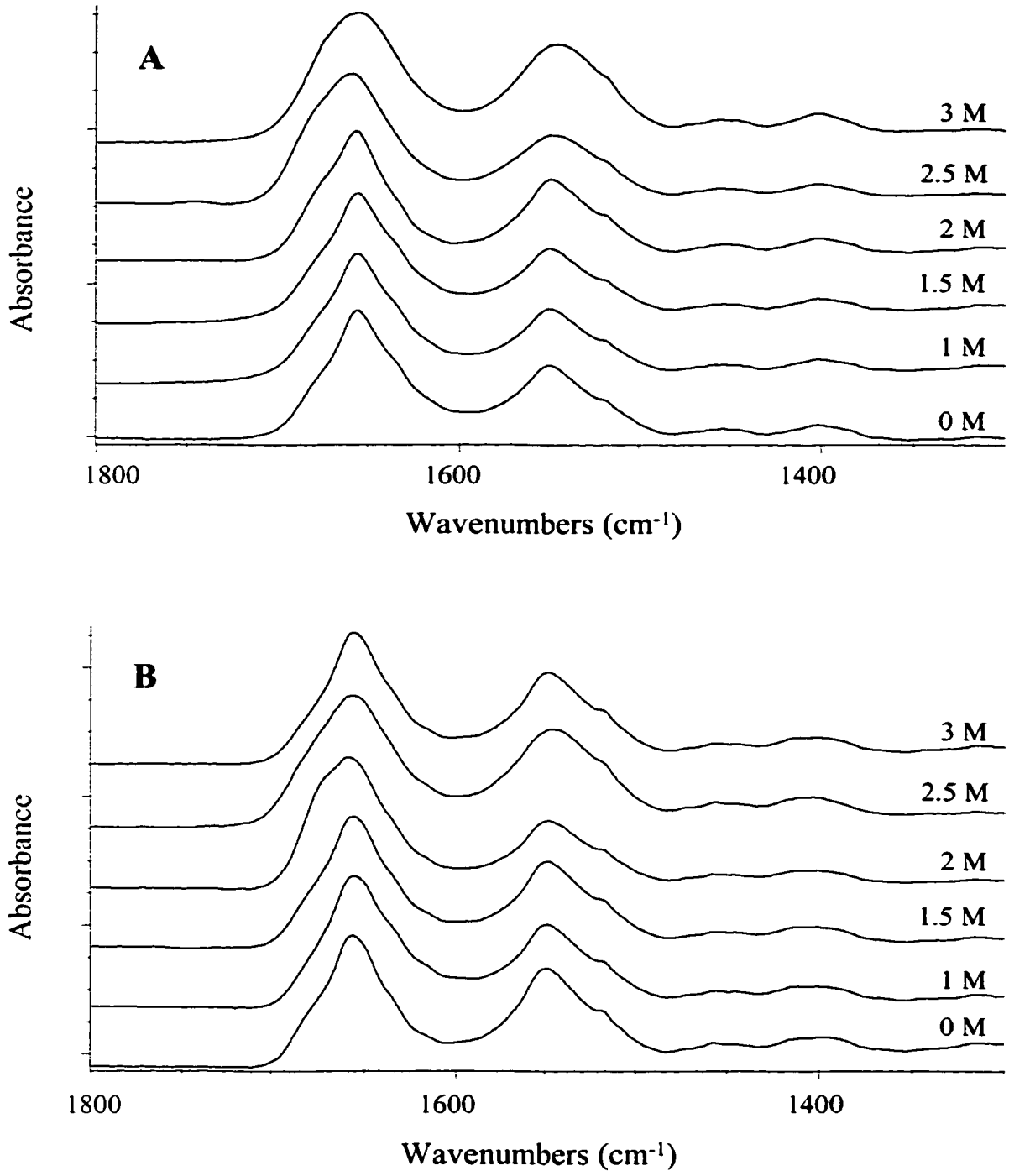

Figure 4.13 Stacked FTIR amide I and II spectra of 2 mM (A) horse and (B) tuna cytochromes c in 0-3 M GdnHCl (in 100 mM NaPi buffer, pH 7, H_2O). Each FTIR spectrum shown represent an average of 256 scans at a resolution of 2 cm^{-1}, acquired using CaF_2 windows with a 6-μM pathlength.

The FTIR amide I and II spectra of horse and tuna c in 0-3 M GdnHCl are stacked in Figure 4.13. As the concentration of GdnHCl is increased, the amide I band of horse c broadens and a high-frequency shoulder appears at 1.5 M GdnHCl and intensifies with increasing concentration of denaturant. For tuna c, a high-frequency shoulder is also apparent in 2-2.5 M GdnHCl. The amide II absorption changes slightly with increasing concentration of GdnHCl.

One of the criteria for background subtraction listed in Section 2.2.2 is that the amide I/II intensity ratios (peak heights) for the native and denatured protein should be as close as possible. The amide I/II intensity ratios for horse and tuna c in 0-3 M GdnHCl are listed in Table 4.2. It is important to note that when background subtraction is performed several criteria must be met, and the subtraction must be optimized using all of the criteria from Section 2.2.2.

Table 4.2: Amide I/II intensity ratios for horse and tuna cytochromes c in 0-3 M GdnHCl

[GdnHCl] (M)	Horse c Amide I/II	Tuna c Amide I/II
0.0	1.3	1.2
1.0	1.3	1.2
1.5	1.2	1.2
2.0	1.4	1.4
2.5	1.5	1.1
3.0	1.5	1.4

The deconvolved FTIR amide I spectra of horse c in 0-3 M GdnHCl are stacked in Figure 4.14, frame A. The native protein was previously analyzed (Figure 4.11). In

1-1.5 M GdnHCl not much change occurs, and the structure is similar to the native form. In 2 M GdnHCl, a slight increase in the 1676-cm^{-1} band is observed due to the presence of turns and loops. In 2.5 M GdnHCl (~$[GdnHCl]_{1/2}$; Figure 4.10), the overall shape of the amide I band becomes broader. In addition, the 1680 cm^{-1} component intensifies, and the β-turns band at 1633 cm^{-1} is lost. In 3 M GdnHCl, the amide I band at 1658 cm^{-1} is even broader and a shoulder at 1675 cm^{-1}, which may be due to turns and loops, is detected. It is also possible that this high frequency band is due to polypeptide-associated GdnHCl. Results from Chapter 2 reveal that GdnHCl preferentially interacts with the polypeptide backbone of PLL in its random coil conformation.

The deconvolved FTIR amide I spectra of tuna c in 0-3 M GdnHCl are shown in Figure 4.14, frame B. Native tuna c was analyzed in Figure 4.11. In 1-1.5 M GdnHCl, there is little change in the spectra, except that the absorbance of the more solvent-exposed α-helices (1650 cm^{-1}) diminishes with increasing concentration of GdnHCl. This is expected since the solvent-exposed α-helices should interact with the denaturant more than buried α-helices. In 2 M GdnHCl, the α-helical signal at 1650 cm^{-1} is no longer detected, and the β-turns band at 1633 cm^{-1} diminishes. Coincidentally, a large band grows in at 1673 cm^{-1}, which may be due to turns and loops or polypeptide-associated GdnHCl. However, the 1673 cm^{-1} band is very intense and may be due to an error in background subtraction. In 2.5 M GdnHCl (~$[GdnHCl]_{1/2}$; Figure 4.10), the amide I band broadens and is similar to that of horse c in 3 M GdnHCl. It appears that tuna c undergoes a large structural change in 3 M GdnHCl since its amide I band sharpens and exhibits a well-defined peak at 1657 cm^{-1}.

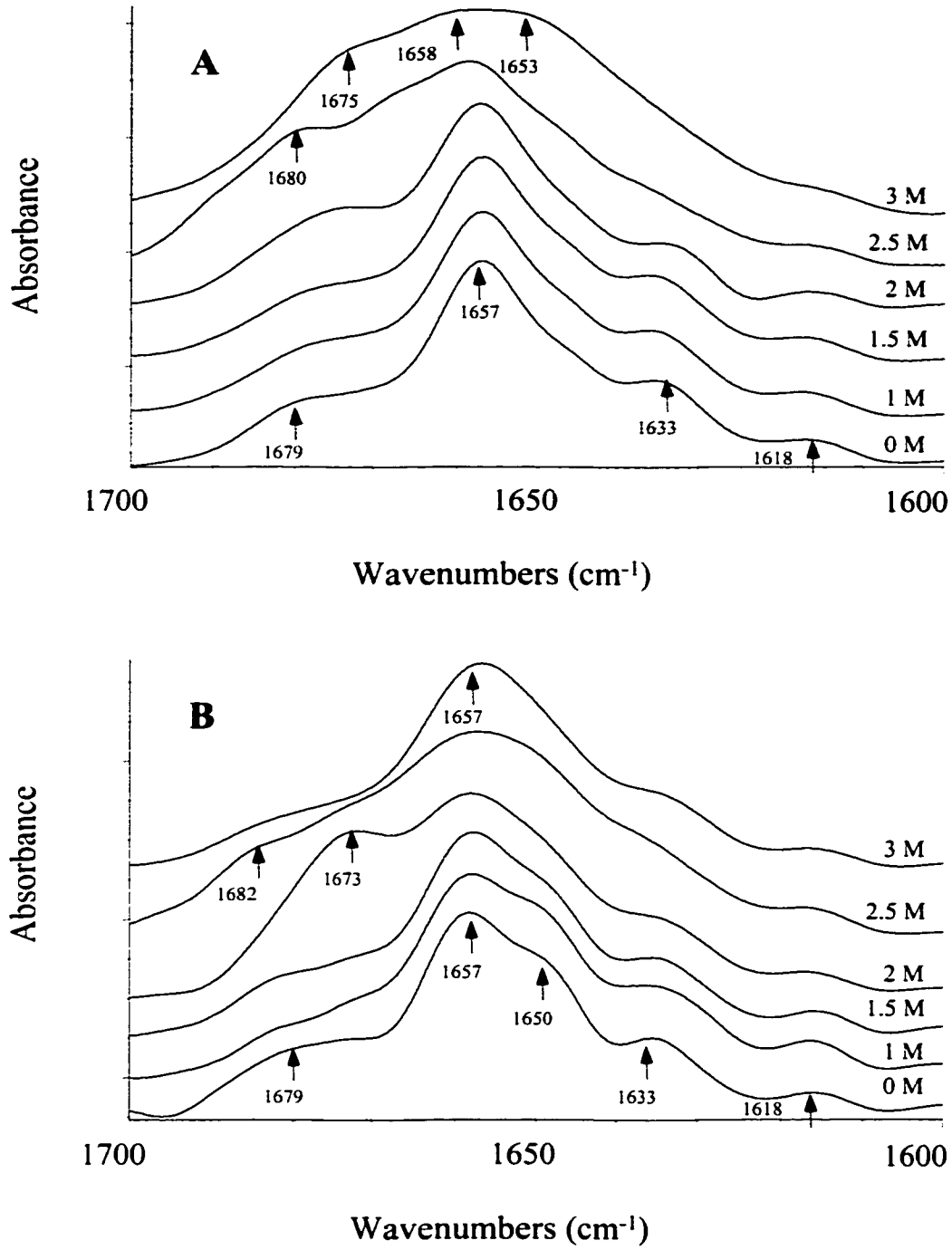

Figure 4.14 Stacked deconvolved FTIR amide I spectra of 2 mM (A) horse and (B) tuna cytochromes c in 0–3 M GdnHCl (in 100 mM NaPi buffer, pH 7, H_2O). Each FTIR spectrum shown represent an average of 256 scans at a resolution of 2 cm^{-1}, acquired using CaF_2 windows with a 6-μM pathlength.

Cytochrome c in Gdn-d_5-DCl (D_2O)

As stated previously, GdnHCl and H_2O have very high absorption in the FTIR amide I region at 1675 and 1644 cm^{-1}, respectively, that overlaps with the absorption of proteins. Therefore, Gdn-d_5-DCl and D_2O were used to red-shift the aforementioned absorptions to 1600 and 1200 cm^{-1}, respectively. Hence, background subtraction problems are alleviated and data processing is not as error-prone as in GdnHCl and H_2O.

The deconvolved FTIR amide I' regions (1700-1600 cm^{-1}) of horse and tuna cytochromes c in buffer (D_2O) are compared in Figure 4.15. As previously demonstrated in H_2O, the amide I' mode is resolved to 4 bands for horse c and 5 bands for tuna c. The common bands found both cytochromes c are: 1673, 1651, 1631 and 1614 cm^{-1}. An additional absorption at 1646 cm^{-1} is detected for tuna c. The frequencies of these secondary structural bands in D_2O are ~ 5 cm^{-1} less than observed in H_2O, which is expected upon deuteration (*31*). Assignment of the components to secondary structural elements is the same as previously determined in GdnHCl/H_2O (Section 4.3.3). Filosa *et al.* (*74*) also analyzed the secondary structures of horse and tuna c in D_2O and found that horse c consists of 23% turns (1641 & 1671 cm^{-1}), 45% α-helices (1653 cm^{-1}), 12% random structures (1641 cm^{-1}) and 18% β-extended chains (1631 cm^{-1}). Their assignments for tuna c are: 24% turns (1644 & 1670 cm^{-1}), 49% α-helices (1644 & 1654 cm^{-1}), 11% random structures (1644 cm^{-1}) and 15% β-extended chains (1630 cm^{-1}).

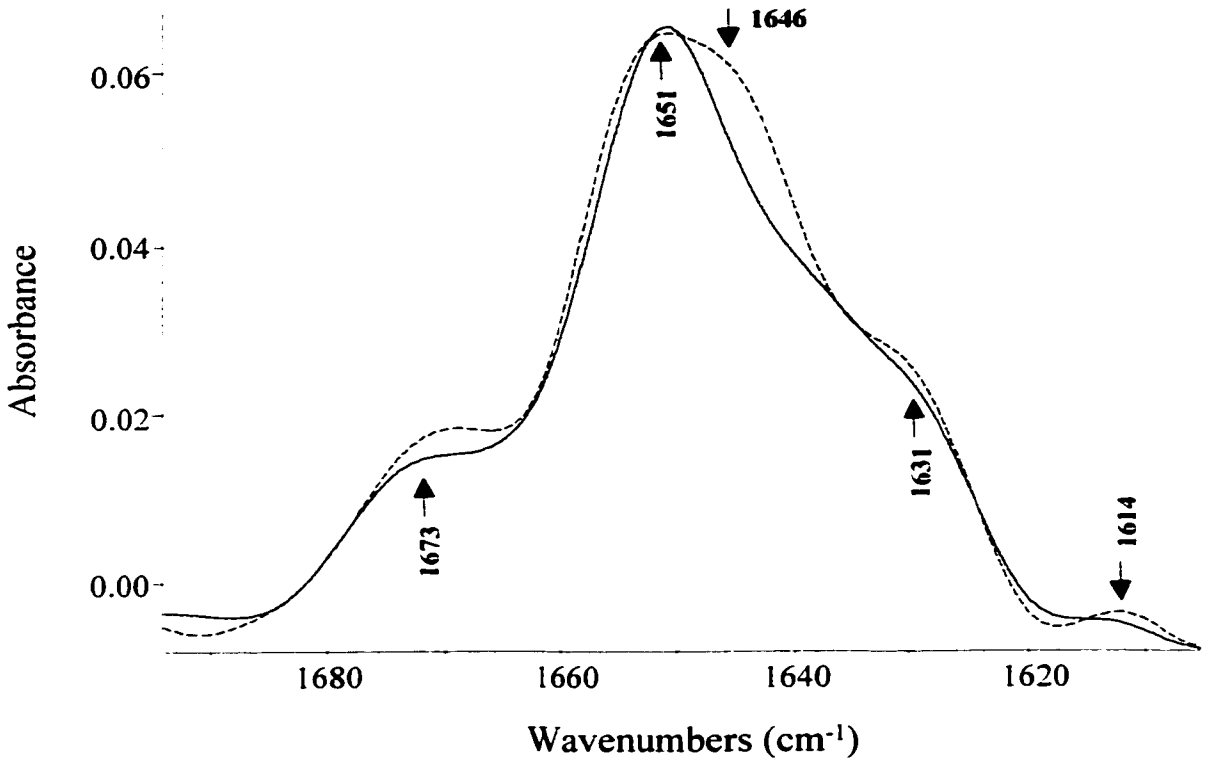

Figure 4.15 Deconvolved FTIR amide I' spectra of 2 mM horse (solid line) and tuna (dashed line) cytochromes c in 100 mM NaPi buffer (pD 7, D_2O). The FTIR spectra shown represent an average of 256 scans at a resolution of 2 cm^{-1}, acquired using CaF_2 windows with a 6-μM pathlength.

The deconvolved FTIR amide I' regions of horse and tuna c in 3 M Gdn-d_5-DCl are presented in Figure 4.16. It appears that the structures of horse and tuna c are much more similar in 3 M Gdn-d_5-DCl (D_2O) than in 3 M GdnHCl (H_2O, Figure 4.12). For horse c, absorptions at 1669, 1659 and 1646 cm^{-1} are tentatively assigned to turns and loops, residual helical structure and random structures, respectively, based on empirical rules from Table 1.1. Bands at approximately the same maxima are observed for tuna c, however, their intensities are higher. It is speculated that the major additional absorption

at 1621 cm^{-1} for both proteins in 3 M GdnHCl is due to polypeptide-associated Gdn-d_5-DCl. PLL (Figure 2.9), a random coil in 3 M Gdn-d_5-DCl, gave rise to a similar absorption at 1622 cm^{-1}, which was assigned to PLL-associated Gdn-d_5-DCl. Since only Gdn-d_5-DCl from bulk solvent can be subtracted out, and not the polypeptide-associated form, the latter absorption must be considered in the assignment of secondary-structural elements.

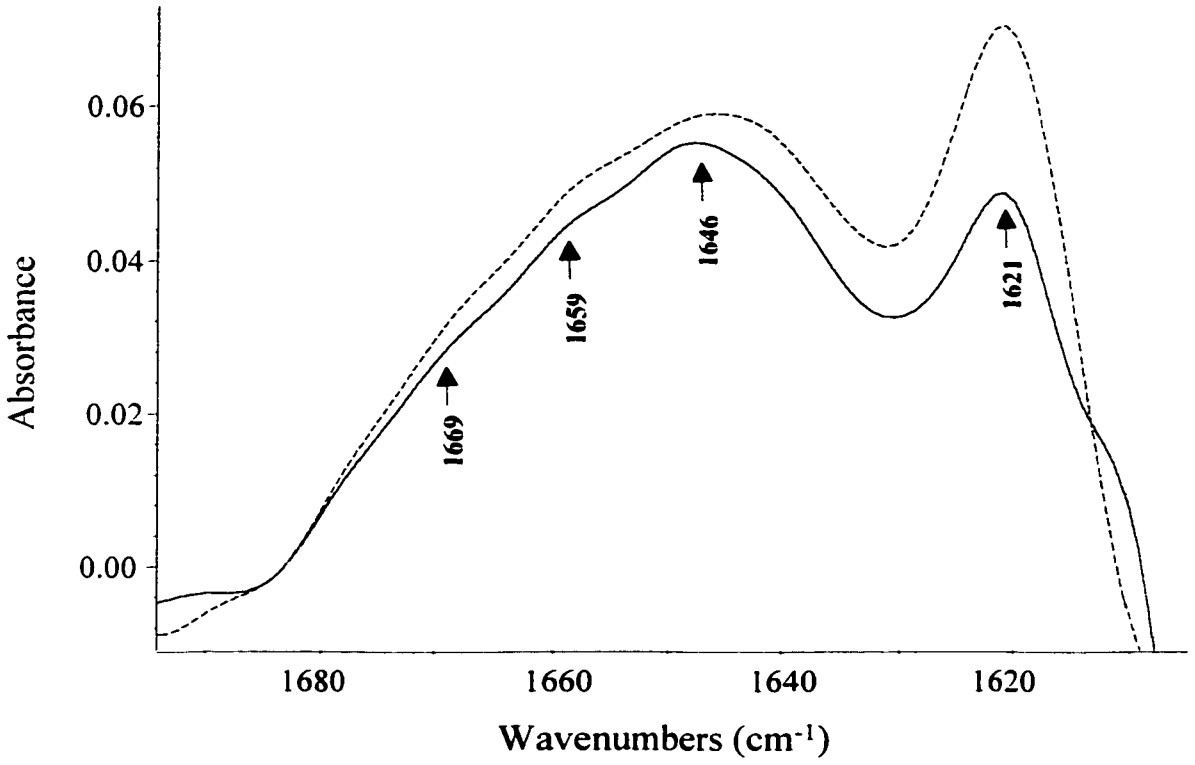

Figure 4.16 Deconvolved FTIR amide I' spectra of 2 mM horse (solid line) and tuna (dashed line) cytochromes c in 3 M Gdn-d_5-DCl (in 100 mM NaPi buffer, pD 7, D_2O). The FTIR spectra shown represent an average of 256 scans at a resolution of 2 cm^{-1}, acquired using CaF_2 windows with a 6-μM pathlength.

The observed FTIR amide I' and II' spectra of horse and tuna c in 0-3 M Gdn-d_5-DCl are stacked in Figure 4.17.

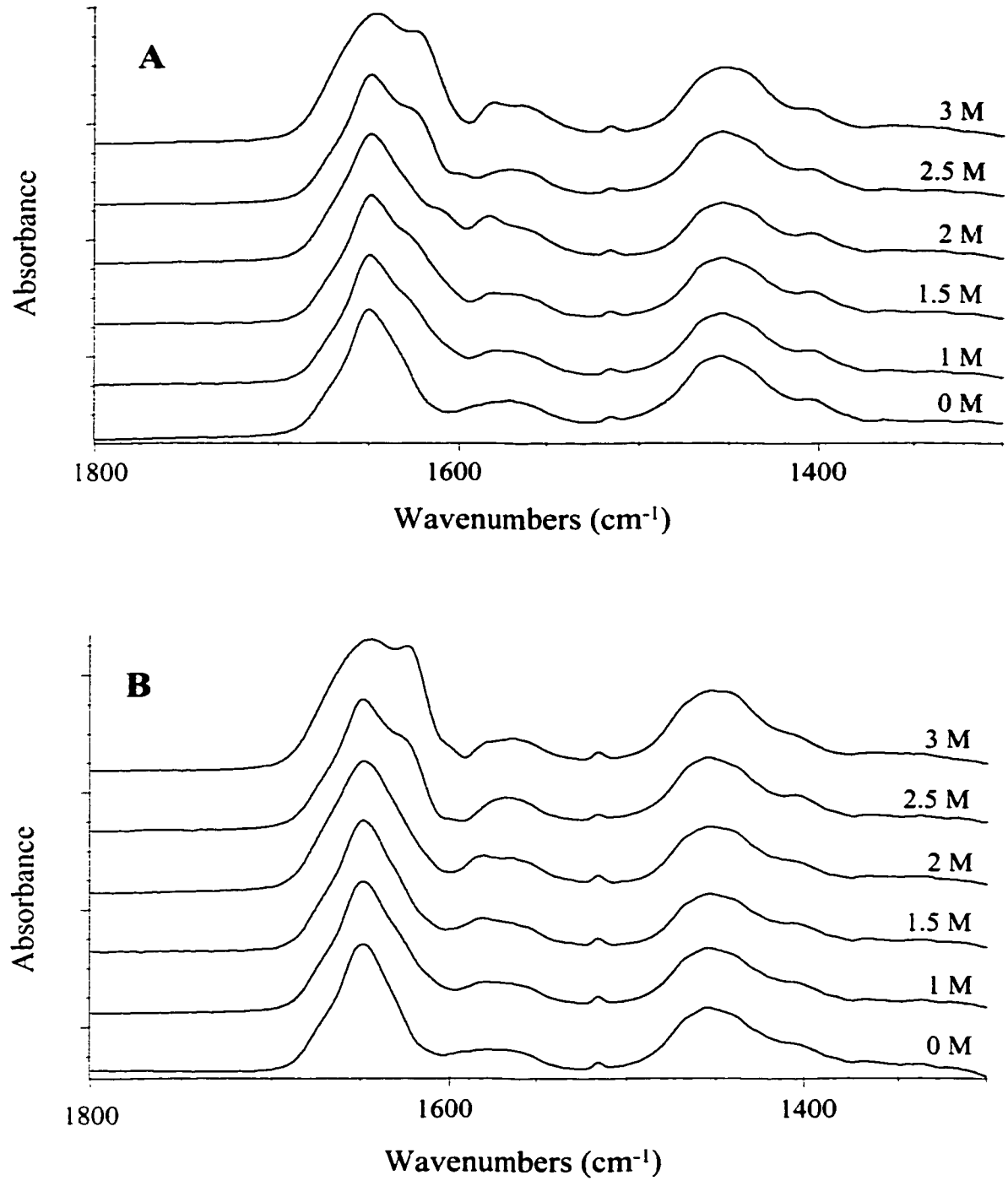

Figure 4.17 Stacked FTIR amide I' and II' spectra of 2 mM (A) horse and (B) tuna cytochromes c in 0-3 M Gdn-d_5-DCl (in 100 mM NaPi buffer, pD 7, D_2O). Each FTIR spectrum shown represent an average of 256 scans at a resolution of 2 cm^{-1}, acquired using CaF_2 windows with a 6-μM pathlength.

It can be seen from Figure 4.17 (frame A) that the FTIR spectra for horse c in 0 to 2 M Gdn-d_5-DCl are very similar. In 2 M Gdn-d_5-DCl, a minor band at the red-end of the amide I' envelope is apparent. The greatest change occurs from 2.5 to 3 M Gdn-d_5-DCl, where the amide I' band broadens, and a new, intense band at 1621 cm^{-1} grows in. The amide II' absorptions are slightly altered with increasing concentration of denaturant. Figure 4.17 frame B reveals that from 0 to 2 M Gdn-d_5-DCl, the tuna c spectra are also similar. In 2 M Gdn-d_5-DCl, the amide I' band broadens slightly, but similar to horse c, the greatest changes occur from 2.5 to 3 M Gdn-d_5-DCl, where additional strong absorption is observed at 1621 cm^{-1}.

As previously stated, a criterion for background subtraction (Section 2.2.2) is that the amide I'/II' intensity ratios (peak heights) for the native and denatured protein should be similar. The amide I'/II' intensity ratios for horse and tuna c in 0-3 M Gdn-d_5-DCl are found in Table 4.3.

Table 4.3: Amide I'/II' intensity ratios for horse and tuna cytochromes c in 0-3 M Gdn-d_5-DCl

[Gdn-d_5-DCl] (M)	Horse c Amide I'/II'	Tuna c Amide I'/II'
0.0	1.4	1.7
1.0	1.7	2.0
1.5	1.7	2.1
2.0	1.8	1.7
2.5	1.8	1.7
3.0	1.7	1.7

The deconvolved structure-sensitive FTIR amide I' bands for horse and tuna c in 0-3 M Gdn-d_5-DCl are stacked in Figure 4.18. Assignment of components in Gdn-d_5-DCl to secondary structures was performed according to the empirical rules (Table 1.1), taking into consideration that frequencies are usually red-shifted ~5 cm^{-1} in D_2O (*74*). The amide I' region of native horse and tuna c in buffer (D_2O) was previously analyzed (Figure 4.15).

In the FTIR amide I' absorption for horse c (Figure 4.18, frame A), no major change in secondary structure is observed in 1-2 M Gdn-d_5-DCl. However, in 1 M Gdn-d_5-DCl, a new band at 1621 cm^{-1} is detected, which intensifies with increasing concentration of denaturant. The greatest change occurs in 3 M Gdn-d_5-DCl, where the overall shape of the amide I' band is broader and the sharp absorption at 1621 cm^{-1}, tentatively assigned to polypeptide-associated Gdn-d_5-DCl, is the most intense. The broad amide I' band at 1646 cm^{-1} in 3 M Gdn-d_5-DCl is assigned to random structures, and the band at 1659 cm^{-1} may be due to residual helical structure or turns.

The deconvolved FTIR spectra of tuna c in 0-3 M Gdn-d_5-DCl are presented in Figure 4.18, frame B. In 0-1.5 M Gdn-d_5-DCl, the absorbance of the more solvent-exposed α-helices (1646 cm^{-1}) diminishes with increasing denaturant concentration, as was observed in GdnHCl/H_2O (Figure 4.14). In 2 M Gdn-d_5-DCl, the amide I' band is broad, whereas in 2.5 M Gdn-d_5-DCl, a relatively sharp peak appears at 1650 cm^{-1} accompanied by a large increase in the 1621-cm^{-1} band. In 3 M Gdn-d_5-DCl, the spectrum changes significantly and the overall shape of the amide I' band is broader, and absorption at 1621 cm^{-1} has intensified significantly.

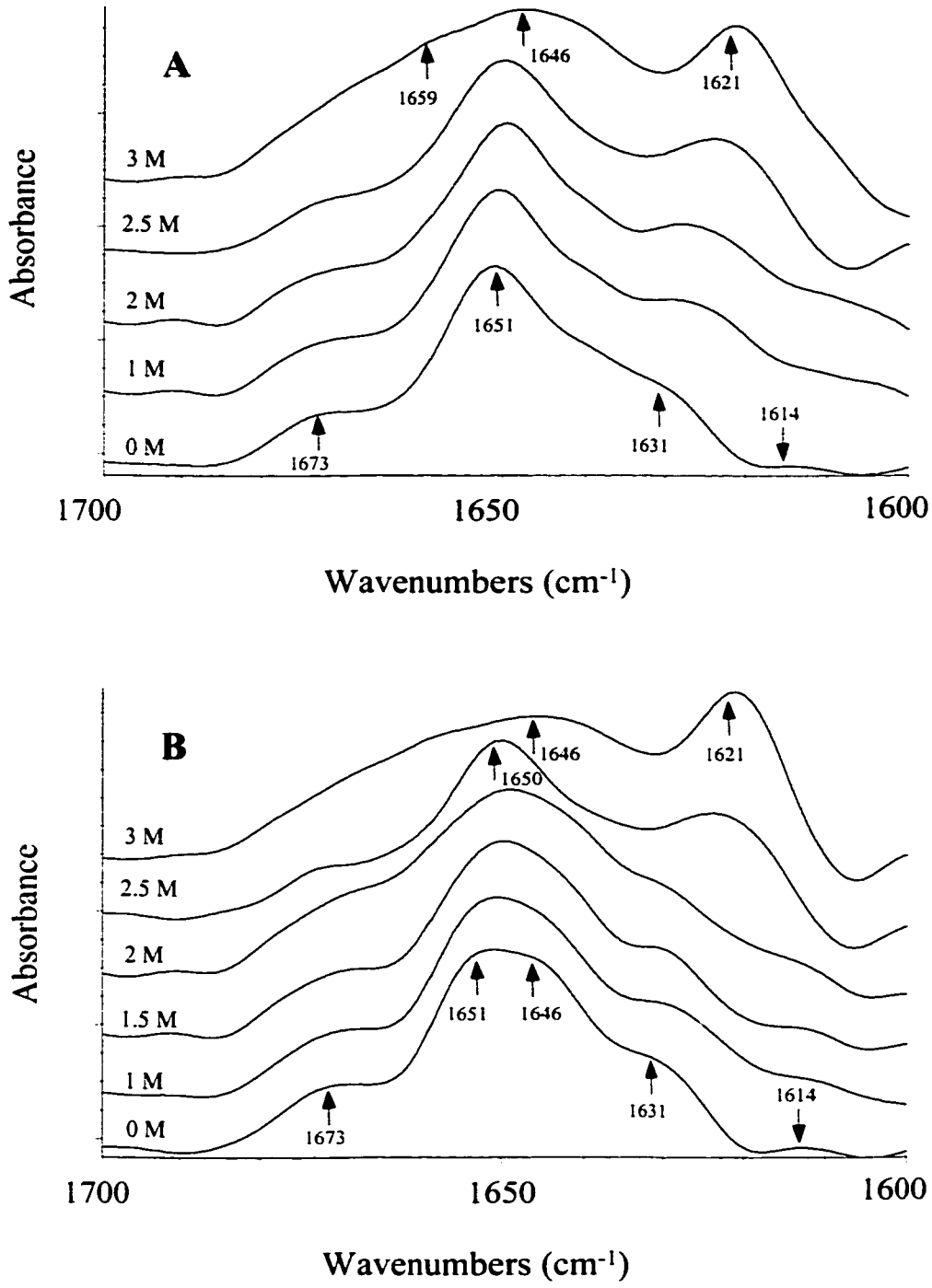

Figure 4.18 Stacked deconvolved FTIR amide I' spectra of 2 mM (A) horse and (B) tuna cytochromes c in 0–3 M Gdn-d_5-DCl (in 100 mM NaPi buffer, pD 7, D_2O). Each FTIR spectrum shown represent an average of 256 scans at a resolution of 2 cm^{-1}, acquired using CaF_2 windows with a 6-μM pathlength.

The deconvolved and curve-fitted FTIR amide I' spectra of horse and tuna c in buffer and in 3 M Gdn-d_5-DCl are shown in Figures 4.19 and 4.20, respectively. These spectra were curve-fitted with Gaussian bands, and the curve-fitting parameters, *i.e.* band assignment, frequency and % area for both proteins in buffer and in 3 M Gdn-d_5-DCl are listed in Tables 4.4 and 4.5, respectively. These results are discussed in the next section.

Table 4.4: Curve-fitting parameters for FTIR amide I' bands of horse and tuna cytochromes c in buffer (D_2O)

Cytochrome	Frequency (cm^{-1})	Secondary structure assignment	% Area
Horse	1671	Antiparallel β-turns	18
	1651	α-helices	50
	1639	Random structures	11
	1631	β-turns	20
	1613	Arg/Lys residues	1
Tuna	1671	Antiparallel β-turns	18
	1653	α-helices	38
	1642	α-helices/Random structures	28
	1629	β-turns	15
	1612	Arg/Lys residues	1

Table 4.5: Curve-fitting parameters for FTIR amide I' bands of horse and tuna cytochromes c in 3 M Gdn-d_5-DCl

Cytochrome	Frequency (cm^{-1})	Secondary structure assignment	% Area
Horse	1666	Turns and loops	25
	1644	Random structures	47
	1620	Polypeptide-associated Gdn-d_5-DCl	28
Tuna	1662	Turns and loops	36
	1640	Random structures	42
	1620	Polypeptide-associated Gdn-d_5-DCl	22

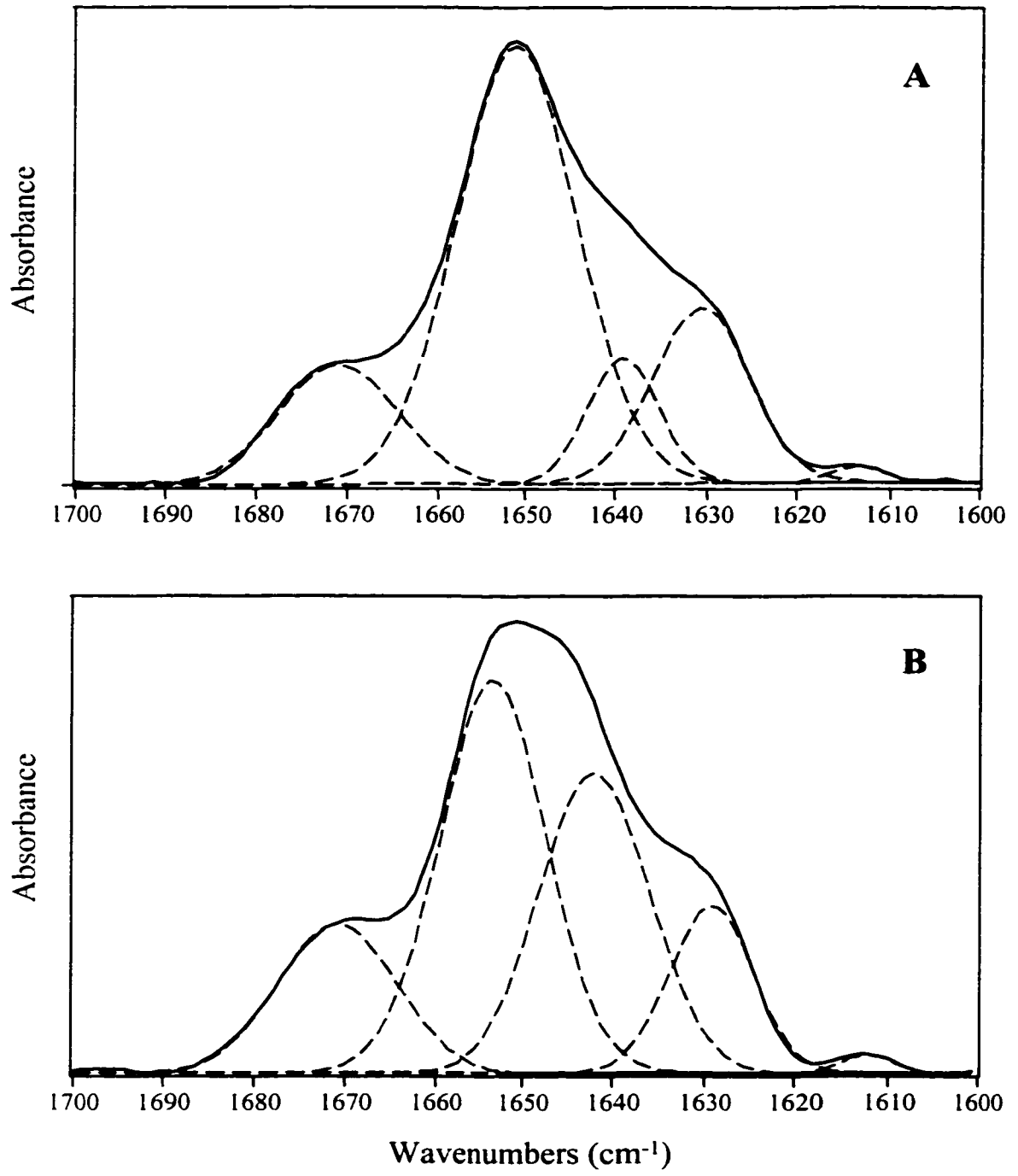

Figure 4.19 Deconvolved and curve-fitted FTIR amide I' spectra of 2 mM (A) horse and (B) tuna cytochromes c in 100 mM NaPi buffer, pD 7, D_2O. The original spectra (solid lines) were fitted using Galactic Peak Solve software and the bands (dashed lines) have Gaussian peak shapes.

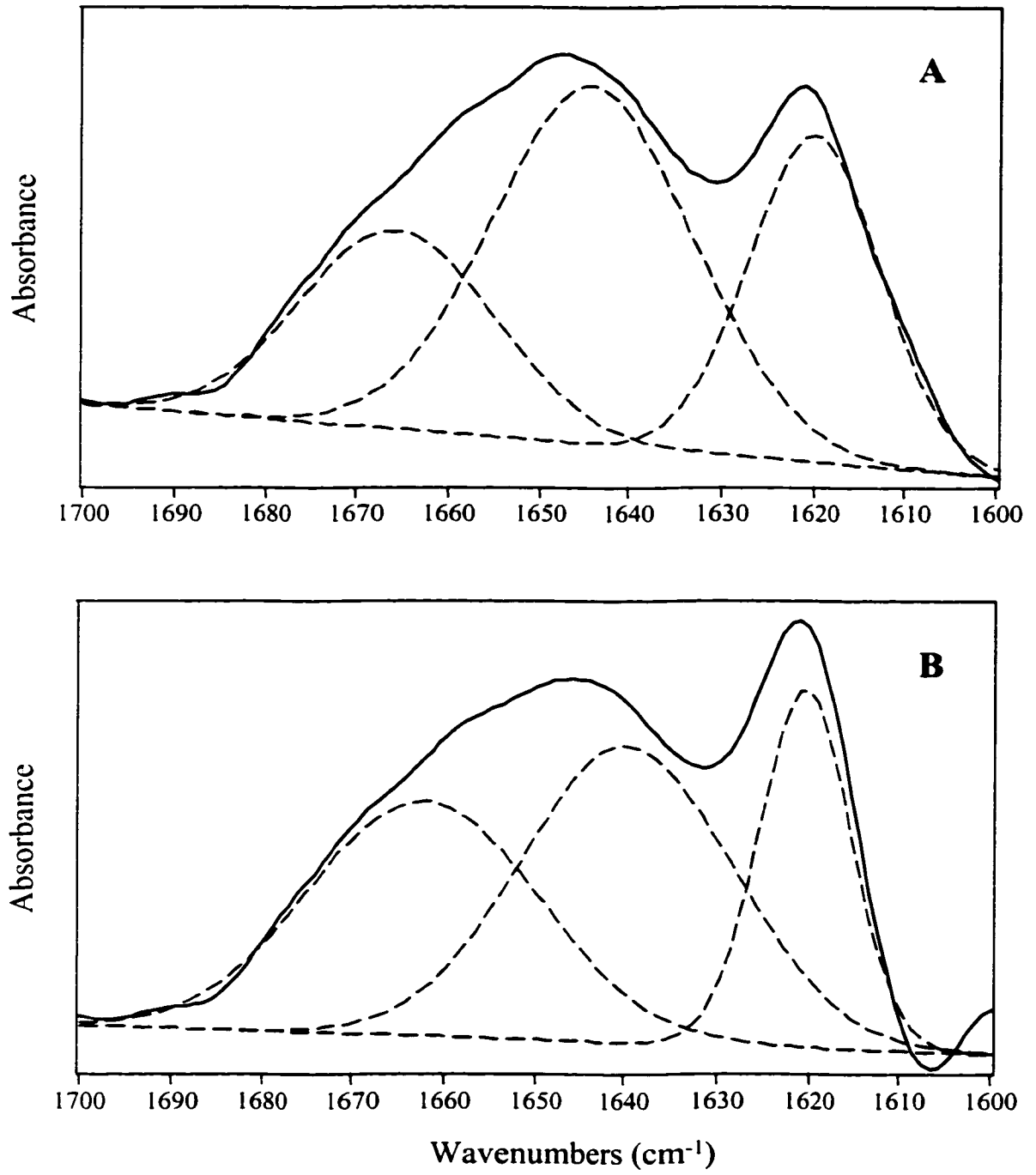

Figure 4.20 Deconvolved and curve-fitted FTIR amide I' spectra of 2 mM (A) horse and (B) tuna cytochromes c in 3 M Gdn-d_5-DCl (in 100 mM NaPi buffer, pD 7, D_2O). The original spectra (solid lines) were fitted using Galactic Peak Solve software and the bands (dashed lines) have Gaussian peak shapes.

4.4 DISCUSSION

The purpose of this work was to characterize the chemically denatured states of horse and tuna cytochromes c using spectroscopic probes, particularly FTIR. The native states of these structurally homologous proteins have been studied extensively, however, relatively little is known regarding their denatured states. Probing the chemically denatured states of proteins by FTIR is a new approach, therefore, fluorescence and CD spectroscopies were used to aid in the interpretation of the FTIR results.

Fluorescence spectroscopy monitored the global unfolding of the polypeptide backbone of both cytochromes c in the presence of GdnHCl. The sigmoidal curves of $\%F_{350}$ *vs* [GdnHCl] in Figure 4.3 were used to determine the $[GdnHCl]_{1/2}$ points. In a two-state model ($N \rightleftharpoons D$), this represents the concentration of GdnHCl at which 50% of the molecules have lost their tertiary structure and are in the denatured state (D). The $[GdnHCl]_{1/2}$ values were found to be 2.7 and 2.9 M for horse and tuna c, respectively. In addition, the fluorescence-monitored denaturation curves have approximately the same sigmoidal shape, suggesting that horse and tuna c have similar cooperativities of unfolding in the presence of GdnHCl.

CD and FTIR spectroscopies are complementary techniques since FTIR is sensitive to turns and sheets (*35*), while CD is preferred for α-helices. Therefore, CD was used to monitor the α-helical content of horse and tuna c in varying amounts of GdnHCl. Changes in the characteristic strong negative α-helical bands at 209 and 222 nm in 0-4 M GdnHCl were observed. In addition, the CD data were acquired using an FTIR cell, which has not been reported in the literature as of yet. This has distinct advantages, which are discussed in Section 2.2.2.

The α-helical far-UV CD spectra for native horse and tuna cytochromes c are not the same (Figure 4.5), despite the fact that both proteins have very similar crystal structures (*58, 75*). However, their sequences differ by 19 residues and most of the substitutions occur in the 60's α-helix (Figure 4.2) (*57*). Even though there are slight differences in the CD spectra of both cytochromes c in 0-2 M GdnHCl, it appears that the α-helicity is not disrupted. However, a dramatic change in the asymmetry of the molecular environment is detected between 2-2.5 M GdnHCl, where most of the α-helical signal is lost. According to the plots of $[\theta]_{222}$ *vs* [GdnHCl] in Figure 4.10, the proteins contain little or no α-helicity in 3-5 M GdnHCl.

The $[GdnHCl]_{1/2}$ values, which represent the concentration at which 50% of the α-helical CD is lost, were found to be 2.6 and 2.4 M for horse and tuna c, respectively. Interestingly, the $[GdnHCl]_{1/2}$ values determined from fluorescence spectroscopy are not the same, as seen in Table 4.6 below. Fluorescence spectroscopy reports on loss of tertiary structure, while CD monitors the loss of the α-helical signal in GdnHCl. According to the two-state model ($N \rightleftharpoons D$), at the $[GdnHCl]_{1/2}$ point, 50% of the molecules are in the denatured state (*D*), while the other 50% are in the native state (*N*). Mc Lendon and Smith (*73*) reported that for a two-state transition, the degree of unfolding should be independent of the technique used. They studied the denaturation curves of donkey, horse and dog cytochromes c in GdnHCl, and found that the transition curves obtained from CD and fluorescence are slightly different.

Table 4.6: Comparison of $[GdnHCl]_{1/2}$ values obtained from fluorescence and CD spectroscopies for horse and tuna cytochromes c in GdnHCl

Technique	Horse c $[GdnHCl]_{1/2}$ (M)	Tuna c $[GdnHCl]_{1/2}$ (M)
Fluorescence	2.7	2.9
CD	2.6	2.4

The far-UV CD spectra of horse and tuna cytochromes c are dissimilar in 3 M (Figure 4.6) and 5 M GdnHCl (Figure 4.7). In 3 M GdnHCl, the CD spectra of both cytochromes contains a positive feature at 197 nm assigned to turns, negative bands between 201 and 206 nm due to random coils as well as a minor absorption at 222 nm which may be due to the presence of residual helical structure. In 5 M GdnHCl, no absorption at 222 nm is detected (Figure 4.7), hence there are no α-helices present in the protein. The spectrum for horse c in 5 M GdnHCl reveals only one strong negative broad band at 201 nm due to random coils, suggesting the absence of any ordered structure. The CD spectra for tuna c in 5 M GdnHCl on the other hand, contain a positive band at 197 nm due to turns and two sharp negative bands at 202 and 206 nm assigned to random coils. Therefore, it appears that in 5 M GdnHCl tuna c has residual ordered structure in its denatured state, whereas horse c does not.

FTIR spectroscopy was utilized to monitor changes in the secondary structures of horse and tuna cytochromes c in GdnHCl and Gdn-d_5-DCl, as well as to probe possible differences in their denatured states. FTIR, as shown previously (*74*), can successfully detect minor differences in the native states of both cytochromes c. The deconvolved

FTIR amide I regions of both native proteins are very similar, except for splitting of the α-helical absorption seen in the spectrum of tuna c (Figures 4.11 and 4.15).

The deconvolved FTIR amide I regions of denatured horse and tuna cytochromes in 3 M GdnHCl are very different (Figure 4.12), suggesting that their denatured states are different. However, it is important to note that assignment of the amide I bands to secondary structures is difficult in GdnHCl because the empirical rules in use (Table 1.3) were designed for model proteins in water, not denaturants. Interactions of the protein with GdnHCl may shift the frequencies of the component bands somewhat. As discussed in Chapter 2 with model studies of PLL at neutral pH, GdnHCl preferentially interacts with random structures, and possibly lysyl side chains. In 3 M GdnHCl, the amide I band is much broader and a high frequency shoulder is observed, which may be due to polypeptide-associated GdnHCl. In high concentrations of denaturant where the predominant secondary structure of cytochrome c is random coil, GdnHCl is likely to associate extensively with these regions of the protein. This would explain the spectral perturbations observed.

Chemical denaturation studies were also performed using Gdn-d_5-DCl in D_2O, which simplified background subtraction and data processing. From the FTIR spectra of horse and tuna c in 3 M Gdn-d_5-DCl (Figure 4.16), it is evident that their denatured states are not as different as suggested from studies in 3 M GdnHCl/H_2O (Figure 4.12). The FTIR spectra of both denatured proteins contained a broad band with an additional strong absorption at 1621 cm^{-1}. PLL, a random coil, gives rise to a similar absorption at 1622 cm^{-1} in 3 M Gdn-d_5-DCl (Figure 2.9), which was assigned to polypeptide-associated Gdn-d_5-DCl. Therefore, this new band at 1621 cm^{-1} in the spectra of both cytochromes is

also assigned to polypeptide-associated Gdn-d_5-DCl. As the concentration of denaturant increases, so does the amount of random structure in the protein, resulting in the growth of the 1621-cm^{-1} band. This is coincident with the appearance of an additional absorption at 201 nm in the CD spectrum (Figure 2.14, in 3 M Gdn-d_5-DCl), as a result of associated guanidine. GdnHCl and Gdn-d_5-DCl from bulk solvent can be subtracted out by mathematical procedures, but not when it is associated to the polypeptide.

Interestingly, in 3 M GdnHCl (H_2O), more dramatic differences between horse and tuna c were observed. This discrepancy between the data sets in H_2O and D_2O is puzzling and suggests that the absorptions of GdnHCl and H_2O may be too high for accurate subtraction. A careful digital subtraction technique with strict criteria (Section 2.2.2) was used (*40*, *41*). The amide I/II and I'/II' intensity ratios (criterion ii) are listed in Tables 4.2 and 4.3. These are the intensity ratios for the background subtracted spectra, and were included to show that criterion ii was met. However, *all* of the criteria must be considered, and not only this one. Intentional over- or under-subtraction was performed to perfect the subtraction technique, as illustrated in Figure 2.3. After considerable manipulations, methods were established to ensure proper background subtraction. However, mode mixing in H_2O may also be a problem. H_2O, GdnHCl and protein vibrations occur at similar frequencies in H_2O, but in D_2O, the water band is shifted to 1200 cm^{-1} and does not interfere with protein vibration.

Curve-fitted FTIR amide I' spectra of horse and tuna c in buffer and in 3 M Gdn-d_5-DCl are shown in Figures 4.19 and 4.20, respectively. The curve-fitting parameters, *i.e.* frequency, secondary structure assignment and % area are listed in Tables 4.4 and 4.5. The frequencies of the curve-fitted bands are shifted somewhat from those

assigned in the deconvolved spectra shown in Figures 4.15 and 4.16. Overlapping components in the amide I' region are resolved and the curve-fitted bands in Figures 4.19 and 4.20 should be more representative of the actual secondary structural elements than those derived from Figures 4.15 and 4.16. A curve-fitted band at 1639 cm^{-1} was discovered for native horse c, not previously detected in Figure 4.15. For horse c in 3 M Gdn-d_5-DCl, bands were resolved at 1666, 1644 and 1620 cm^{-1}, and assigned to turns and loops (25%), random structures (47%) and polypeptide-associated Gdn-d_5-DCl (28%). For tuna c components were detected at 1662, 1640 and 1620 cm^{-1}, and assigned to turns and loops (36%), random structures (42%) and polypeptide-associated Gdn-d_5-DCl (22%). Bands at 1644 and 1640 cm^{-1} for the denatured cytochromes may also be due to residual helical structure. Therefore, the denatured states of both cytochromes in 3 M Gdn-d_5-DCl have residual structure, as evidenced by the bands resolved using curve-fitting (Figure 4.20). Similarly, CD spectra (Figure 4.6) revealed a small absorption at 222 nm in 3 M GdnHCl, which was assigned to residual helical structure.

Bowler *et al.* (*9*) performed similar studies and monitored the GdnHCl-denatured states of iso-1-cytochrome c from *yeast* in 0-3 M GdnHCl using FTIR spectroscopy. This is the most relevant literature report to compare with the present results, although yeast c differs from horse and tuna c by 46 amino acids (~56% sequence homology). Bowler's results revealed that the FTIR amide I band broadens and shifts to higher wavenumbers with increasing GdnHCl concentration. This blue-shift is away from the frequency normally associated with random structures (~1645 cm^{-1}). However, as yeast c is denatured, it is expected that the amount of random structures will increase, hence there is an increased probability that GdnHCl will associate with the polypeptide. This is

consistent with results for horse and tuna c in this study, where the amide I band broadened and shifted to higher wavenumbers (Figure 4.13) upon GdnHCl denaturation.

Although, FTIR is not widely used for the study of protein chemical denaturation, it has been used extensively to study protein thermal denaturation (*74*, *59*, *76*). The FTIR amide I' spectra of fully heat-denatured horse and tuna c at 85°C are shown in Figure 4.21 (data from Angelo Filosa). According to Filosa *et al.* (*74*), loss of secondary structure and protein aggregation occur at 70°C for horse c and 65°C for tuna c.

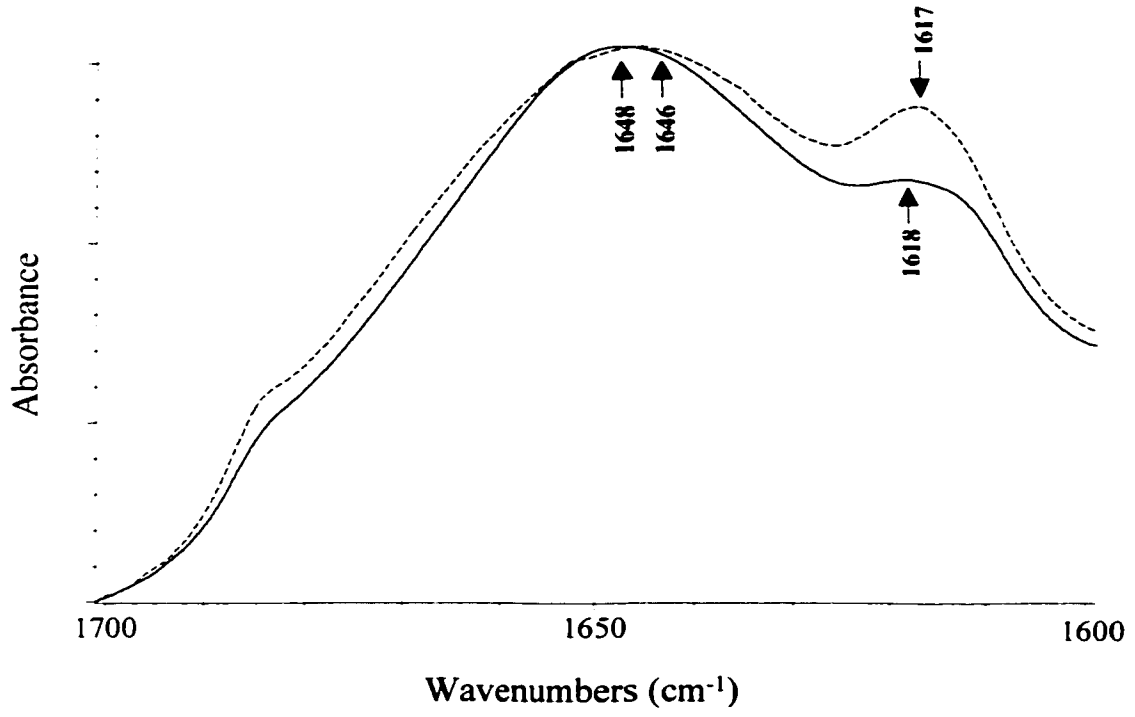

Figure 4.21 FTIR amide I' spectra of 4 mM horse (solid line) and tuna (dashed line) cytochromes c at 85 °C (in 50 mM NaPi buffer, pD 7, D_2O). The FTIR spectra shown represent an average of 256 scans at a resolution of 2 cm^{-1}, acquired using CaF_2 windows with a 56-μM pathlength. Spectra were obtained from Angelo Filosa.

In Figure 4.21, the FTIR spectrum of horse c exhibits a broad band centered at 1648 cm^{-1} assigned to random structures, and a low frequency band at 1618 cm^{-1} due to aggregated strands. Similarly, the FTIR spectrum of tuna c also reveals bands at 1646 and 1617 cm^{-1} due to random structures and aggregation. The chemically denatured counterparts shown in Figure 4.20, appear to have more residual structure. Both cytochromes in 3 M Gdn-d_5-DCl exhibit bands at ~1662-1666 cm^{-1} and ~1644-1640 cm^{-1}, tentatively assigned to turns and loops and random structures, respectively (Table 4.5.) In addition, a major absorption at 1620 cm^{-1} was detected and assigned to polypeptide-associated Gdn-d_5-DCl (Section 4.3.3), and not aggregated strands since thermally-denatured proteins can aggregate, while chemically-denatured ones do not (*9*).

Protein thermal and chemical denaturation were contrasted by CD spectroscopy. The thermally and GdnHCl-denatured states of iso-1-cytochrome c from yeast were compared using CD spectroscopy (*8*). CD absorption for both denatured forms was different, and the chemically denatured state was found to have more residual structure than the thermally denatured one. The GdnHCl-denatured protein adopted a denaturant-stabilized helical structure, which may result from GdnHCl-association with the protein. The heat-denatured protein, on the other hand, resembled a random coil.

4.5 CONCLUSIONS

These results demonstrate the power of FTIR spectroscopy in probing the denatured states of horse and tuna cytochromes c in the presence of GdnHCl and Gdn-d_5-DCl. FTIR is a very sensitive technique and was successfully applied to detect subtle differences in the native states of horse and tuna cytochromes c, despite their

structural homology. Only slight differences in their denatured states were observed via FTIR and CD spectroscopies, and it was demonstrated that their denatured states contained residual structure.

Fluorescence and CD spectroscopies were used to facilitate the FTIR data interpretation. From the fluorescence-monitored loss of protein tertiary structure, $[GdnHCl]_{1/2}$ values were found to be 2.7 and 2.9 M for horse and tuna c, respectively. CD spectroscopy was employed to study the loss of α-helicity, which is the predominant secondary structure in both cytochromes. The $[GdnHCl]_{1/2}$ values were 2.6 and 2.4 M for horse and tuna cytochromes c, respectively. As discussed in Section 4.4, the $[GdnHCl]_{1/2}$ values obtained from independent techniques like CD and fluorescence should be the same, as is observed for horse c (~0.1 M difference). Tuna c, on the other hand exhibits a difference of ~0.5 M in its $[GdnHCl]_{1/2}$ values obtained from CD and fluorescence, which suggests that the transition from $N \rightleftharpoons D$ state might involve contributions from an intermediate species.

Upon comparison of the FTIR spectra in H_2O and D_2O, it was found that the D_2O data were easier to interpret. This is due to fewer uncertainties in the background subtraction and less potential for mode mixing, since the absorption for water in D_2O is shifted to 1200 cm^{-1}, away from the amide I' window. The FTIR spectra of the denatured cytochromes in 3 M Gdn-d_5-DCl (Figure 4.16) revealed an additional strong absorption at 1621 cm^{-1}. A random-coil homopolypeptide, PLL, gave rise to a similar FTIR absorption at 1622 cm^{-1} in 3 M Gdn-d_5-DCl (Figure 2.9), which strongly supports the hypothesis that Gdn-d_5-DCl associates with the polypeptide. It is also possible that Gdn-d_5-DCl preferentially associates with the Lys-rich regions of cytochrome c. Therefore, this new

band at 1621 cm^{-1} is attributed to polypeptide-associated Gdn-d_5-DCl. The CD spectra of horse and tuna c in Gdn-d_5-DCl also exhibited an additional absorption at 201 nm, which may result from immobilized Gdn-d_5-DCl.

CHAPTER 5: GENERAL CONCLUSIONS AND SUGGESTIONS FOR FUTURE STUDY

5.1 GENERAL CONCLUSIONS

The aim of this study was to demonstrate that FTIR be used as a reliable research tool for probing protein structures in chemical denaturants. The interaction of GdnHCl and Gdn-d_5-DCl with a random coil model was analyzed to gain further insight on the denaturant's mode of action, which promotes unfolding and destabilizes the peptide or protein. Initially, it was speculated that the denaturant preferentially interacted with random structures, which unlike helices, sheets and turns, are not held together by strong H-bonds nor side-chain interactions. Therefore, in order to confirm this hypothesis, the interaction of GdnHCl and Gdn-d_5-DCl with model systems was investigated.

This research is important since proteins play crucial roles and have a broad array of functions in almost every biological process (*71*). Proteins fold in unique ways and their three-dimensional structures mediate their functions. Therefore, understanding how proteins denature is a key element for advancement in the study of protein stability and folding. Exploration of protein denaturation by spectroscopic techniques provided additional insight on this subject and may have applications for the clinical diagnosis of diseases.

Probing the GdnHCl-denatured states of proteins by FTIR spectroscopy is a novel technique. Therefore, in order to develop this technology, fluorescence and CD spectroscopies were used to complement the FTIR results. Fluorescence was chosen to study the loss of protein tertiary structure in GdnHCl by reporting on changes in the

heme-to-Trp distance, while CD selectively monitored changes in the α-helical content via the signature α-helical 222-nm band.

To date, the majority of FTIR studies on protein denaturation were performed on thermally denatured systems. Chemical denaturation by FTIR is challenging since denaturants (GdnHCl ~1675 cm^{-1} and urea ~1645 cm^{-1}) as well as H_2O (1650 cm^{-1}) absorb very strongly in the amide I region (1600-1700 cm^{-1}) and overlap with the protein's absorption. Switching to Gdn-d_5-DCl and D_2O shifted the solvent absorbance to 1600 and 1200 cm^{-1}, respectively, and simplified data processing. The potential for mode mixing is reduced in D_2O since water absorbs out of the amide I' window.

Three biomolecules were investigated in an attempt to find a suitable model system to develop FTIR as a research tool for the characterization of chemically denatured states. PLL, a random coil peptide model, was selected to study the interaction of GdnHCl and Gdn-d_5-DCl with random structures. PLL was also chosen to gain further insight on the interaction of the denaturants with the Lys-rich regions of cytochrome c. Spectroscopic evidence proved HRP to be unsuitable for this exploratory research due to the complex time-dependent spectral changes it underwent in GdnHCl. Cytochromes c from two homologous species (horse and tuna) were chosen as protein models for the structural characterization of their denatured states.

PLL exists as a random coil in the solution conditions studied, therefore no 'unfolding' was expected to occur in the denaturant. Therefore, any spectral changes observed were attributable to interactions of the polypeptide with the solvent. Since the surface of a random coil is very hydrated (*54*), it is not surprising that the solvation of PLL is different in water than in GdnHCl, as reported by FTIR and CD. At high

concentrations of denaturant, more GdnHCl molecules populate the environment surrounding the peptide chain, which should influence the interaction between the polypeptide backbone and the solvent molecules (H_2O *vs* GdnHCl).

Spectral evidence strongly suggests that GdnHCl associates with PLL. FTIR bands were observed at intermediate frequencies between PLL (~1645 cm^{-1}) and GdnHCl (~1675 cm^{-1}), as well as PLL and Gdn-d_5-DCl (~1600 cm^{-1}). Association with the polypeptide augmented at concentrations of denaturant >1.5 M. Generally, at high concentrations of GdnHCl or Gdn-d_5-DCl, some degree of unfolding has occurred in proteins, and hence a greater population of random coil exists.

The association of GdnHCl with proteins has not been addressed in the literature. Bowler *et al.* (*9*) hinted that immobilized GdnHCl may perturb the FTIR spectra of yeast cytochrome c, but did not interpret their data accordingly. Their FTIR results showed that the amide I band was blue-shifted in GdnHCl; away from the frequency normally assigned to random coil, but towards that obtained for GdnHCl. This is consistent with the data presented in this study. As the concentration of GdnHCl increases, the amount of random coil increases, and hence the amide I should be shifted towards the frequency associated with random coils. Instead, a new population grows in at an intermediate frequency between the absorption of the protein and the denaturant.

The nature of the association of GdnHCl and Gdn-d_5-DCl with PLL is of great interest. The denaturant can either interact with the polypeptide backbone or the lysyl side chains of PLL. According to the FTIR spectrum of PLL in 3 M Gdn-d_5-DCl, the absorption at 1645 cm^{-1} (80%, Figure 2.13) due to the polypeptide backbone of PLL appears relatively unaltered compared to its absorption in D_2O (76%, Figure 2.12 B).

This suggests that Gdn-d_5-DCl associates with the lysyl side chains of PLL, rather than with the backbone. A new population (~1620 cm^{-1}, 15%) grows in at an intermediate frequency between the random coil (~1645 cm^{-1}) and Gdn-d_5-DCl (~1600 cm^{-1}) absorptions. Since the lysyl side chain contains a C_4 hydrophobic chain (Figure 2.1), it is not surprising that association with the denaturant does not appear to affect the absorption of the backbone. Interestingly, Lys absorbs at 1629 cm^{-1} (Table 1.2, NH_3^+ asymmetric vibrations) and the band at 1622 cm^{-1} is likely due to Gdn-d_5-DCl–Lys association.

Lysyl side chains appear to be a target for GdnHCl and Gdn-d_5-DCl association. PLL, which is composed entirely of Lys residues, generates an intense FTIR absorption at 1622 cm^{-1}, which was assigned to polypeptide-associated Gdn-d_5-DCl. Spectroscopic data indicated that association of Gdn-d_5-DCl with cytochrome c also occurred. Interestingly, cytochromes c from horse and tuna consists of ~17% Lys (*57*), which is the most abundant amino acid present in the protein. It can be inferred that association of the denaturant with HRP was not observed since the protein contains only ~2% Lys residues. In addition, HRP studies were performed in 1 M GdnHCl, which may be insufficient to observe association with the protein.

It was common in the past to assume that the protein denatured state was a featureless random coil in order to simplify the data interpretation. However, this assumption is clearly wrong. Many recent studies have reported residual structure in denatured proteins (*4, 7-9, 27*). If further insight can be gained on the denatured state, then this might shed some light on the native state. Discovery on how unique native protein structures form would enrich our understanding of protein stability and folding.

The FTIR spectra of horse and tuna c in GdnHCl and Gdn-d_5-DCl were compared and their denatured states were characterized. Due to fewer uncertainties in the background subtraction, a greater emphasis was placed on the results in D_2O and Gdn-d_5-DCl. Horse and tuna c in 3 M Gdn-d_5-DCl were found to contain residual structure. The curve-fitted bands of horse c in 3 M Gdn-d_5-DCl were assigned to turns and loops (25%), random and residual helical structures (47%) and polypeptide-associated Gdn-d_5-DCl (28%). For tuna c, bands were assigned to turns and loops (36%), random and residual helical structures (42%) and polypeptide-associated Gdn-d_5-DCl (22%). Although the structural assignments were the same for both cytochromes, differences in their frequencies and integrated intensities were reported. This confirms that the denatured states of horse and tuna c are not the same in 3 M Gdn-d_5-DCl. It appears that horse c contains a greater amount of random coil, and hence polypeptide-associated Gdn-d_5-DCl, while tuna c has more turns and loops.

The thermally (Figure 4.21) and Gdn-d_5-DCl–denatured (Figure 4.16) forms of horse and tuna c were compared. Although the FTIR spectra of both denatured forms revealed a low frequency band at ~1620 cm^{-1}, their identity was different. In the thermally denatured form, bands due to aggregated strands are observed at 1618 and 1617 cm^{-1} for horse and tuna c, respectively. Thermally denatured proteins are known to aggregate at high temperatures, while chemically denatured ones do not (*9*). The bands at 1620 cm^{-1} in the Gdn-d_5-DCl–denatured form are assigned to polypeptide-associated Gdn-d_5-DCl.

As discussed in Section 1.2.1, it is advantageous to use FTIR for the structural characterization of proteins, and this technique can be applied to many other fields, such

as medicine. In addition to proteins, FTIR can be used to study biological fluids or diseased tissues. In clinical chemistry, FTIR is a practical technique since no reagents are needed to acquire data, all IR active components are monitored simultaneously and the concentration of multiple analytes from biological fluids can be determined from the same spectrum (*77*). FTIR can also be used for pathology studies since it provides information regarding the molecular structure of tissues and there is no need for fixation or staining of cells (*77*).

In conclusion, it has been demonstrated that FTIR is a powerful tool for probing the chemically denatured states of model protein systems, with potential applications for other biomolecules. Spectroscopic studies of PLL and cytochrome c in GdnHCl and Gdn-d_5-DCl strongly suggest that the denaturant preferentially interacts with random structures and associates with the polypeptide at high concentration of denaturant.

5.2 SUGGESTIONS FOR FUTURE STUDY

It is recommended that FTIR studies aimed at probing the chemically denatured states of biomolecules be performed using Gdn-d_5-DCl and D_2O. This will simplify data processing as well as the interpretation of results. It is also advantageous to acquire both CD and FTIR data using an FTIR cell as described in Section 2.2.2. This is a novel technique which, to my knowledge, has not been reported in the literature.

The following are suggestions for future study:

(i) Investigate the interaction of Gdn-d_5-DCl with other model proteins that adopt only one dominant secondary structure. Examples of biomolecules with predominately

α-helical and β-sheet structures are myoglobin (*83*) and concanavalin A (*32*), respectively.

(ii) Perform chemical denaturation studies using other guanidinium salts such as GdnSCN, to investigate how the counter ion influences the potency of the denaturant.

(iii) Investigate the interaction of GdnHCl with other charged homopolypeptides, for example poly-Asp or poly-Arg.

(iv) Execute FTIR experiments using isotopically labeled urea. From *et al.* (*7*) performed FTIR denaturation studies using deuterated ^{13}C-urea which absorbs out of the amide I' window at 1562 cm^{-1}.

(v) Utilize two-dimensional infrared (2D-IR) spectroscopy for protein chemical denaturation studies. This novel concept improves resolution of overlapping bands by spreading them over a second dimension, which simplifies complex spectra (*78-81*).

(vi) Obtain further proof that Gdn-d_5-DCl interacts with lysyl side chains of PLL, rather than the polypeptide backbone. Molecular modeling by computer simulations is proposed.

(vii) NMR studies would provide complementary information to the FTIR data on the GdnHCl-denatured states of horse and tuna c. NMR can be used to pinpoint the precise locations in the amino acid sequences (*36*) of both cytochromes, which are responsible for the differences in their denatured states.

REFERENCES

1. Creighton, T. E. (1997), IRL press, New York.
2. Chick, H., and Martin, C. J. (1911) *J. Physiol. 43*, 1.
3. Wu, H. (1929) *Am. J. Physiol. 90*, 952.
4. Dill, K. A., and Shortle, D. (1991) *Annu. Rev. Biochem. 60*, 795-825.
5. Shortle, D. (1996) *FASEB 10*, 27-34.
6. Hammack, B., Attfield, K., Clayton, D., Dec, E., Dong, A., Sarisky, C., and Bowler, B. E. (1998) *Protein Sci. 7*, 1789-1795.
7. From, N. B., and Bowler, B. E. (1998) *Biochemistry 37*, 1623-1631.
8. Herrmann, L. M., and Bowler, B. E. (1997) *Protein Sci 6*, 657-665.
9. Bowler, B. E., Dong, A., and Caughey, W. S. (1994) *Biochemistry 33*, 2402-2408.
10. Martensson, L. G., and Jonsson, B. H. (1993) *Biochemistry 32*, 224-231.
11. Petrescu, A. J., Receveur, V., Calmettes, P., Durand, D., and Smith, J. C. (1998) *Protein Sci. 7*, 1396-1403.
12. Qian, H., and Chan, S. I. (1999) *J. Mol. Biol. 286*, 607-616.
13. Yang, M., Liu, D., and Bolen, D. W. (1999) *Biochemistry 38*, 11216-11222.
14. Dill, K. A. (1990) *Biochemisrty 29*, 7133-7155.
15. Hibbard, L. S., and Tulinsky, A. (1978) *Biochemistry 17*, 5460-5468.
16. Creighton, T. E. (1993) *Proteins: Structures and molecular properties*, 2nd ed., W.H. Freeman and company, New York.
17. Segel, D. J., Fink, A. L., Hodgson, K. O., and Doniach, S. (1998) *Biochemistry 37*, 12443-12451.
18. Tanford, C. (1964) *J. Am. Chem. Soc. 86*, 2050-2059.

19. Ibarra-Molero, B., Loladze, V. V., Makhatadze, G. I., and Sanchez-Riuz, J. M. (1999) *Biochemistry 38*, 8138-8149.

20. Hagihara, Y., Tan, Y., and Goto, Y. (1994) *J. Mol. Biol. 237*, 336-348.

21. Doss-Pepe, E. W., Carew, E. L., and Korentz, J. F. (1998) *Exp. Eye Res. 67*, 657-679.

22. Moosavi-Movahedi, A. A., and Nazari, K. (1995) *Int. J. Biol. Macromol. 17*, 43-47.

23. Pappa, H. S., and Cass, A. E. G. (1993) *Eur. J. Biochem. 212*, 227-235.

24. Smulevich, G., Mantini, A. R., English, A. M., and Mauro, M. (1989) *Biochemistry 28*, 5058-5064.

25. Timasheff, S. N. (1992) *Biochemistry 31*, 9857-9864.

26. Makhatadze, G. I., and Privalov, P. (1992) *J. Mol. Biol. 226*, 491-505.

27. Denisov, V. P., Jonsson, B. H., and Halle, B. (1999) *Nat. Struct. Biol. 6*, 253-260.

28. Barron, L. D., Hecht, L., and Wilson, G. (1997) *Biochemistry 36*, 13143-13147.

29. Schellman, J. A. (1994) *Biopolymers 34*, 1015-1026.

30. Staniforth, R. A., Burston, S. G., Smith, C. J., Jackson, G. S., Badcoe, I. G., Akinson, T., Holbrook, J. J., and Clarke, A. R. (1993) *Biochemistry 32*, 3842-3851.

31. Jackson, M., and Mantsch, H. H. (1995) *Crit. Rev. Biochem. Mol. Biol. 30*, 95-120.

32. Haris, P. I., and Chapman, D. (1995) *Biopolymers 37*, 251-263.

33. Haris, P. I., and Chapman, D. (1992) *Trends Biochem. Sci. 17*, 328-333.

34. Markovich, R. J., and Pidgeon, C. (1991) *Pharm. Res. 8*, 663-675.

35. Surewicz, W. K., Mantsch, H. H., and Chapman, D. (1993) *Biochemistry 32*, 389-394.

36. Mantsch, H. H., Perczel, A., Hollosi, M., and Fasman, G. D. (1993) *Biopolymers 33*, 201-207.

37. Goormaghtigh, E., Cabiaux, V., and Ruysschaert, J. M. (1990) *Eur. J. Biochem. 193*, 409-420.

38. Stuart, B. (1997) *Biological applications of infrared spectra.*

39. Venyaminov, S., and Kalnin, N. N. (1990) *Biopolymers 30*, 1243-1257.

40. Dong, A. C., Huang, P., and Caughey, W. S. (1992) *Biochemistry 31*, 182-189.

41. Dong, A., Huang, P., and Caughey, W. S. (1990) *Biochemistry 29*, 3303-3308.

42. Susi, H., and Byler, D. M. (1986) *Methods Enzymol. 130*, 290-311.

43. Skoog, D. A., and Leary, J. J. (1992) *Principles of instrumental analysis*, 4th ed., Saunders College Publishing, USA.

44. Meyers, R. A. (1995) in *Circular dichroism in protein analysis* (Price, N. C., Ed.), VCH Publishers Inc., New York.

45. Strickland, E. H. (1974) *CRC Crit. Rev. Biochem. 2*, 113-175.

46. Fox, T., Ferreira-Rajabi, L., Hill, B. C., and English, A. M. (1993) *Biochemistry 32*, 6938-6943.

47. Das, T. K., and Mazumdar, S. (1995) *Eur. J. Biochem. 227*, 823-828.

48. Colon, W., Elove, G. A., Wakem, L. P., Sherman, F., and Roder, H. (1996) *Biochemistry 35*, 5538-5549.

49. Mines, G. A., Pascher, T., Lee, S. C., Winkler, J. R., and Gray, H. B. (1996) *Chem. Biol. 3*, 491-497.

50. Mathews, and Houde, V. (1990) , Cummings Publishing, California.

51. Arunkumar, A. I., Kumar, T. K., Sivaraman, T., and Yu, C. (1997) *Int. J. Biol. Macromol. 21*, 299-305.

52. Fukushima, K., Sakamoto, T., Tsuji, J., Kondo, K., and Shimozawa, R. (1994) *Biochim. Biophys. Acta 1191*, 133-140.

53. Chiou, J. S., Tatara, T., Sawamura, S., Kaminoh, Y., Kamaya, H., Shibata, A., and Ueda, I. (1992) *Biochim. and Biophys. Acta 1119*, 211-217.

54. Shibata, A., Yamamoto, M., Yamashita, T., Chiou, J. S., Kamaya, H., and Ueda, I. (1992) *Biochemistry 31*, 5728-5733.

55. Jackson, M., Haris, P. I., and Chapman, D. (1989) *Biochimica and Biophysica Acta 998*, 75-79.

56. Martinez, G., and Millhauser, G. (1995) *Journal of Structural Biology 114*, 23-27.

57. Gao, Y., Lee, A. D., Williams, R. J., and Williams, G. (1989) *Eur. J. Biochem. 182*, 57-65.

58. Bushnell, G. W., Louie, G. V., and Brayer, G. D. (1990) *J. Mol. Biol. 214*, 585-595.

59. Holzbaur, I. E., English, A. M., and Ismail, A. A. (1996) *Biochemistry 35*, 5488-5494.

60. Welinder, K. G. (1979) *Eur. J. Biochem. 96*, 483-502.

61. Tams, J. W., and Welinder, K. G. (1995) *Analytical Biochemistry 228*, 48-55.

62. Gajhede, M., Schuller, D. J., Henriksen, A., Smith, A. T., and Poulos, T. L. (1997) *Nat. Struct. Biol. 4*, 1032-1038.

63. Chattopadhyay, K., and Mazumdar, S. (2000) *Biochemistry 39*, 263-270.

64. Tsaprailis, G., Chan, D. W., and English, A. M. (1998) *Biochemistry 37*, 2004-2016.

65. Ellis, W. D., and Dunford, H. B. (1968) *Biochemistry 7*, 2054-2062.

66. Tsaprailis, G., and English, A. M. (1997) *Biochemistry*.

67. Edelhoch, H. (1967) *Biochemistry 6*, 1948-1954.

68. Yeh, S. R., and Rousseau, D. L. (1998) *Nat. Struct. Biol. 5*, 222-228.

69. Wittung-Stafshede, P. (1998) *Biochim. Biophys. Acta 1382*, 324-332.

70. Moore, G. R., and Williams, R. J. (1980) *Eur. J. Biochem. 103*, 533-541.

71. Stryer, L. (1988) , W.H. Freeman and company, New york.

72. Margoliash, E., and Frohwirt, N. (1959) *Biochem. J. 71*, 570-572.

73. McLendon, G., and Smith, M. (1978) *J. Biol. Chem. 253*, 4004-4008.

74. Filosa, A., Ismail, A. A., and English, A. M. (1999) *JBIC 4*, 717-726.

75. Takano, T., and Dickerson, R. E. (1981) *J. Mol. Biol. 153*, 95-115.

76. Reinstadler, D., Fabian, H., Backmann, J., and Naumann, D. (1996) *Biochemistry 35*, 15822-15830.

77. Jackson, M., Sowa, M. G., and Mantsch, H. H. (1997) *Biophysical Chemistry 68*, 109-125.

78. Noda, I. (1990) *Applied Spectroscopy 44*, 550-561.

79. Noda, I. (1993) *Applied Spectroscopy 47*, 1329-1336.

80. Muller, M., Buchet, R., and Fingeli, U. P. (1996) *J. Phys. Chem. 100*, 10810-10825.

81. Nabet, A., and Pezolet, M. (1997) *Applied Spectroscopy 51*, 466-469.